Spring 2019 – Epigenetics and Systems Biology
Discussion Session (Systems Biology)
Michael K. Skinner – Biol 476/576
Week 4 (January 31)

Systems Biology (Omics Technology)

Primary Papers

1. Wu, et al. (2014) J Theor Biol 362:44-52
2. Davidsen, et al. (2016) J Appl Physiol 120:297-309
3. ENCODE Consortium (2012) Nature 489:57-74

Discussion

Student 7 – Ref #1 above

- What protocols and technology are used?
- What integration was required for the technology?
- How can the information be used in therapeutic design?

Student 8 – Ref #2 & 3 above

- What omics technology was integrated?
- What correlations with physiological parameters were made?
- Did the molecular insights help understand the physiology?

Student 9 – Ref #3 above

- What is ENCODE?
- What types of technology and data was obtained?
- What novel observations were made?

Journal of Theoretical Biology 362 (2014) 44–52

Contents lists available at ScienceDirect

Journal of Theoretical Biology

journal homepage: www.elsevier.com/locate/yjtbi

Pathway and network analysis in proteomics

Xiaogang Wu [a,b,c], Mohammad Al Hasan [d], Jake Yue Chen [a,b,d,e,*]

[a] Institute of Biopharmaceutical Informatics and Technology, Wenzhou Medical University, Wenzhou, Zhejiang Province, China
[b] School of Informatics and Computing, Indiana University-Purdue University, Indianapolis, IN 46202, USA
[c] Institute for Systems Biology, Seattle, WA 98109, USA
[d] Department of Computer Science and Information Science Purdue University, Indianapolis, IN 46202, USA
[e] Indiana Center for Systems Biology and Personalized Medicine, Indiana University, Indianapolis, IN 46202, USA

ARTICLE INFO

Article history:
Received 1 January 2014
Received in revised form
15 May 2014
Accepted 21 May 2014
Available online 6 June 2014

Keywords:
Pathway analysis
Functional analysis
Hybrid strategy
Network modules
Complex networks

ABSTRACT

Proteomics is inherently a systems science that studies not only measured protein and their expressions in a cell, but also the interplay of proteins, protein complexes, signaling pathways, and network modules. There is a rapid accumulation of Proteomics data in recent years. However, Proteomics data are highly variable, with results sensitive to data preparation methods, sample condition, instrument types, and analytical methods. To address the challenge in Proteomics data analysis, we review current tools being developed to incorporate biological function and network topological information. We categorize these tools into four types: tools with basic functional information and little topological features (e.g., GO category analysis), tools with rich functional information and little topological features (e.g., GSEA), tools with basic functional information and rich topological features (e.g., Cytoscape), and tools with rich functional information and rich topological features (e.g., PathwayExpress). We first review the potential application of these tools to Proteomics; then we review tools that can achieve automated learning of pathway modules and features, and tools that help perform integrated network visual analytics.

1. Introduction

Proteomics, the collective study of all measured proteins in cells of a given condition, is inherently a systems science that requires the understanding of not only the independent parts – protein constituents and their expressions in a cell – but also the interplay of proteins, protein complexes, signaling pathways, and network modules as a whole for achieving biochemical functions. Ideker et al. (2001) introduced an integrated approach to identify metabolic networks and build cellular pathway models, by using measurements from DNA microarrays, protein expressions, and protein interaction knowledge. This work provides systems biology researchers with a practical example how biological networks could be used to perform integrative functional genomics data analysis. By gaining system-wide perspectives of protein functions, Proteomics promises to further study which subsets of proteins are essential in regulating specific biological process. In Proteomics analysis, the incorporating of prior knowledge how groups of proteins work in concert with each other or with other genes and metabolites has made it possible to unravel the complexity inherent in the analysis of cellular functions (MacBeath, 2002). New network biology and systems biology techniques have emerged in recent Proteomics studies (Bensimon et al., 2012; Sabidó et al., 2012) including cancer (Goh and Wong, 2013).

There has been a rapid accumulation of data due to advances in Proteomics technologies (MacBeath, 2002). Proteomics data are often generated from high-throughput experimental platforms, e.g., two-dimensional (2D) gel, liquid chromatography coupled tandem mass spectrometers (LC–MS/MS), multiplexed immunoassays, and protein microarrays (Altelaar et al., 2013; Kingsmore, 2006). These platforms can assay thousands of proteins simultaneously from complex biological samples (Aebersold and Mann, 2003) to measure the relative abundance of proteins or peptides in various biological conditions. More accurate quantitative measure of peptides could also be performed with isotopic labelling of proteins in two different samples (Ong and Mann, 2005). Similar to Genomics, Proteomics studies have been widely used to extract functional and temporal signals identified in biological systems (Blagoev et al., 2004). Popular experimental techniques to measure protein–protein interactions include the yeast two-hybrid (Y2H) system (Ito et al., 2001).

In contract to the recent accelerated application of next-generation sequencing (NGS) in biology, a primary hurdle that slows down Proteomics' applications is the Proteomics data's high

* Corresponding author at: Indiana University School of Informatics & Computing, Indiana Center for Systems Biology and Personalized Medicine, Indiana University - Purdue University Indianapolis, 719 Indiana Avenue, Indianapolis, IN 46202, USA. Tel.: +1 317 278 7604; fax: +1 317 278 9201.
E-mail address: jakechen@iupui.edu (J.Y. Chen).
URL: http://bio.informatics.iupui.edu/ (J.Y. Chen).

http://dx.doi.org/10.1016/j.jtbi.2014.05.031
0022-5193/

variability, which makes it difficult to interpret Proteomics data analysis results biologically (Colinge and Bennett, 2007). Possible sources of data variations arise from biological sample heterogeneity, sample preparation variance, protein separation variance, detection limits of various proteomics techniques, and pattern-matching peptide/protein identification or quantification inaccuracies from Proteomics data management software. The unusual high level of data noises inherent in Proteomics studies in contrast to those in DNA microarrays or NGS instruments have made Proteomics experiments difficult to repeat, and many statistical methods developed for Genomics applications ineffective. There are plenty of reviews that cover the computational challenges (Vitek, 2009; Noble and MacCoss, 2012; Barla et al., 2008) and solutions to apply statistical machine learning approaches to the problem, e.g., with the use of support vector machines (SVM) (Elias et al., 2004), Markov clustering (Krogan et al., 2006), ant colony optimization (Ressom et al., 2007), and semi-supervised learning (Käll et al., 2007) techniques. The ultimate challenge, however, is how to extract functional and biological information from a long list of proteins identified or discovered from high-throughput Proteomic experiments, in order to provide biological insights into the underlying molecular mechanisms of different conditions (Khatri et al., 2012). Therefore, additional protein functional knowledge, e.g., the abundance of proteins, cellular locations, protein complexes, and gene/protein regulatory pathways, should be incorporated in the second phase of proteomics analysis in order to filter out noisy protein identifications missed in the first statistical analysis phase of Proteomics analysis.

Pathway and network analysis techniques can help address the challenge in interpreting Proteomics results. Analysis of proteomic data at the pathway level has become increasingly popular (Fig. 1). For pathway analysis, we refer to data analysis that aims to identify activated pathways or pathway modules from functional proteomic data. Biological pathways can be viewed as signaling pathways, gene regulatory pathways, and metabolic pathways, all of which are curated carefully in reputable scientific publications. Pathway analysis can help organize a long list of proteins onto a short list of pathway knowledge maps, making it easy to interpret molecular mechanisms underlying these altered proteins or their expressions (Khatri et al., 2012). For network analysis, we refer to data analysis that build, overlay, visualize, and infer protein interaction networks from functional Proteomics and other systems biology data. Network analysis usually requires the use of graph theory, information theory, or Bayesian theory. Different from pathway analysis, network analysis aims to use comprehensive network wiring diagram derived both from prior experimental sources and new in silico prediction to gain systems-level biological meanings (Wu and Chen, 2009). Many large knowledge bases on biological pathways and protein networks have been published, e.g., BioGRID (Chatr-aryamontri et al., 2013), STRING (Franceschini et al., 2013), KEGG (Kanehisa and Goto, 2000), Reactome (Matthews et al., 2009), BioCarta (Nishimura, 2001), PID (Schaefer et al., 2009), HAPPI (Chen et al., 2009), HPD (Chowbina et al., 2009), and PAGED (Huang et al., 2012) databases.

Compared to pathway and network analysis approaches applied in genomics, the advantages of the related researches in proteomics are listed below: (1) Pathway analysis for proteomic data can be directly interpreted in signaling pathways with signal proteins. (2) Network analysis for proteomic data can have direct evidences supported by protein–protein interaction data validated by in-vitro experiments. (3) Both pathway analysis and network analysis for proteomic data can be visualized in a functional protein network with transcriptional factors labeled, which are all measured indirectly in genomic studies.

2. Pathway and network analysis for proteomics

Many pathway databases and pathway analysis software tools have become available in the last decade (Khatri et al., 2012; Ramanan et al., 2012), with some directly applicable to Proteomics (Goh and Wong, 2013; Goh et al., 2012). In Proteomics, statistically significant proteins identified from high-throughput Proteomic instruments often suffer from high false discovery rate (Vitek, 2009), partly because the inherently high level of variance in Proteomics data can make it difficult to identify true biological signals (Noble and MacCoss, 2012). To assess the biological significance of Proteomics results, additional information such as Gene Ontology (GO) and pathways is needed. While there are numerous approaches to incorporate biological pathway and network data into Proteomics data analysis, we categorize existing approaches into two major characteristics, one focusing on integration of "functional information" and the other focusing on integration of "topological information". For functional information, we refer to functional descriptions that aggregate genes into common protein complexes, biological pathways, network modules, and other genes sets consisting of genes playing similar roles. For topological information, we refer to regulatory relationships that exist among

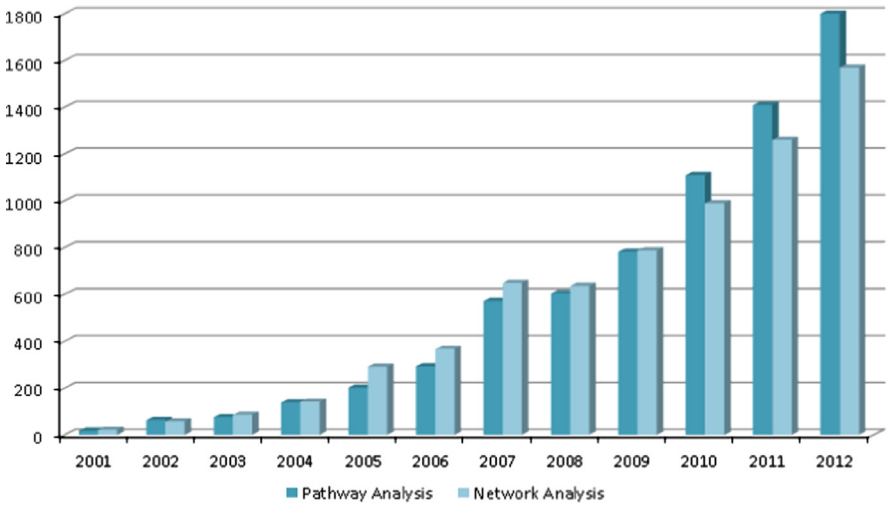

Fig. 1. Trends of pathway and network analysis in Proteomics from decade publications (searched in Google Scholar with terms of ["pathway analysis" AND "Proteomics"], and ["network analysis" AND "Proteomics"]).

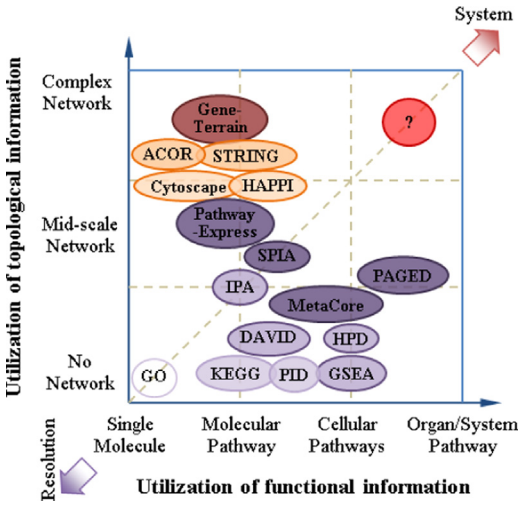

Fig. 2. Conceptual plot of different pathway analysis tools according to the utilization of functional information and/or topological information (positions are NOT absolute).

genes, protein complexes, biological pathways, and biological network modules. In Fig. 2, we organize the two independent characteristics as the *x*- and *y*- axis to categorize representative pathway and network analysis tools in a two-dimensional space. With this framework, we can further categorize existing pathway analysis tools into roughly four quadrants:

- Basic functional information and basic topological features ($\mathbf{F}^{-}\mathbf{T}^{-}$). An example is the uses of minimal additional information, e.g., GO categories, to interpret Proteomics results. Since the GO categories contain curated and known functions, and the interaction or regulation relationship information is not tested, the value for pathway and network analysis from the $\mathbf{F}^{-}\mathbf{T}^{-}$ quadrant may be quite limited. We also consider the traditional feature selection method (e.g., linear programming based feature selection approach (Wang et al., 2012) or heterogeneous set identification (Ren et al., 2013)) in the $\mathbf{F}^{-}\mathbf{T}^{-}$ quadrant, which is based on the classification algorithm and purely used the data itself. When facing simple problems that only require obtaining basic functional information from proteomic data, approaches in the $\mathbf{F}^{-}\mathbf{T}^{-}$ quadrant will work very well.
- Basic functional information but rich topological features ($\mathbf{F}^{-}\mathbf{T}^{+}$). An example is the use of protein interaction or gene regulatory networks to help prioritize top-ranked proteins retrieved from the Proteomics results. Since the protein–protein interaction or gene regulatory network contains the biological context, pathway and network analysis from the $\mathbf{F}^{-}\mathbf{T}^{+}$ quadrant can help reduce false discovery rate. A latest example is NOA (Network Ontology Analysis) (Wang et al., 2011). If the applications are related to cascade regulation or signaling relationships, approaches from the $\mathbf{F}^{-}\mathbf{T}^{+}$ quadrant will be more suitable than the ones from the $\mathbf{F}^{-}\mathbf{T}^{-}$ quadrant.
- Rich functional information but basic topological features ($\mathbf{F}^{+}\mathbf{T}^{-}$). An example is the use of gene set knowledge and corresponding knowledge to characterize significant biological phenomena that are strongly associated with Proteomics results. Since the gene set information – including both characterized and uncharacterized pathway-related gene sets – can be quite comprehensive, integrated Proteomics data analysis using computational techniques such as the GSEA analysis from the $\mathbf{F}^{+}\mathbf{T}^{-}$ quadrant can reveal significant biological insights. If the applications are related to complex functional identification, especially for protein biomarker discovery, approaches from the $\mathbf{F}^{+}\mathbf{T}^{-}$ quadrant will be more suitable than the ones from the $\mathbf{F}^{-}\mathbf{T}^{-}$ quadrant.
- Rich functional information and rich topological features ($\mathbf{F}^{+}\mathbf{T}^{+}$). An example is the simultaneous use of both protein interaction/gene regulation information and curated gene set knowledge to build biological networks at different functional categorical levels (i.e., multiple biosystems scales). Since the multi-scale pathway interaction/regulation network can be complex, the $\mathbf{F}^{+}\mathbf{T}^{+}$ model can properly mimic the actual biological systems to provide the highest value to Proteomics researchers. Pathway-Express (Draghici et al., 2007) is an exemplar tool showing how to move toward this new quadrant. Once we meet problems related to both cascade regulation/signaling relationships and complex functional identification, especially for complex disease biomarker discovery, approaches shown in the $\mathbf{F}^{+}\mathbf{T}^{+}$ quadrant could be considered as our first options.

2.1. *Pathway analysis using protein functional category information*

Many pathway analysis tools in the $\mathbf{F}^{-}\mathbf{T}^{-}$ or the $\mathbf{F}^{-}\mathbf{T}^{+}$ quadrant use basic functional information, since these tools focus on protein functional annotation or basic "functional enrichment analysis" among an unordered set of proteins identified from Proteomics data analysis (Sherman and Lempicki, 2009). These approaches aim to identify proteins with statistical significance first and functional significance subsequently. For example, GoMiner (Zeeberg et al., 2003) can organize lists of "interesting" genes/proteins for biological interpretation in the context of GO terms, which is at the single-molecule level. DAVID (Dennis et al., 2003) provides a comprehensive set of functional annotation tools which cannot only identify enriched biological themes, particularly GO terms, but also discover enriched functionally-related gene groups and visualize genes/proteins in pathway diagrams based on the famous pathway databases—KEGG (Kanehisa and Goto, 2000) and BioCarta (Nishimura, 2001). To provide broad pathway data coverage, the Human Pathway Database (HPD) (Chowbina et al., 2009) integrated KEGG (Kanehisa and Goto, 2000), Reactome (Matthews et al., 2009), BioCarta (Nishimura, 2001), and PID (Schaefer et al., 2009) databases ranges from molecular pathways to cellular pathways. The functional enrichment analysis of Proteomics results against these database resources is performed usually with an overlap cut-off score, e.g., as in the single enrichment analysis (SEA) (Sherman and Lempicki, 2009); therefore true signals that are marginally significant from statistical tests may be filtered out prematurely.

Pathway analysis tools moving from the $\mathbf{F}^{-}\mathbf{T}^{-}$ quadrant to the $\mathbf{F}^{+}\mathbf{T}^{-}$ quadrant is able to better integrate statistical significance from Proteomics data analysis into functional enrichment. Compared with SEA, gene set enrichment analysis (GSEA) (Subramanian et al., 2005) evaluates statistical significance of a ranked list of genes/proteins (i.e. gene sets) against one or more pathway data set. GSEA not only can detect group-wise statistically-significant genes and proteins, but also enriched pathway gene sets against a large database of gene sets previously characterized in functional genomic studies. To support GSEA, databases such as the Molecular Signature Database (MSigDB) (Liberzon et al., 2011), GeneSigDB (Culhane et al., 2010), and PAGED (Huang et al., 2012) have been developed to integrate GO categories, pathways from KEGG (Kanehisa and Goto, 2000), gene regulatory targets from TRANSFAC (Wingender et al., 2000), micro-RNA targets, and curated gene sets that are co-expression signatures from literature. GSEA and comprehensive databases populated pathway modules can help streamline statistical and

functional determination of groups of proteins identified from generally "noisy" Proteomics results.

2.2. Pathway analysis using network topological information

Moving from the $\mathbf{F}^{-}\mathbf{T}^{-}$ quadrant to the $\mathbf{F}^{-}\mathbf{T}^{+}$ quadrant, tools take a different strategy to perform pathway analysis, i.e., to treat pathways and pathway models as a form of network data structure from which one may incorporate network topological information into the Proteomic data analysis. Here, we refer to biological pathways and biological pathway models interchangeably. In practice, however, biological pathways refer to signaling pathways, gene regulatory networks and metabolic pathways (Bader et al., 2006), whereas biological pathway models refer to computer representation of actual biological events that have been abstracted. Network representation of biological pathway models involve topologically connected molecules (e.g., genes, proteins, or metabolites) and molecular events (e.g., protein interactions, gene regulations, or metabolite reactions) that are carefully assembled into a graph. While there are 550 biological pathway data sources according to Pathguide (http://www.pathguide.org/), only approximately 10% of them provide pathway diagrammatic details suitable as pathway models; the remaining 90% may only be useful for functional category analysis described earlier. Cytoscape (Shannon et al., 2003) is an open-source biological network analysis platform to visualize and analyze biological pathways based on network topological information. IPA from Ingenuity and MetaCore from GeneGo are commercially available to perform network and pathway analysis for manual pathway data analysis and modeling. However, manual examination of a given biological pathway structure is no longer scalable when it involves more than a few dozen nodes and several hundred edges in the network.

To address scalability issues, tools in the $\mathbf{F}^{-}\mathbf{T}^{+}$ quadrant must evaluate both statistical significance and topological significance with computational method. An example is Pathway-Express (Draghici et al., 2007), which develops "impact analysis" techniques to prioritize biologically-significant genes/proteins with lower FDRs. Impact analysis measures network topological information as degree of connectivity and clustering coefficient and applies it as weight for given genes/proteins in the biological pathway to calculate an "impact factor" for the entire pathway. It further evaluates whether the impact factor obtained is significant due to a possible network perturbation event or a random chance. Separately, signaling pathway impact analysis (SPIA) combines both functional evidences from classical enrichment analysis and topological evidences represented as perturbation factor on a given pathway under a given condition (Tarca et al., 2009). Network analysis using partial network modules are also promising, e.g., developing pathway biomarkers from proteomic data (Zhang and Chen, 2010) and breast cancer subtyping from plasma proteins (Zhang and Chen, 2013). In all, these pathway/network analysis tools integrates network topological information at a limited scale, either at the protein interaction network level or at the network module level. For a list of representative software tools, refer to Table 1.

2.3. Pathway analysis using a multi-scale hybrid strategy

To understand complex molecular mechanisms associated with a biological condition using Proteomics, a researcher must not only study specific proteins whose expressions are altered or specific pathways in which signaling cascades take place, but also understand how external and internal stimuli translates into coordinated changes of genes, proteins, metabolites, signaling network modules, pathways, and other functional components in a

Table 1
Selected pathway/network analysis resource that can benefit Proteomics data analysis.

Name	Description	Link	Reference	Functional info using	Topological info using
GoMiner	Gene ontology (GO) analysis for omic data	http://discover.nci.nih.gov/gominer/	Zeeberg et al. (2003)	Single molecule	Non
KEGG	Kyoto encyclopedia of genes and genomes	http://www.genome.jp/kegg/	Kanehisa and Goto (2000)	Molecular pathway	Non
DAVID	The database for annotation, visualization and integrated discovery	http://david.abcc.ncifcrf.gov/	Dennis et al. (2003)	Molecular pathway	Small-scale
PID	Pathway interaction database	http://pid.nci.nih.gov/	Schaefer et al. (2009)	Cellular pathway	Non
HPD	Human pathway database	http://bio.informatics.iupui.edu/HPD	Chowbina et al. (2009)	Cellular pathway	Small-scale
GESA	Gene set enrichment analysis	http://www.broadinstitute.org/gsea/	Subramanian et al. (2005)	Cellular pathway	Small-scale
IPA	Ingenuity pathway analysis	http://www.ingenuity.com/	N/A	Molecular pathway	Small-scale
MetaCore	Thomson Reuters pathway analysis and knowledge mining	http://thomsonreuters.com/metacore/	N/A	Cellular pathway	Small-scale
Pathway-Express	A systems biology approach for pathway level impact analysis	http://vortex.cs.wayne.edu/projects.htm	Draghici et al. (2007)	Molecular pathway	Mid-Scale
SPIA	Signaling pathway impact analysis	http://www.bioconductor.org/packages/2.12/bioc/html/SPIA.html	Tarca et al. (2009)	Molecular pathway	Mid-Scale
PAGED	An integrated pathway and gene enrichment database	http://bio.informatics.iupui.edu/PAGED	Huang et al. (2012)	System pathway	Mid-Scale
HAPPI	Human annotated and predicted protein interaction database	http://bio.informatics.iupui.edu/HAPPI	Chen et al. (2009)	Single molecule	Large-scale
STRING	Search tool for the retrieval of interacting genes/proteins	http://string.embl.de/	Franceschini et al. (2013)	Single molecule	Large-scale
CytoScape	An open source platform for complex network analysis and visualization	http://www.cytoscape.org/	Shannon et al. (2003)	Molecular pathway	Large-scale
ACOR	Ant colony optimization reordering	N/A	Wu et al. (2009), (2009b), (2009c), (2012)	Molecular pathway	Large-scale
Gene-Terrain	Terrain-based visual analysis for complex networks	N/A	Kim et al. (2001), You et al. (2010)	Network module	Large-scale

cell. This is why tools in the $\mathbf{F}^{+}\mathbf{T}^{+}$ quadrant must be developed. For example, the concept of "GO functional crosstalk network" was introduced in 2008, based on graph representations that use GO functional categories as nodes and enriched protein interactions between GO functional categories as edges (Li et al., 2008). In this work, researchers integrated network topological information and functional information together, resulting in enhanced characterization of complex ovarian cancer drug resistance development mechanism from Proteomics tandem mass spectrometry data. Similarly, pathway similarity networks can be built from heterogeneous pathway data as nodes and pathway–pathway similarity measurement as edges (Chowbina et al., 2009). Pathway association networks (PAN) as a more special form of "GO functional crosstalk networks" can be built from heterogeneous pathway data as nodes and significant protein–protein interaction enrichments as edges (Wu and Chen, 2012). The concept of PANs have already been successfully applied into complex disease modeling for cancer progression (Edelman et al., 2008), Alzheimer's disease (Liu et al., 2010), and colorectal cancer (Pradhan et al., 2012). Recently, a comprehensive approach to construct multi-edge gene-set networks based on co-memberships, protein interactions, and co-enrichment has also been proposed (Parikh et al., 2012).

Tools in the $\mathbf{F}^{+}\mathbf{T}^{+}$ quadrant can benefit significantly from knowledge bases that build relationships between different molecular biosystem components, e.g., pathways, disease-associated gene sets, molecular signatures, microRNA and all their gene targets, and protein interaction network modules. Using molecular biosystem component similarity measures for human in PAGED, a PAN can

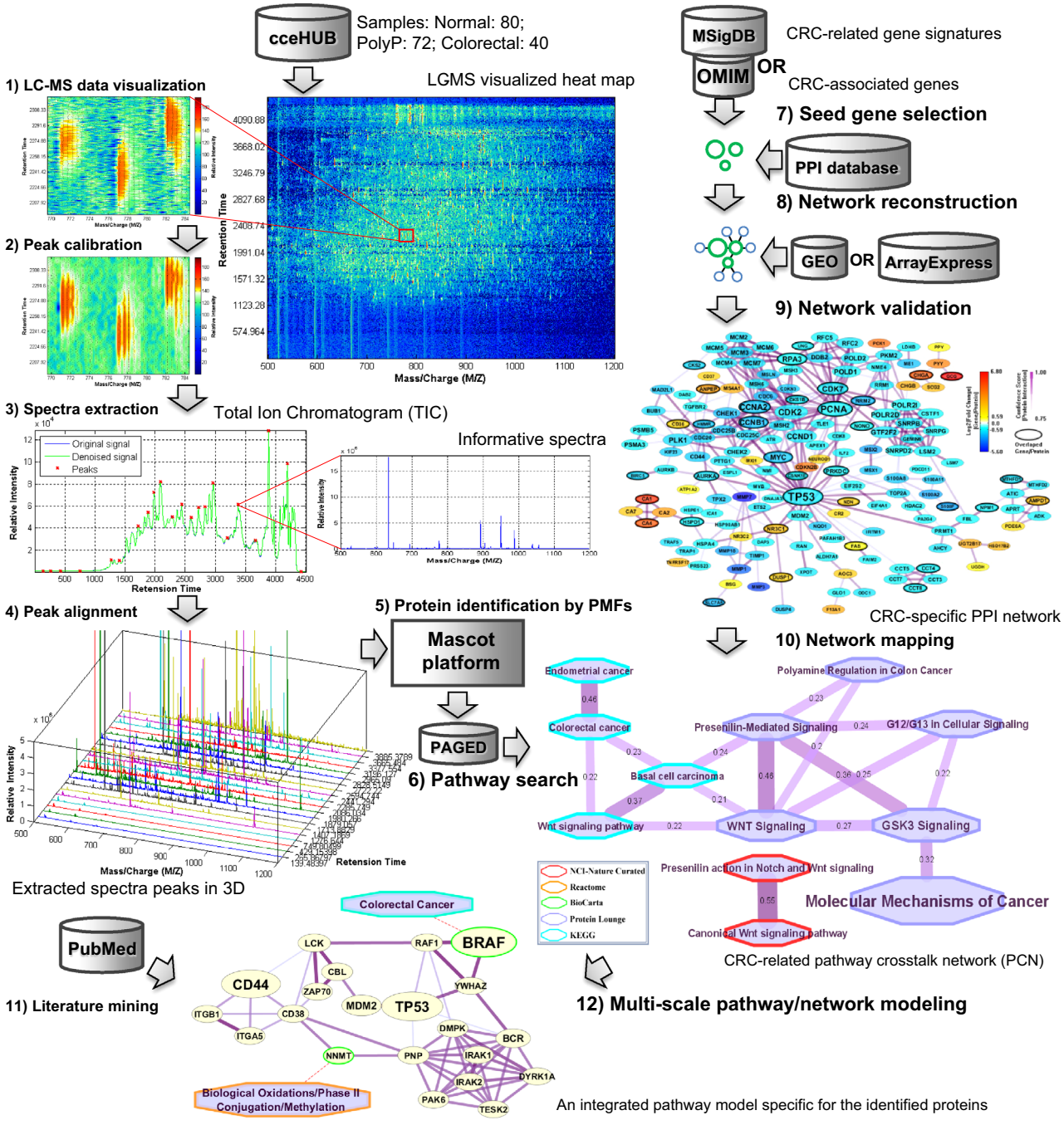

Fig. 3. Illustration of multi-scale pathway analysis using colorectal cancer proteomic data as an example. The protein–protein interaction (PPI) database for the Step 8) could use STRING or HAPPI.

be developed to serve as a system-level pathway model for interpretation of complex molecular profiling study results. In Fig. 3, we demonstrate a workflow platform with which we apply multi-scale pathway analysis to the characterization of colorectal cancer MS-based proteomic data. The input LC–MS data comes from the cceHUB web portal (The Cancer Care Engineering project, hosted at https://ccehub.org/). This workflow utilizes both functional information from the PAGED (Huang et al., 2012) and topological information from the protein–protein interaction (PPI) database, such as HAPPI or STRING. The functional information validates Proteomics results obtained from LC–MS experiments of the colorectal cancer sample, while the final findings are subsequently examined in the integrated pathway model constructed from protein–protein interaction databases. In this study, we not only confirmed BRAF as a prognostic biomarker for colorectal cancer (Yokota et al., 2011), but also discovered NNMT to be a potential biomarker worth experimental validations (Roeßler et al., 2005).

2.4. Automated learning of pathway modules and features

Functional and network information related to pathway models can be either extracted from large existing databases, or learned automatically from functional genomics and Proteomics data sets. There are two types of knowledge discovery tasks. The first is the discovery of pathway modules from pathway and network data relevant to Proteomics results. The second is the discovery of network topological features.

In the first type, “pathway module discovery”, one can assume that there is a close relationship between common protein function categories and proteins closely regulated in the same pathway or network (Barabási et al., 2011). Existing pathway knowledge or other functional information could also be used to validate newly-discovered pathway models or pathway modules. Hartwell et al. (1999) define “network module” as an entity comprising of different types of interacting molecules with strong connections within each other but weak connections outside of the entity. Network modules may map to protein complexes or molecular pathways, consisting of a large number of molecules that co-regulate each other to perform particular cellular functions. Due to the difficulty by human curators to read hundreds of research articles and document molecular regulation details in biological networks, computerized techniques to identify network modules usually involve some form of automated graph clustering of the biological network data (Dittrich et al., 2008; He et al., 2012; Pereira-Leal et al., 2004)

In the second type, “network feature discovery”, automated network-based learning of topological and functional information can be done with nonlinear dynamical modeling, when there is no absolute rank for each protein as the node and no clear cluster network module boundaries in the network (Barabási and Oltvai, 2004). Hence, traditional network analysis approaches, such as node ranking and graph clustering, are not directly applicable (Barabási, 2009). The lack of absolute rank or cluster boundaries is characteristic of scale-free biological networks and is also common in other nonlinear systems such as fractals (multi-scale self-similarity), chaos, and phase transitions (Strogatz, 2001). Nonlinear dynamical modeling approach, e.g., ant colony optimization (ACO) (Dorigo and Birattari, 2010), has already been applied to the analysis Proteomic data in 2007 (Ressom et al., 2007). An ACO-based network reordering (ACOR) algorithm has been show effective in analyzing complex networks to reveal fractal-like patterns in the studies of yeast lethal gene study (Wu et al., 2009a), breast cancer (Wu et al., 2009b), and Alzheimer’s disease (AD) (Wu et al., 2009c). A recent study to classify AD and normal brain tissue samples showed that prediction based on the ACOR algorithm had better performance than even the best available approaches using either node ranking or graph clustering alone (Wu et al., 2012). In contract, Proteomics biomarker results obtained from traditional network analysis approaches such as (Chuang et al., 2007; Lee et al., 2008; Taylor et al., 2009) reported that sometimes breast cancer metastasis predictions consisting of multiple genes cannot compete well in performance against optimized single-gene classifiers by comparison (Staiger et al., 2012).

3. Network analysis for complex protein networks

Complex protein networks are often characterized by scale-free properties (Barabási and Oltvai, 2004), i.e., their node distribution follow power laws. Such networks are highly robust to node communication errors, even with unrealistically high failure rates (Albert et al., 2000). The ability of error tolerance not only appears in complex protein networks, but also has been found in many other types of scale-free networks, such as World-Wide Web (WWW), the Internet, social networks and cell networks (Barabási, 2009). This suggests that network modeling and analysis methods originally designed for complex social networks can be also applied to analyzing complex protein networks.

The motivation for network analysis specific for complex protein networks derives from complex disease (e.g. various cancers, Alzheimer’s disease and type II diabetes etc.) network biomarker discovery, since there are thousands of genes/proteins respond to disease driving factors and drug sensitivity/resistance. As we all know, a complex disease is usually not one disease, but multiple subtypes of disease phenotypes. To discover hidden molecular mechanisms for early diagnosis, prognosis, and drug response, we have to deal with large-scale disease-specific protein networks with hierarchical functional relationships under different conditions, in order to develop tailored therapies for different subtypes of patients, which is the main goal of personalized medicine. Here we will introduce several cutting-edge works for modeling and analyzing large-scale complex protein networks, utilizing vast topological information and group functional information.

3.1. Network reordering using global topological information

A complex network with scale-free property may also have high-degree “inseparability”, which means that there is no “absolute rank” for each node or no “clear cluster” in the network. Hence, traditional network analysis approaches, such as node ranking and graph clustering, often failed when facing complex networks. Scale-free is an analogy to the situation where power laws arise and no single characteristic scale can be identified, which also happens in other nonlinear phenomena, such as fractals (multi-scale self-similarity), chaos, and phase transitions (Strogatz, 2001). Based on this connection, nonlinear dynamical modeling may have great potential in analyzing complex protein networks. As a typical nonlinear dynamical modeling approach, ant colony optimization (ACO) (Dorigo and Birattari, 2010), which has been already applied to analyzing MS-based proteomic data in 2007 (Ressom et al., 2007), can be also employed for complex protein network analysis. An ACO-based network reordering (ACOR) algorithm was developed in 2009 to analyze complex networks and the results revealed fractal-like patterns in protein interaction networks for yeast lethal gene study (Wu et al., 2009a), breast cancer (BRCA) research (Wu et al., 2009b), and Alzheimer’s disease (AD) diagnosis (Wu et al., 2009c), respectively. These interesting patterns might be closely related to scale-free properties.

Different with traditional network analysis approaches only using local topological information, the ACOR algorithm can

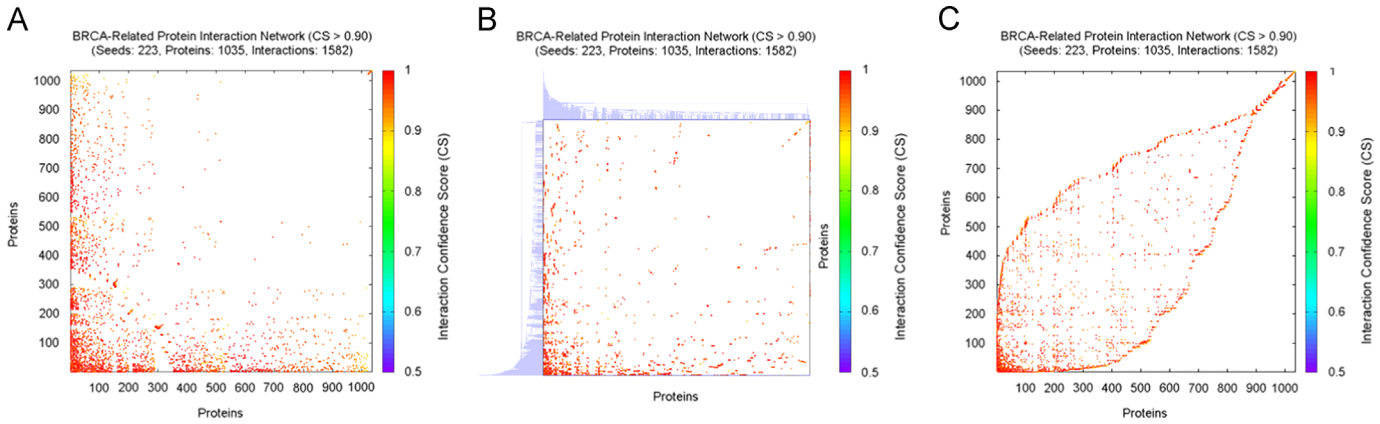

Fig. 4. Re-ordered network adjacency matrices of a weighted BRCA-related protein interaction network with 1035 proteins and 1582 interaction, expanded in HAPPI from 223 breast cancer associated genes from OMIM. (A) The result ranked by GeneRank (similar to PageRank algorithm used by Google), (B) The result clustered by 2D hierarchical clustering in Matlab Bioinformatics Toolbox, and (C) The result reordered by Ant Colony Optimization Reordering (ACOR) algorithm. (CS: confidence score for protein interaction in the HAPPI database)

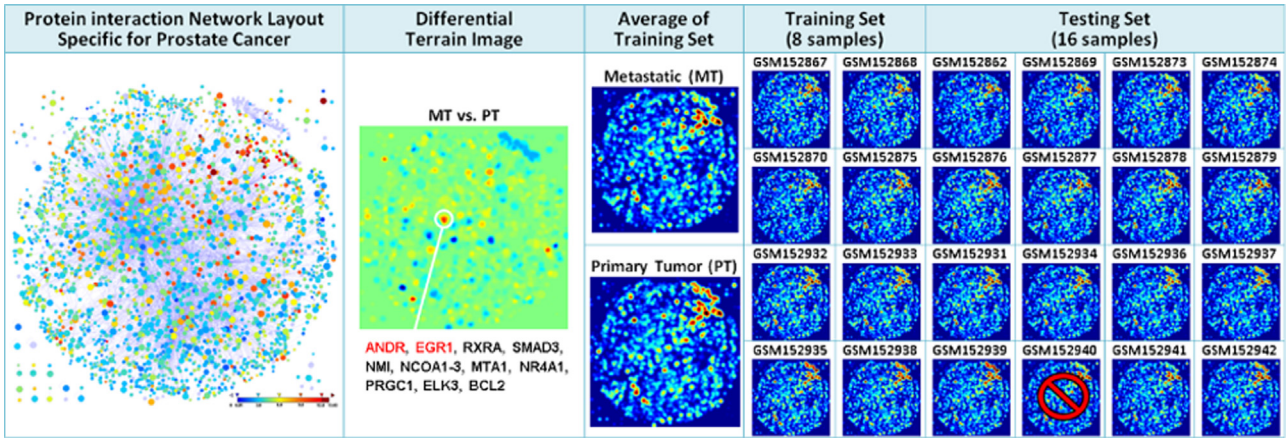

Fig. 5. Prostate cancer microarray classification between primary prostate tumor (PT) samples and metastatic (MT) samples by using terrain-based visual analytics approach. The terrain model derived from a PC-specific protein interaction network containing 2637 proteins and 5772 interactions. 24 gene expression profiles (12 PT samples and 12 MT samples) are randomly selected from a microarray dataset GSE6919 in GEO. The only one PT sample classified incorrectly is marked.

efficiently extract global topological information in a complex network, through assigning each node an order number—"relative rank" in "overlapped clusters". In a recent case study on microarray classification for brain tissue samples of AD patients vs. normal controls, prediction based on the ACOR algorithm showed better performance than the one using either node ranking or graph clustering (Wu et al., 2012). Interestingly, the prediction power of these traditional network analysis approaches is only at the same level with the one using random-ordering but still keeping node degree values—typical local topological information. Another case study on breast cancer metastasis prediction also showed that several most popular pathway or network-based approaches (Chuang et al., 2007; Lee et al., 2008; Taylor et al., 2009) even cannot compete with a simple, single genes based classifier in an extensive and critical comparison (Staiger et al., 2012). In Fig. 4, we showed an intuitional comparison of the results respectively produced by conventional network-based gene ranking (similar to PageRank algorithm used by Google) (Morrison et al., 2005), 2D hierarchical clustering (Bar-Joseph et al., 2001) and ACOR (Wu et al., 2009a, 2009b, 2009c), for analyzing a BRCA-related protein interaction network (Wu et al., 2009b). From this comparison, we can see directly that only ACOR approach can reorder the adjacency matrix of the BRCA-related protein network to a meaningful pattern, which has many clusters closely overlapped. All the evidences showed here directly point to an important conclusion—utilization of global topological information is the key of analyzing complex protein networks.

3.2. *Visual analytics using both topological and functional information*

A complex protein network usually consists of thousands proteins, which make the network layout looks like a messy hair ball on conventional network visualization platforms. An example of complex protein network visualization by Cytoscape can be seen in Fig. 5. One way to overview complex networks is to visualize them at the functional level. A functional category crosstalk network was constructed based on protein interaction networks for ovarian cancer drug resistance study in 2007. This network was first shown as a matrix of interactions between related GO terms, also called GO–GO interactions (Chen et al., 2007), which took the advantages of both local topological information and group functional information. Another way to simplify complex network visualization is to use the concept of molecular network terrain. Molecular network terrain visualization grows from the work of Kim et al. (2001), who assembled data from C. Elegans DNA microarray experiments, and visualized grouped co-regulated genes in a three-dimensional (3D) expression map that displays correlations of gene expression profiles as distances in two dimensions and gene density in the third dimension. In a subsequent study, You et al. (2010) visualized an Alzheimer's

disease (AD) specific protein interaction network as a 3D terrain, and successfully differentiated the three distinct stages of AD. The visual analytics approach based on molecular network terrains could increase accuracy and noise endurance for sample molecular classifications, by utilizing both global topological information and group functional information.

As shown in Fig. 5, the terrain-based classification approach exhibited amazing performance in a case study on prostate cancer (PC) microarray classification between primary prostate tumor (PT) samples and metastatic (MT) samples. We randomly selected 24 gene expression profiles (12 PT samples and 12 MT samples) from a microarray dataset (GSE6919 (Yu et al., 2004; Chandran et al., 2007)) in GEO. We only used 4 PT samples and 4 MT samples as training set, and used the left 16 samples as testing set. Although all the terrain images here look like the same, they can be easily distinguished by computer program. We applied a terrain model, derived from a PC-specific protein interaction network containing 2637 proteins and 5772 interactions (also shown in Fig. 5), and simply used the distance between a testing terrain image and average terrain image to determine its group for two-group classification. Although these metastatic samples derive from different organs, and are highly heterogeneous in expression, the left 8 MT samples are all correctly classified (100%), and the left 7 of 8 PT samples are also correctly classified (87.5%), which makes the total accuracy reach 93.75%. Moreover, as clearly shown in Fig. 5, the differential terrain image between two groups identified a crucial gene clusters, including androgen receptor (ANDR) and early growth response protein (EGR1), which are all well-known, and have been validated to be closely related to PC metastasis previously (Chandran et al., 2007). This case study demonstrates again the power of using global topological information. Furthermore, it shows that utilization of group functional information (from network modules) not only can be an important supplement to pathway analysis, but also brings great convenience to the interpretation for complex network analysis.

4. Summary

Due to the data variability issues inherent in Proteomics measurements, statistical significance alone is insufficient to the evaluation of Proteomics results. We believe both pathway models' functional information and topological information should be integrated to make Proteomics data interpretation relevant to biological mechanism. With the availability of two types of information, one in protein functional categories and the other in network topological features, we can categorize pathway analysis tools available to Proteomics researchers today as falling into any one of the 2×2 quadrants as described in this review. GSEA enables molecular signature-based statistical significance testing, which integrates protein functional category information effectively with statistical testing of functional genomics or Proteomics results. Cytoscape enables network-based data analysis of biological data in situations where functional information may or may not be available. SPIA enables pathway-based statistical assessment by combining both functional annotation and local topological annotation of the network. Ultimately, future tools must support elucidation of complex molecular mechanisms suggested from Proteomics results from multi-scale network data and molecular signature data. A workflow with a hybrid strategy for multi-scale pathway analysis of LC–MS proteomic data was presented. New tools to extract and integrate gene set knowledge from public databases using PAGED and ACOR can be promising. Ultimately, the use of terrain-based visual analytics can be more fruitful, because it gives users inexperienced with network biology or systems biology analysis a rich user experience based on a visualization interface. However, there are still significant challenges in designing next-generation network/pathway analysis tools. In large complex gene regulatory networks and pathway association networks, network coverage can be poor. Accurate protein or protein group functional information at each network scale may be missing. Proposed findings of molecular mechanisms at the network module level can also be more challenging to validate experimentally than at the individual protein level. Nonetheless, the opportunity to discover novel complex mechanisms of biological processes will keep researchers in the field occupied for quite some time.

Acknowledgements

This work is partly supported by Indiana Center for Systems Biology and Personalized Medicine (CSBPM) and Wenzhou Medical University.

References

Aebersold, R., Mann, M., 2003. Mass spectrometry-based proteomics. Nature 422 (6928), 198–207.
Albert, R., Jeong, H., Barabási, A.-L., 2000. Error and attack tolerance of complex networks. Nature 406 (6794), 378–382.
Altelaar, A.M., Munoz, J., Heck, A.J., 2013. Next-generation proteomics: towards an integrative view of proteome dynamics. Nat. Rev. Genet. 14 (1), 35–48.
Bader, G.D., Cary, M.P., Sander, C., 2006. Pathguide: a pathway resource list. Nucleic Acids Res. 34 (Suppl. 1), D504–D506.
Bar-Joseph, Z., Gifford, D.K., Jaakkola, T.S., 2001. Fast optimal leaf ordering for hierarchical clustering. Bioinformatics 17 (Suppl. 1), S22.
Barabási, A.-L., 2009. Scale-free networks: a decade and beyond. Science 325 (5939), 412–413.
Barabási, A.-L., Oltvai, Z.N., 2004. Network biology: understanding the cell's functional organization. Nat. Rev. Genet. 5 (2), 101–113.
Barabási, A.-L., Gulbahce, N., Loscalzo, J., 2011. Network medicine: a network-based approach to human disease. Nat. Rev. Genet. 12 (1), 56–68.
Barla, A., Jurman, G., Riccadonna, S., Merler, S., Chierici, M., Furlanello, C., 2008. Machine learning methods for predictive proteomics. Brief. Bioinf. 9 (2), 119–128.
Bensimon, A., Heck, A.J., Aebersold, R., 2012. Mass spectrometry-based proteomics and network biology. Annu. Rev. Biochem. 81, 379–405.
Blagoev, B., Ong, S.-E., Kratchmarova, I., Mann, M., 2004. Temporal analysis of phosphotyrosine-dependent signaling networks by quantitative proteomics. Nat. Biotechnol. 22 (9), 1139–1145.
Chandran, U., Ma, C., Dhir, R., Bisceglia, M., Lyons-Weiler, M., Liang, W., Michalopoulos, G., Becich, M., Monzon, F., 2007. Gene expression profiles of prostate cancer reveal involvement of multiple molecular pathways in the metastatic process. BMC Cancer 7 (1), 64.
Chatr-aryamontri, A., Breitkreutz, B.-J., Heinicke, S., Boucher, L., Winter, A., Stark, C., Nixon, J., Ramage, L., Kolas, N., O'Donnell, L., 2013. The BioGRID interaction database: 2013 update. Nucleic Acids Res. 41 (D1), D816–D823.
Chen, J., Mamidipalli, S., Huan, T., 2009. HAPPI: an online database of comprehensive human annotated and predicted protein interactions. BMC Genomics 10 (Suppl. 1), S16.
Chen, J.Y., Yan, Z., Shen, C., Fitzpatrick, D.P., Wang, M., 2007. A systems biology approach to the study of cisplatin drug resistance in ovarian cancers. J. Bioinform. Comput. Biol. 5 (02a), 383–405.
Chowbina, S.R., Wu, X., Zhang, F., Li, P.M., Pandey, R., Kasamsetty, H.N., Chen, J.Y., 2009. HPD: an online integrated human pathway database enabling systems biology studies. BMC Bioinf. 10 (Suppl. 11), S5.
Chuang, H.-Y., Lee, E., Liu, Y.-T., Lee, D., Ideker, T., 2007. Network-based classification of breast cancer metastasis. Mol. Syst. Biol. 3, 1.
Colinge, J., Bennett, K.L., 2007. Introduction to computational proteomics. PLoS Comput. Biol. 3 (7), e114.
Culhane, A.C., Schwarzl, T., Sultana, R., Picard, K.C., Picard, S.C., Lu, T.H., Franklin, K. R., French, S.J., Papenhausen, G., Correll, M., et al., 2010. GeneSigDB—a curated database of gene expression signatures. Nucleic Acids Res. 38, D716–D725 (Database issue).
Dennis Jr, G., Sherman, B.T., Hosack, D.A., Yang, J., Gao, W., Lane, H.C., Lempicki, R.A., 2003. DAVID: database for annotation, visualization, and integrated discovery. Genome Biol. 4 (5), P3.
Dittrich, M.T., Klau, G.W., Rosenwald, A., Dandekar, T., Müller, T., 2008. Identifying functional modules in protein–protein interaction networks: an integrated exact approach. Bioinformatics 24 (13), i223–i231.
Dorigo, M., Birattari, M., 2010. Ant colony optimization, Encyclopedia of Machine Learning. Springer, pp. 36–39.

Draghici, S., Khatri, P., Tarca, A.L., Amin, K., Done, A., Voichita, C., Georgescu, C., Romero, R., 2007. A systems biology approach for pathway level analysis. Genome Res. 17 (10), 1537–1545.
Edelman, E.J., Guinney, J., Chi, J.-T., Febbo, P.G., Mukherjee, S., 2008. Modeling cancer progression via pathway dependencies. PLoS Comput. Biol. 4 (2), e28.
Elias, J.E., Gibbons, F.D., King, O.D., Roth, F.P., Gygi, S.P., 2004. Intensity-based protein identification by machine learning from a library of tandem mass spectra. Nat. Biotechnol. 22 (2), 214–219.
Franceschini, A., Szklarczyk, D., Frankild, S., Kuhn, M., Simonovic, M., Roth, A., Lin, J., Minguez, P., Bork, P., von Mering, C., 2013. STRING v9. 1: protein–protein interaction networks, with increased coverage and integration. Nucleic Acids Res. 41 (D1), D808–D815.
Goh, W.W., Lee, Y.H., Chung, M., Wong, L., 2012. How advancement in biological network analysis methods empowers proteomics. Proteomics 12 (4–5), 550–563.
Goh, W.W.B., Wong, L., 2013. Networks in proteomics analysis of cancer. Curr. Opin. Biotechnol..
Hartwell, L.H., Hopfield, J.J., Leibler, S., Murray, A.W., 1999. From molecular to modular cell biology. Nature 402 (6761 Suppl.), C47–C52.
He, J., Li, C., Ye, B., Zhong, W., 2012. Efficient and accurate greedy search methods for mining functional modules in protein interaction networks. BMC Bioinf. 13 (Suppl. 10), S19.
Huang, H., Wu, X., Sonachalam, M., Mandape, S.N., Pandey, R., MacDorman, K.F., Wan, P., Chen, J.Y., 2012. PAGED: a pathway and gene-set enrichment database to enable molecular phenotype discoveries. BMC Bioinf. 13 (Suppl. 15), S2.
Huang, H., Wu, X., Sonachalam, M., Mandape, S.N., Pandey, R., MacDorman, K.F., Wan, P., Chen, J.Y., 2012. PAGED: a pathway and gene-set enrichment database to enable molecular phenotype discoveries. BMC Bioinf. 13 (Suppl. 15), S2.
Ideker, T., Thorsson, V., Ranish, J.A., Christmas, R., Buhler, J., Eng, J.K., Bumgarner, R., Goodlett, D.R., Aebersold, R., Hood, L., 2001. Integrated genomic and proteomic analyses of a systematically perturbed metabolic network. Science 292 (5518), 929–934.
Ito, T., Chiba, T., Ozawa, R., Yoshida, M., Hattori, M., Sakaki, Y., 2001. A comprehensive two-hybrid analysis to explore the yeast protein interactome. Proc. Nat. Acad. Sci. 98 (8), 4569–4574.
Käll, L., Canterbury, J.D., Weston, J., Noble, W.S., MacCoss, M.J., 2007. Semi-supervised learning for peptide identification from shotgun proteomics datasets. Nat. Methods 4 (11), 923–925.
Kanehisa, M., Goto, S., 2000. KEGG: kyoto encyclopedia of genes and genomes. Nucleic Acids Res. 28 (1), 27–30.
Khatri, P., Sirota, M., Butte, A.J., 2012. Ten years of pathway analysis: current approaches and outstanding challenges. PLoS Comput. Biol. 8 (2), e1002375.
Kim, S.K., Lund, J., Kiraly, M., Duke, K., Jiang, M., Stuart, J.M., Eizinger, A., Wylie, B.N., Davidson, G.S., 2001. A gene expression map for Caenorhabditis elegans. Science 293 (5537), 2087–2092.
Kingsmore, S.F., 2006. Multiplexed protein measurement: technologies and applications of protein and antibody arrays. Nat. Rev. Drug Discovery 5 (4), 310–321.
Krogan, N.J., Cagney, G., Yu, H., Zhong, G., Guo, X., Ignatchenko, A., Li, J., Pu, S., Datta, N., Tikuisis, A.P., 2006. Global landscape of protein complexes in the yeast *Saccharomyces cerevisiae*. Nature 440 (7084), 637–643.
Lee, E., Chuang, H.-Y., Kim, J.-W., Ideker, T., Lee, D., 2008. Inferring pathway activity toward precise disease classification. PLoS Comput. Biol. 4 (11), e1000217.
Li, Y., Agarwal, P., Rajagopalan, D., 2008. A global pathway crosstalk network. Bioinformatics 24 (12), 1442–1447.
Liberzon, A., Subramanian, A., Pinchback, R., Thorvaldsdóttir, H., Tamayo, P., Mesirov, J.P., 2011. Molecular signatures database (MSigDB) 3.0. Bioinformatics 27 (12), 1739–1740.
Liu, Z.-P., Wang, Y., Zhang, X.-S., Chen, L., 2010. Identifying dysfunctional crosstalk of pathways in various regions of Alzheimer's disease brains. BMC Syst. Biol. 4 (Suppl. 2), S11.
MacBeath, G., 2002. Protein microarrays and proteomics. Nat. Genet. 32, 526–532.
Matthews, L., Gopinath, G., Gillespie, M., Caudy, M., Croft, D., de Bono, B., Garapati, P., Hemish, J., Hermjakob, H., Jassal, B., 2009. Reactome knowledgebase of human biological pathways and processes. Nucleic Acids Res. 37 (Suppl. 1), D619–D622.
Morrison, J.L., Breitling, R., Higham, D.J., Gilbert, D.R., 2005. GeneRank: using search engine technology for the analysis of microarray experiments. BMC Bioinf. 6 (1), 233.
Nishimura, D., 2001. BioCarta. Biotech. Softw. Internet Rep.: Comput. Softw. J. Sci. 2 (3), 117–120.
Noble, W.S., MacCoss, M.J., 2012. Computational and statistical analysis of protein mass spectrometry data. PLoS Comput. Biol. 8 (1), e1002296.
Ong, S.-E., Mann, M., 2005. Mass spectrometry–based proteomics turns quantitative. Nat. Chem. Biol. 1 (5), 252–262.
Parikh, J.R., Xia, Y., Marto, J.A., Multi-Edge Gene, S.E.T., 2012. Networks reveal novel insights into global relationships between biological themes. PLoS One 7 (9), e45211.
Pereira-Leal, J.B., Enright, A.J., Ouzounis, C.A., 2004. Detection of functional modules from protein interaction networks. Proteins: Struct., Funct. Bioinf. 54 (1), 49–57.
Pradhan, M.P., Nagulapalli, K., Palakal, M.J., 2012. Cliques for the identification of gene signatures for colorectal cancer across population. BMC Syst. Biol. 6 (Suppl. 3), S17.
Ramanan, V.K., Shen, L., Moore, J.H., Saykin, A.J., 2012. Pathway analysis of genomic data: concepts, methods, and prospects for future development. Trends Genet. 28 (7), 323–332.
Ren, X., Wang, Y., Chen, L., Zhang, X.-S., Jin, Q., 2013. ellipsoidFN: a tool for identifying a heterogeneous set of cancer biomarkers based on gene expressions. Nucleic Acids Res. 41 (4), e53 (e53).
Ressom, H.W., Varghese, R.S., Drake, S.K., Hortin, G.L., Abdel-Hamid, M., Loffredo, C.A., Goldman, R., 2007. Peak selection from MALDI-TOF mass spectra using ant colony optimization. Bioinformatics 23 (5), 619–626.
Roeßler, M., Rollinger, W., Palme, S., Hagmann, M.-L., Berndt, P., Engel, A.M., Schneidinger, B., Pfeffer, M., Andres, H., Karl, J., 2005. Identification of nicotinamide *N*-methyltransferase as a novel serum tumor marker for colorectal cancer. Clin. Cancer Res. 11 (18), 6550–6557.
Sabidó, E., Selevsek, N., Aebersold, R., 2012. Mass spectrometry-based proteomics for systems biology. Curr. Opin. Biotechnol. 23 (4), 591–597.
Schaefer, C.F., Anthony, K., Krupa, S., Buchoff, J., Day, M., Hannay, T., Buetow, K.H., 2009. PID: the pathway interaction database. Nucleic Acids Res. 37 (Suppl. 1), D674–D679.
Shannon, P., Markiel, A., Ozier, O., Baliga, N.S., Wang, J.T., Ramage, D., Amin, N., Schwikowski, B., Ideker, T., 2003. Cytoscape: a software environment for integrated models of biomolecular interaction networks. Genome Res. 13 (11), 2498–2504.
Sherman, B.T., Lempicki, R.A., 2009. Bioinformatics enrichment tools: paths toward the comprehensive functional analysis of large gene lists. Nucleic Acids Res. 37 (1), 1–13.
Staiger, C., Cadot, S., Kooter, R., Dittrich, M., Müller, T., Klau, G.W., Wessels, L.F., 2012. A critical evaluation of network and pathway-based classifiers for outcome prediction in breast cancer. PLoS One 7 (4), e34796.
Strogatz, S.H., 2001. Exploring complex networks. Nature 410 (6825), 268–276.
Subramanian, A., Tamayo, P., Mootha, V.K., Mukherjee, S., Ebert, B.L., Gillette, M.A., Paulovich, A., Pomeroy, S.L., Golub, T.R., Lander, E.S., 2005. Gene set enrichment analysis: a knowledge-based approach for interpreting genome-wide expression profiles. Proc. Nat. Acad. Sci. U.S.A. 102 (43), 15545–15550.
Tarca, A.L., Draghici, S., Khatri, P., Hassan, S.S., Mittal, P., Kim, J.-S., Kim, C.J., Kusanovic, J.P., Romero, R., 2009. A novel signaling pathway impact analysis. Bioinformatics 25 (1), 75–82.
Taylor, I.W., Linding, R., Warde-Farley, D., Liu, Y., Pesquita, C., Faria, D., Bull, S., Pawson, T., Morris, Q., Wrana, J.L., 2009. Dynamic modularity in protein interaction networks predicts breast cancer outcome. Nat. Biotechnol. 27 (2), 199–204.
Vitek, O., 2009. Getting started in computational mass spectrometry–based proteomics. PLoS Comput. Biol. 5 (5), e1000366.
Wang, J., Huang, Q., Liu, Z.-P., Wang, Y., Wu, L.-Y., Chen, L., Zhang, X.-S., 2011. NOA: a novel network ontology analysis method. Nucleic Acids Res. 39 (13), e87 (e87).
Wang, Y., Wu, Q.-F., Chen, C., Wu, L.-Y., Yan, X.-Z., Yu, S.-G., Zhang, X.-S., Liang, F.-R., 2012. Revealing metabolite biomarkers for acupuncture treatment by linear programming based feature selection. BMC Syst. Biol. 6 (Suppl. 1), S15.
Wingender, E., Chen, X., Hehl, R., Karas, H., Liebich, I., Matys, V., Meinhardt, T., Prüß, M., Reuter, I., Schacherer, F., 2000. TRANSFAC: an integrated system for gene expression regulation. Nucleic Acids Res. 28 (1), 316–319.
Wu, X., Chen, J.Y., 2009. Molecular interaction networks: topological and functional characterizations. In: Alterovitz, G., Benson, R., Ramoni, M. (Eds.), Automation in Proteomics and Genomics: An Engineering Case-Based Approach. Wiley.
Wu X., Chen J.Y.2012. An evaluation for merging signaling pathways by using protein–protein interaction data. In: IEEE International Workshop on Genomic Signal Processing and Statistics,(GENSIPS), 2012. pp. 203–206.
Wu X., Pandey R., Chen J.Y., 2009a. Network topological reordering revealing systemic patterns in yeast protein interaction networks. In: IEEE Annual International Conference of the Engineering in Medicine and Biology Society (EMBC), 2009, pp. 6954–6957.
Wu, X., Harrison, S.H., Chen, J.Y., 2009b. Pattern discovery in breast cancer specific protein interaction network. Summit Trans. Bioinf. 2009, 1.
Wu, X., Huan, T., Pandey, R., Zhou, T., 2009c. Finding fractal patterns in molecular interaction networks: a case study in Alzheimer's disease. Int. J. Comput. Biol. Drug Des. 2 (4), 340–352.
Wu, X., Huang, H., Sonachalam, M., Reinhard, S., Shen, J., Pandey, R., Chen, J.Y., 2012. Reordering based integrative expression profiling for microarray classification. BMC Bioinf. 13 (Suppl. 2), S1.
Yokota, T., Ura, T., Shibata, N., Takahari, D., Shitara, K., Nomura, M., Kondo, C., Mizota, A., Utsunomiya, S., Muro, K., 2011. BRAF mutation is a powerful prognostic factor in advanced and recurrent colorectal cancer. Br. J. Cancer 104 (5), 856–862.
You, Q., Fang, S., Chen, J.Y., 2010. GeneTerrain: visual exploration of differential gene expression profiles organized in native biomolecular interaction networks. Inf. Visual. 9 (1), 1–12.
Yu, Y.P., Landsittel, D., Jing, L., Nelson, J., Ren, B., Liu, L., McDonald, C., Thomas, R., Dhir, R., Finkelstein, S., 2004. Gene expression alterations in prostate cancer predicting tumor aggression and preceding development of malignancy. J. Clin. Oncol. 22 (14), 2790.
Zeeberg, B.R., Feng, W., Wang, G., Wang, M.D., Fojo, A.T., Sunshine, M., Narasimhan, S., Kane, D.W., Reinhold, W.C., Lababidi, S., 2003. GoMiner: a resource for biological interpretation of genomic and proteomic data. Genome Biol. 4 (4), R28.
Zhang, F., Chen, J., 2010. Discovery of pathway biomarkers from coupled proteomics and systems biology methods. BMC Genomics 11 (Suppl. 2), S12.
Zhang, F., Chen, J.Y., 2013. Breast cancer subtyping from plasma proteins. BMC Med. Genet. 6 (Suppl. 1), S6.

J Appl Physiol 120: 297–309, 2016.
First published November 5, 2015; doi:10.1152/japplphysiol.01110.2014.

Synthesis Review

Multilevel functional genomics data integration as a tool for understanding physiology: a network biology perspective

Peter K. Davidsen,[1] Nil Turan,[2] Stuart Egginton,[3] and Francesco Falciani[1]

[1]*Institute of Integrative Biology, University of Liverpool, Liverpool, United Kingdom;* [2]*School of Biosciences, University of Birmingham, Birmingham, United Kingdom; and* [3]*School of Biomedical Sciences, Faculty of Biological Sciences, University of Leeds, Leeds, United Kingdom*

Submitted 17 December 2014; accepted in final form 4 November 2015

Davidsen PK, Turan N, Egginton S, Falciani F. Multilevel functional genomics data integration as a tool for understanding physiology: a network biology perspective. *J Appl Physiol* 120: 297–309, 2016. First published November 5, 2015; doi:10.1152/japplphysiol.01110.2014.—The overall aim of physiological research is to understand how living systems function in an integrative manner. Consequently, the discipline of physiology has since its infancy attempted to link multiple levels of biological organization. Increasingly this has involved mathematical and computational approaches, typically to model a small number of components spanning several levels of biological organization. With the advent of "omics" technologies, which can characterize the molecular state of a cell or tissue (intended as the level of expression and/or activity of its molecular components), the number of molecular components we can quantify has increased exponentially. Paradoxically, the unprecedented amount of experimental data has made it more difficult to derive conceptual models underlying essential mechanisms regulating mammalian physiology. We present an overview of state-of-the-art methods currently used to identifying biological networks underlying genomewide responses. These are based on a data-driven approach that relies on advanced computational methods designed to "learn" biology from observational data. In this review, we illustrate an application of these computational methodologies using a case study integrating an in vivo model representing the transcriptional state of hypoxic skeletal muscle with a clinical study representing muscle wasting in chronic obstructive pulmonary disease patients. The broader application of these approaches to modeling multiple levels of biological data in the context of modern physiology is discussed.

systems biology; data integration; genomics

MODELING IN PHYSIOLOGICAL SCIENCES

PHYSIOLOGY HAS EVOLVED AS a series of subdisciplines attempting to understand organismal function as a combination of interacting components and systems. The last decade or so has witnessed the development of systems biology as an investigative approach and its application in different areas of biology, ranging from engineering/synthetic biology (e.g., design of bacterial strains with improved properties) to health sciences (e.g., disease biomarker identification). Despite the lack of a concise definition acceptable to the majority of the community (30, 32), systems biology is frequently understood to be the study of complex regulatory interactions in biological systems using a holistic approach. This is often achieved by integrating different experimental approaches within the conceptual framework of a computational model (i.e. a mathematical representation of a system that allows simulation of its behavior). Physiology is probably one of the few research areas in biological sciences that has traditionally adopted such an approach. It has long sought to understand the behavior of complex biological processes and cellular systems using an integrative approach and has extensively adopted mathematical modeling in its tool set. Classical examples include August Krogh's tissue cylinder model of oxygen transport to skeletal muscle (34j), and Huxley's two-state cross-bridge model of muscle contraction (26), which are still used by investigators today. Indeed, this shows that using modeling to study a system as a whole has been a key component of physiology from its early days.

As often happens when a distinct discipline branches out of another, there developed over time a separation of ideas based in part on confusion arising from use of esoteric terminology, similar concepts masked by unfamiliar language. There is, therefore, a need for an overview of this relatively new discipline, to both emphasize the essential links with basic physiological principles and demystify the approach such that the available tools may become more widely adopted in physiological research. The overall aim of this opinion-based review is to describe, using concepts that will be intuitive to physiology researchers, different key methodologies available from the systems biology community. In addition, we provide a practical step-by-step guide for integrating multilevel data

Address for reprint requests and other correspondence: F. Falciani, Centre for Computational Biology and Modelling, Institute for Integrative Biology, Univ. of Liverpool, Crown St., Liverpool L69 7ZB, UK (e-mail: f.falciani@liverpool.ac.uk).

within an analysis pipeline based around inferred interactions of variables, modeled as a network based on statistical correlations, using a worked example in the field of physiological sciences.

THE ADVENT OF FUNCTIONAL GENOMICS: A CHALLENGE FOR PHYSIOLOGICAL MODELING

It is now clear that much of the complex mammalian physiology or pathophysiology cannot be understood in sufficient detail through a reductionist approach alone. Although this approach has proved valuable in explaining broad phenomena and individual mechanisms, linking multiple mechanisms and effects has proved challenging. For example, a disease phenotype is rarely caused by a single dysfunctional gene or protein. Instead, genetic variability, epigenetic modifications, posttranscriptional regulation mechanisms, etc., all act in concert to determine a specific high-level phenotypic response (43). The potential for such complex interaction makes data interpretation much more complicated than originally envisioned, highlighting the need to move away from the widespread "candidate gene" approach (39).

Triggered by the advent of genome sequencing, inspired by the Human Genome Project, dramatic technological advances within the last decade or so have led to increased throughput in genomewide molecular analyses (i.e., genomics, epigenomics, transcriptomics, proteomics, metabolomics). The comprehensive data acquisition tools developed to cope with large datasets have allowed investigators to determine the molecular state of cells, tissues, or even entire organs in a single experiment. Such cost-effective omics approaches are now becoming prevalent in biological and medical research and, consequently, have been responsible for the generation of an incredibly large amount of multivariate molecular data. A large proportion of this data is available in the public domain via different online databases [e.g., NCBI Gene Expression Omnibus (5), EBI ArrayExpress (7), and PRIDE (29)].

For example, mRNA microarray technology and more recently mRNA sequencing has provided insight into the transcriptional response of skeletal muscle to prolonged endurance exercise training, highlighting a pronounced interindividual variation at the molecular level that is consistent with the heterogeneous response observed in a population of individuals at the physiology level (31, 59). Statistical models built to explain such variation as a function of gene expression data can be exploited to identify underlying mechanisms controlling tissue homeostasis. The transcriptional signatures identified in such studies likely explain, at least in part, why some people show great improvements in aerobic capacity [maximum O_2 uptake ($\dot{V}O_{2max}$)], whereas others only experience smaller benefits, despite completing the same supervised exercise training program. Another example of applying omics technology to better understand human physiology concerns the quantification of individual levels of different proteins in health and disease; by use of proteomics methodology, Holloway et al. (24) were the first to investigate adaptations in human muscle protein content to long-term exercise training on a large scale.

While such omics-based studies hint at the potential of a data-driven approach, they also illustrate the difficulty in deriving conceptual models underlying the essential mechanisms regulating physiology, as most are restricted to only one aspect of regulation. Perhaps surprisingly, the exponential growth in publicly available omics data (35, 37) has not resulted in a paradigm shift in our understanding of biology. The main reason is the continuing challenge of integrating multivariate datasets spanning multiple organization levels in a way that allows the identification of discrete, small biomolecular networks that are truly important in the context of a specific biological response (47). Such a task cannot be achieved simply using unaided human interpretation. Rather, complex computational techniques are needed that are able to integrate and automatically "learn" the structure of a biological system. Such a modeling framework is very different from what physiological sciences have traditionally employed.

TOWARD DATA-DRIVEN PREDICTIVE BIOLOGY

Although the modeling approach traditionally used by physiologists has been extremely successful, it suffers from severe limitations when challenged with extensive omics data. For example, physiological modeling relies to various degrees on a mechanistic understanding of the biological system of interest (16), which automatically limits the number of components that can be included due to gaps in our current knowledge (19, 47). Moreover, estimation of model parameters, which is usually a challenging task because of experimental limitations (e.g., due to limited amount and quality of data), makes the approach difficult to scale up to a larger number of components and their interactions. Perhaps the most comprehensive example to date is modeling the cardiac cycle based on ion channel kinetics (44).

With such large multivariate datasets, and little knowledge about the way biomolecules are connected with each other and to key phenotypic switches, the fundamental question is whether or not we can "learn" the structure of biological interaction networks from high-throughput data. Clearly, there is a need for sophisticated computational tools that are able to *1*) integrate genomewide measurements spanning multiple levels of biological organization (ranging from subcellular to organ level); *2*) identify key biomolecular components of the system; and finally *3*) statistically infer the way that these biomolecules interact in a pairwise manner to generate an observed biological response.

Central to these approaches is the concept of interaction networks, a mathematical representation of a system of biomolecules. Networks are commonly used to describe biological systems at different levels of complexity (e.g., metabolic and signal transduction networks). They can be descriptive models built using a wide spectrum of qualitative data (e.g., biological knowledge of protein-protein interactions, transcription factor binding, etc.), or they can be inferred from quantitative measurements using complex computational models. In this case, they can be used to predict the behavior of the system when perturbed.

In the following section, we summarize specific methodologies that can be applied to achieve such tasks.

COMPUTATIONAL APPROACHES FOR THE ANALYSIS OF COMPLEX DATASETS

The process of modeling a biological system from complex multilevel datasets can, for the sake of convenience, be divided

into four conceptually distinct yet interconnected approaches (Fig. 1).

The first approach is biomarker discovery (Fig. 1*A*), which perhaps is most widely used in the analysis of functional genomics datasets. Here the objective is to identify measurable variables that are predictive of a given outcome (e.g., the response to physical training in a population of individuals). Such measurements can be molecular (e.g., gene expression, protein levels, metabolite concentrations, genetic mutations) and/or more traditional physiological endpoints (e.g., endurance, $\dot{V}O_{2max}$). The identification of predictive biomarkers can be achieved by use of univariate and multivariate variable selection strategies that aim to identify the most relevant explanatory measurement(s), while developing a computational model that can accurately predict an outcome (60). Univariate methods will test every variable (e.g., expression of a given gene) on its own, whereas multivariate methods test combinations of variables for their ability to explain a given outcome. Clearly, multivariate approaches better resemble the complex nature of biological networks and, therefore, are more likely to provide insights into the mechanisms underlying a complex phenotypic trait. Consistent with this notion, multigene biomarkers are often required for robust predictions in independent datasets.

The second approach (Fig. 1*B*) consists of "reverse engineering" biomolecular networks from observational data (i.e., infer regulatory interactions between quantified biomolecules based on mathematical principles). Here the overall aim is to reconstruct the underlying structure of interactions between biological molecules profiled using omics tools (ideally from multiple data sources) and rigorous statistics. Such a network inference framework can be achieved by applying a multitude of approaches with varying underlying data assumptions and modeling principles, including ordinary differential equation-based methods (3), probabilistic modeling techniques (e.g., Bayesian theory models) (42, 64), state-space representation models (23), and correlation-based methods. Note, while the first three approaches are able to infer directed networks, their capability is currently limited to inferring smaller networks with few variables due to increased computational complexity than possible with correlation approaches.

Importantly, this network inference part may potentially benefit from a biomarker discovery phase, since it has been shown that identified predictive variables are more likely to be directly controlling important physiological processes and, therefore, are good candidates to include in a network (47). Similarly, whole networks can be used as an input for biomarker discovery procedures. It has been shown that often the overall "activity" of a biological network (e.g., a specific signaling pathway) is a better predictor than a few key individual genes, proteins, and/or metabolites. This implies that, in the coming years, predictive biomarkers are more likely to consist of a relatively large panel of measurements, possibly spanning multiple levels of complexity within a pathway. Current omics platforms are experiencing a rapid development, as well as drop in costs, making routine collection of large datasets a feasible option. Once a robust biological network has been inferred, this may serve as a good basis for developing a more conventional modeling approach to provide explanations for observed phenomena that requires a mechanistic understanding of the system (Fig. 1*C*).

Finally, multiple computational models that initially were developed independently can be integrated into larger and more complex models, which allow responses to physiological/pathological challenges to be simulated, thus integrating effects across multiple organs and/or pathways. These complex

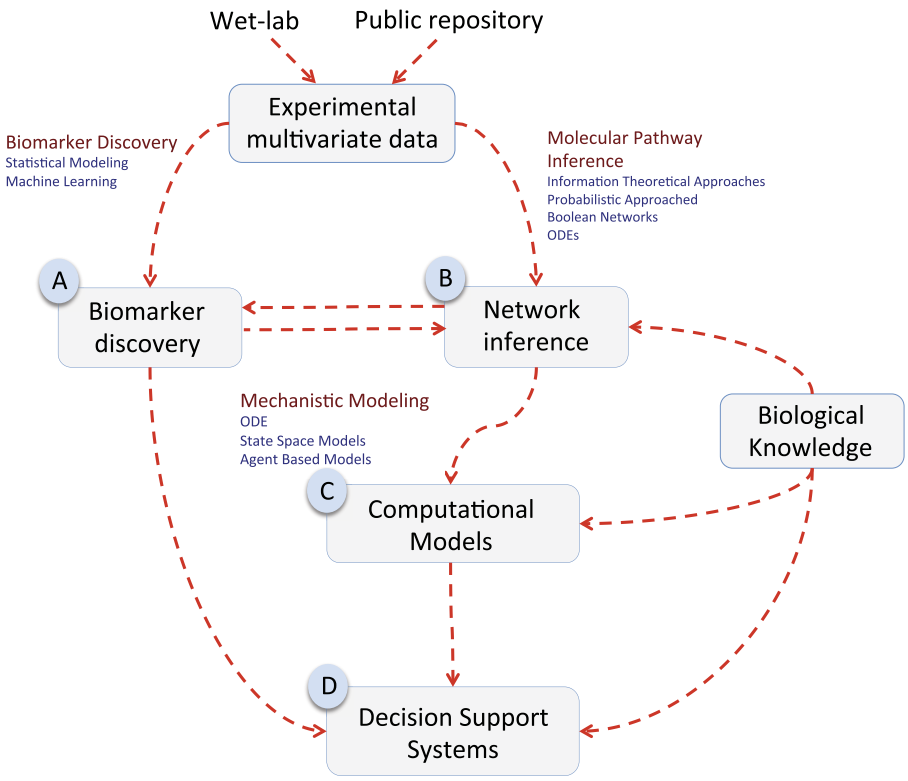

Fig. 1. Schematic representation of the process involved in modeling a biological system by integrating knowledge from various sources, and complex multilevel datasets. The process can be conceptually subdivided into four distinct yet interconnected approaches (*A–D*). The experimental data used can either be novel multivariate data generated in your own (wet) laboratory, or taken from a public repository. These may then be used to identify predictive biomarkers, i.e., variables that are predictive of a defined outcome (e.g., response to exercise training), and also to inform development of important networks that infer such outcomes; experimental data and other source of biological knowledge may also be useful in refining these representations of complex interactions. Such networks may in turn aid biomarker discovery, but are an essential precursor to computational models that are able to explore underlying molecular mechanisms; again, knowledge of specific biological issues may help in their refinement. Finally, incorporation of these models into larger scale analyses offer the potential for in silico experimentation, whereby, e.g., the effect of different therapeutic interventions on disease outcome may be tested.

models are often referred to as decision support systems because of their potential to provide information about the expected outcome of a therapeutic intervention (Fig. 1*D*).

Several large international projects aiming at the development of such technology into systems medicine integrated frameworks have been established so far, e.g., the Virtual Physiological Human project funded by the European Commission 7th Framework Programme, which aims to aid clinically relevant research by establishing a framework for handling and integrating various mechanistic models spanning different levels of organizational complexity (ranging from molecular components to organ function). By unifying the modeling languages employed across the different mathematical models included, parameters of a particular model in the hierarchy can be processed by other appropriate models at a lower hierarchical level. These global initiatives should be considered long-term goals, aiming at understanding human physiology quantitatively as a dynamic system.

Developing a comprehensive model of a biological system requires integrating mechanistic and probabilistic inferences. The mathematics for performing such a task is in its infancy, and more development is needed. However, a successful example is illustrated by the anatomically based model of human heart ventricles (44). In the following sections, we aim to provide an overview of some of the methodologies that can be used to infer biomolecular networks, as well as introduce one particular approach we have found useful in our research.

Inference of Biological Networks from Observational Data

Reverse engineering is an evolving field within network-based systems biology. The rapid accumulation of omics data in the postgenomic era has made it possible to infer (a.k.a., "reverse engineer") models of cellular systems with the overall aim of deducing the regulatory structure at a subcellular level. Most of the network-based approaches that have been developed are in fact general and can be applied to any type of experimental data. However, because the mRNA expression profiling technology is the most mature omics discipline, most applications have been developed to reconstruct transcriptional networks (i.e., decode the mechanisms of transcriptional control). However, recently it has become apparent that, irrespective of the methodology used to generate data, to be able to recapitulate the complex behavior of a biological system, it is essential to integrate multiple types and scales of experimental data (e.g., transcriptomic, proteomic, metabolomic).

Static vs. Dynamic Networks

Biological networks can be reconstructed from two different types of experimental studies: either cross-sectional, e.g., representing a population of individuals at a given time (i.e., steady-state measurements following an experimental perturbation), or prospective, where the experimental data are available across a defined time course. In reverse engineering, statistical inference of biological causality is an important goal (10a). A simple example of causality could, for example, be a transcription factor regulating the expression of several target genes. Since determining cause and effects implies a direction (i.e., the cause precedes the effect), inference of causality from cross-sectional studies presents a challenge due to their static nature, one that is less difficult when a time course is available. However, it must be stressed that both approaches are often used in combination to, for example, integrate clinical cross-sectional studies (thereby providing the researcher with a static network representation) and experimental intervention studies that can provide dynamic (prospective) models of the process being studied. At present, most of the developed techniques infer regulatory networks without any causality information (likely due to the scarcity of time course datasets due to their higher costs). However, a small number of causality detection techniques have been proposed in the literature, such as dynamic Bayesian networks (48) and Granger causality (46). It is also important to point out that true time course datasets can only be developed when the sequence of events is measured within the same cells/tissues. This is, for example, achieved with imaging techniques that require complex molecular probes and can typically be only applied to measure a relatively small number of system components (14). Omics technologies unfortunately are disruptive, so time course data derived using these approaches are in fact a sequence of independent snapshots, which clearly limits the potential use of dynamic modeling tools.

A Primer for Network Inference Methods

The simplest method for inferring statistical relationships between experimental variables is computing the pairwise correlation coefficient across a large collection of heterogeneous samples (8). Usually such an approach is not able to identify complex nonlinear dependencies and does not discriminate between direct and indirect connections. More complex methods, such as the mutual information (MI) based ARACNE (Algorithm for the Reconstruction of Accurate Cellular Networks) (38), also aim at establishing a statistical relationship between pairs of variables but have a stronger theoretical foundation. Because of the added mathematical complexity, they can capture a broader range of biologically relevant dependencies between variables, including nonlinear, nonmonotonic relationships; importantly, they can distinguish between direct and indirect relationships. ARACNE is a free tool for which a Java-based graphical user interface exists; hence investigators do not need any programming skills to use the software.

ARACNE relies on estimating the probability that a variable (e.g., the expression of a gene or a protein) assumes a certain "state" (i.e., abundance), given the state of another biomolecule (conditional probability). A number of alternative MI-based implementations have been proposed during the last decade [e.g., context likelihood relatedness (13), minimum redundancy/maximum relevance networks (41)], which mainly differ by the way inferred indirect relationships (so-called "edges") are removed once the dependencies between all pairs of variables have been mathematically formulated. In such analyses, unwanted indirect interactions occur by default if there is strong correlation between *biomolecule 1* and *biomolecule 2*, and between *biomolecule 1* and *biomolecule 3* in a three-node clique (i.e., a triplet of connected variables).

An MI value of zero means that there is no dependency (i.e., no information flow) between two variables, whereas an MI value of 1 indicates a perfect association between them, and, therefore, a likely strong regulatory interaction between them. For each inferred dependency, a *P* value is calculated based on

the distribution of MI values between random permutations of the original dataset, thereby allowing the elimination of all nonstatistically relevant dependencies by thresholding using an appropriate (user-defined) cutoff level. Importantly, the quality of the inferred interaction network depends on the arbitrarily selected probability cutoff. A small threshold (e.g., $P = 0.05$) gives a high recall (i.e., fraction of true dependencies that could be inferred) but low precision, whereas a higher threshold (e.g., $P = 10^{-6}$) yields better precision (i.e., fraction of inferred dependencies that really are in the network), while suffering from a low recall. A further advantage of MI as an information-theoretical measure of dependency between variables concerns its relatively low computational requirements for building an interaction network. Hence, MI is able to handle very large data matrixes with thousands of experimental variables, whereas most of the other more advanced techniques mentioned (e.g., Bayesian methods) can only deal with much smaller numbers of variables ($<$100) because of the high computational complexity. However, to infer robust statistical associations based on MI, a fairly large sample size is required ($>$50-100 biological replicates), due to the required estimation of the (joint) frequency distribution of the connectivity. Interaction networks derived from such reverse engineering methodologies can be visualized and further analyzed using various freeware software tools, such as Cytoscape (55), Pajak (6), and BioLayout (18). A comprehensive list of visualization tools focused on interaction networks and their web-links has recently been reviewed (17).

Up to now, these information-theoretic approaches have usually been employed on gene expression data only, due to the wealth of such data available. However, as physiologists have known for many decades, biological systems are usually more complex and multilayered. Indeed, despite some popularist science writing to the contrary, genes on their own are merely permissive elements within biological systems (43). Furthermore, it has been shown that, when multiple types of data (e.g., copy number variants, protein, or microRNA expression levels) are incorporated in the network inference pipeline, the accuracy of the learned network topology increases (49). Hence, at present there is a call for methodologies that can embed multiple data sources in a single computational framework. Our recent work has focused on methods that are able to handle large-scale, multidimensional genomic datasets (9, 21).

Topological Analysis of Inferred Biological Networks Provides Useful Biological Insight

Up to now, we have described some of the most widely used methodologies for inferring regulatory networks. However, an immediate challenge arises in interpreting these often large, complex networks that visually present as a "hairball" (i.e., too dense a collection of connections to comprehend as a whole) (40). A simple solution, although not very objective, is to focus the analysis around a favorite gene(s). In this scenario, the investigator typically examines the manually selected subnetwork to identify unknown or unexpected biological relationships, which in turn may be used to formulate new hypotheses. Such "discovery-led" science may be useful when there is insufficient information to generate hypothesis.

Alternatively, the topological properties of the network can be used to identify interesting genes and subnetworks that can be interpreted. We and others have demonstrated the existence of a higher-level, modular organization in biological networks (47, 52, 54), i.e., components of biological systems that act in collaboration to carry out specific biological processes. Consequently, several modularization approaches have now been developed to help group subsets of cellular components based on a given property, such as topological structure or functional role. Such decomposition of a large complex network into relatively independent subnetworks (or "modules") has been shown to be an effective way to deduce the underlying structure of the fully connected network containing many hundred variables (so-called "nodes"), as each module can then be analyzed independently. In addition, studies have demonstrated that such identified network modules can serve as better predictors of a physiological response than the classic biomarker discovery approach (see Fig. 1).

In biomolecular interaction networks, as well as subnetworks, nodes have different levels of connectivity (i.e., number of interactions with other nodes). It has been shown that such interaction networks have so-called "scale-free" structure properties, as their node connectivity distribution fits a power law (4). Such a power law degree distribution implies that most of the connections between biomolecules is linked to a small number of highly connected nodes, such that a large proportion of the molecular state of a cell can be explained by a small subset of biomolecules (so-called "hub" nodes; e.g., a transcription factor that regulates many more genes than average). Hence, in biological networks a hub is often assumed to be a key component of a regulatory networks, hence important for the function of a cell/tissue under investigation. This assumption is supported by the fact that random node disruption does not significantly affect the network architecture, whereas deletion of hub nodes leads to a complete breakdown of the network structure (1). Hence, adjusting the spatial position of each node according to its interconnectivity has been shown to be a simple, yet effective way of visualizing large complex interaction networks (57).

More advanced methods to extract information from complex networks exist that aim to identify functional modules (i.e., subnetworks of biomolecules that are linked to the same biological function), e.g., by integrating both physical interactions (i.e., experimentally validated protein-protein interactions) and mRNA expression data (27). In this context, an identified functional module represents a putative multiprotein complex that is transcriptionally regulated in a specific experimental condition (e.g., treatment vs. control). Hence, by considering additional data on a different level of organization, one can potentially infer a clearer composite picture of the underlying biological function.

Finally, to generate objective hypotheses about biological processes controlled by a specific hub node or subnetwork, functional enrichment analysis can be performed on all of its direct neighbors (i.e., all of the adjacent nodes that are directly connected to the hub) (25). Such enrichment analysis aims at reducing complexity by defining groups of molecules (represented by gene sets) that share similar biological functions (e.g., a class of adhesion molecules). To accommodate the latest advances in knowledge, the different annotation databases used for this purpose [e.g., gene ontology (GO) (2) and

KEGG (Kyoto Encyclopedia of Genes and Genomes) (45)] are frequently updated by curators. Using software tools like the web-based application DAVID (Database for Annotation, Visualization, and Integrated Discovery) (11) or applications such as BiNGO (36) developed specifically for use with software visualization tools like Cytoscape, one can quickly determine whether any gene sets are statistically over-represented, thus generating hypotheses on the biological processes controlled by those factors outlined above.

CASE STUDY: INFERENCE OF OXYGEN-DEPENDENT PATHWAYS IN SKELETAL MUSCLE

The main purpose of this case study is to illustrate in a step-by-step manner the application of reverse engineering to integrate supracellular physiological measures and genome-wide expression profiling. From a more biological perspective, we aim to identify a clinically relevant signature of hypoxia in skeletal muscles.

This analysis uses two different datasets. The first is a publicly available dataset (GSE27536) representing a cohort of chronic obstructive pulmonary disease (COPD) patients and healthy controls matched for age and smoking history (10) (see Table 1 for subject characteristics), which includes gene expression profiling in vastus lateralis muscle and whole body physiological variables [e.g., $\dot{V}O_{2max}$, minute ventilation, arterial oxygen tension (Pa_{O_2})] (50, 61). The second dataset represents an unpublished, genomewide transcriptional response of mouse soleus muscle to a gradual decline in atmospheric oxygen concentration (GSE64076).

Using the first dataset, representing the transcriptional state of skeletal muscles in a COPD cohort (Fig. 2*A*), we first show how to infer connections between oxygen availability (e.g., $\dot{V}O_{2max}$), oxidative stress (protein carbonylation), and gene expression signatures (Fig. 2, *A–C*).

Having defined an oxygen-related signature in the disease setting, we then transpose these findings in a mouse model of gradual hypoxia (second dataset, Fig. 2, *D–E*). Here we use a different computational approach to develop a hierarchical dynamic model explaining the transcriptional response of oxidative leg muscles to a prolonged gradual reduction in blood oxygenation (hypoxemia) (Fig. 2, *F* and *G*). The model we describe below validates the notion that the signature identified using the clinical study may be truly triggered by changes in oxygen availability. Moreover, the model contributes to the understanding of the transient events following oxygen depletion that cannot be observed using a cross-sectional clinical study.

Table 1. *Anthropometric characteristics defining the COPD cohort used in the case study*

	Healthy Controls	COPD, Normal BMI	COPD, Low BMI
Sex (M/F)	10/2	9/0	6/0
Age, yr	65.3 ± 2.9	69.4 ± 1.5	69.2 ± 4.6
BMI, kg/m^2	26.3 ± 1.1	27.4 ± 1.4	19.7 ± 1.0^{b,e}
FFMI, kg/m^2	21.0 ± 0.8	21.5 ± 0.7	16.7 ± 0.9^{b,e}
$\dot{V}_E$, l/min	71.2 ± 5.6	40.5 ± 3.6^c	33.0 ± 3.8^c
FEV_1, liters	3.46 ± 0.2	1.41 ± 0.09^c	1.21 ± 0.21^c
FEV_1/FVC, %	75.9 ± 2.4	44.0 ± 2.7^c	39.5 ± 4.5^c
RV, %predicted	103.9 ± 5.2	145.0 ± 13.3	160.0 ± 28.6^a
$\dot{V}O_{2max}$, l·min^{-1}·kg^{-1}	22.3 ± 1.4	13.9 ± 1.7^b	14.4 ± 1.5^b
Peak power, W	117 ± 8	60 ± 7^c	47 ± 9^c
6MWD, m	584 ± 24	469 ± 30^a	367 ± 59^c
BODE index	0.1 ± 0.1	2.3 ± 0.4^b	4.0 ± 1.0^{c,d}

Values are means ± SE. COPD, chronic obstructive pulmonary disease; BMI, body mass index; M, male; F, female; FFMI, fat-free mass index; $\dot{V}_E$, lung ventilation; FEV_1, forced expiratory volume in 1 s; FVC, forced vital capacity; RV, residual volume; $\dot{V}O_{2max}$, maximum O_2 uptake; 6MWD, 6-min walking distance; BODE: BMI, airflow obstruction, dyspnea, and exercise. $^aP < 0.05$, $^bP < 0.01$, and $^cP < 0.001$ vs. controls. $^dP < 0.05$ and $^eP < 0.01$ vs. COPD patients with a normal BMI. Comparisons were analyzed using one-way ANOVA and Tukey's post hoc test.

Step 1. Linking Physiological Measurements and Gene Expression Data in the COPD Cohort

To reconstruct an interaction network spanning multiple levels of organization, we have utilized the following strategy that was developed earlier (61).

Combining measurements from different data sources. To combine gene expression data with whole body physiological readouts, all variables need to have the same units of measurement (as the range of, e.g., VEGF mRNA expression values are very different from those of $\dot{V}O_{2max}$). All such raw scale units can be unified by simply "transforming" each experimental variable to have the same dynamic range, e.g., this can be achieved by standardizing measurements across samples to have a mean of zero with a SD of 1. Such an established approach, called *z*-scoring, enables us to treat the physiological indicators as individual "nodes" in the inferred interaction network with states (just as each gene on the array is treated).

DEFINITION OF A BIOLOGICAL FRAMEWORK FOR DATA-DRIVEN NETWORK INFERENCE. The outcome of data-driven reverse engineering of biological networks, in the absence of any biological assumption(s), often provides results that are difficult to interpret due to the large number of inferred significant interactions. Thus, to reduce complexity of the problem, we decided to focus the analysis on the set of physiological parameters and genes encoding for enzymes in the central bioenergetic pathways (i.e., TCA cycle, oxidative phosphorylation, glycolysis) (see http://pcwww.liv.ac.uk/~herberjm/JAPreview/Table_S2.pdf for additional tables). The latter choice is reasonable considering the paramount importance of these molecular pathways in skeletal muscle adaptation. The overall strategy is, therefore, to identify biomolecules that are highly correlated (based on MI) with biologically important experimental variables. Such a focused analysis will generate multiple network modules of interacting biomolecules, each with a bioenergetic hub gene or physiological measurement at its center. Two modules will be linked together if a specific gene is statistically linked to both hubs.

Reverse engineering. To infer robust regulatory relationships between variables in the integrated multilevel dataset, we used the ARACNE algorithm. This choice was based on the large number of measured variables to be considered by the mathematical framework. By combining all genes expressed in human skeletal muscle (>10,000 mRNAs) with the list of physiological variables, we far exceed the number of variables that can be handled by more advanced network inference methods (e.g., Bayesian methods). Hence, we infer a static network without any obvious hierarchical organization. The result of an ARACNE run is an "adjacency matrix" containing

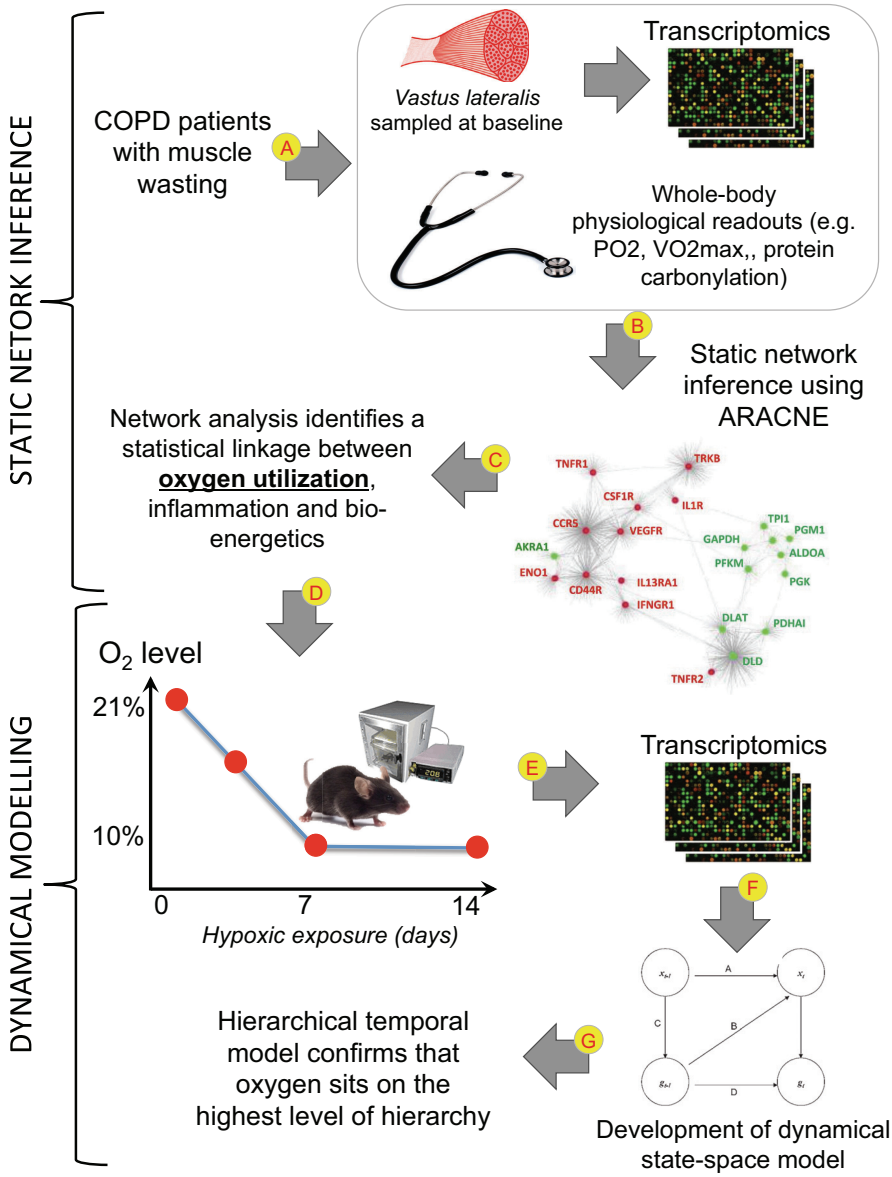

Fig. 2. Schematic representation of the analysis strategy used in the case study, highlighting how the inferred static multiscale network from the clinical chronic obstructive pulmonary disease (COPD) cohort (*A–C*) can be bridged to the inference of a dynamic network representing the temporal progression of events following an experimental challenge (hypoxic exposure) in a murine animal model (*D–G*). Having identified a clinical condition with known outcome (exercise intolerance in patients with respiratory disease), we could target unknown mechanisms by focusing on one likely source of functional limitation (skeletal muscle dysfunction ± central limitation on O_2 supply) and generate data characterizing the phenotype. Both genomic and physiological readouts were used to construct a network of inferred interactions, which was then interrogated to identify statistically robust linkages among broad biological functions. While very useful in providing a list of useful biomarkers, there remains a potential limitation with single-point associations. The dynamic nature of relationships is captured by repeated measures across a suitable time scale (which will vary for different molecular, physiological, and structural responses) using an animal model of respiratory distress, where the transcriptome-based model demonstrated the central importance of oxygen in the response. $\dot{V}O_{2max}$, maximum O_2 uptake; ARACNE, Algorithm for the Reconstruction of Accurate Cellular Networks.

MI values for all pairwise interactions above the specified MI threshold, which can be visualized automatically in Cytoscape.

After calculating MI-based dependencies between all of the different variables in our multilevel data matrix, all of those inferred regulatory interactions with an MI value < 0.22 (corresponding to a P value cutoff of 10^{-6}) were removed. Such filtering of weaker statistical dependencies is an important step in the generation of a more sparse interaction network, which can more easily be interpreted by the investigator. The stringent P value cutoff means that the remaining associations have been inferred with high precision at the cost of a lower recall rate.

Network visualization. Data visualized as a network are often easier to interpret than long lists of biomolecules and their associated statistical dependencies. Hence, the numeric output of ARACNE, which contains MI values for all pairwise associations, was imported into Cytoscape for visualization, a conventional way of analyzing interaction networks. Briefly, we reconstruct the network neighborhood of each of the bioenergetic "seed" genes (i.e., all variables directly connected to them) (see http://pcwww.liv.ac.uk/~herberjm/JAPreview/Table_S2.pdf for additional tables). The neighboring variables can either be genes expressed in muscle and/or physiological variables. Figure 3 summaries key regulatory associations (based on MI) between this seed set of genes and their immediate neighbors.

Functional analysis of the network hubs. We further explored whether the direct interacting neighbors of each central metabolism pathway mapped to functional categories (i.e., GO terms) as well as KEGG pathways. Notably, a marked enrichment of the different bioenergetic compartments was observed (Fig. 3, *A–C* boxes) that clearly highlights the interconnected nature of the bioenergetic machinery, i.e., functionally related genes appear to be coexpressed.

Biological interpretation. The most important finding of the current analysis is that, among the direct neighbors to each bioenergetic pathway, particularly the two oxidative ones, we noted a statistical over-representation of genes encoding his-

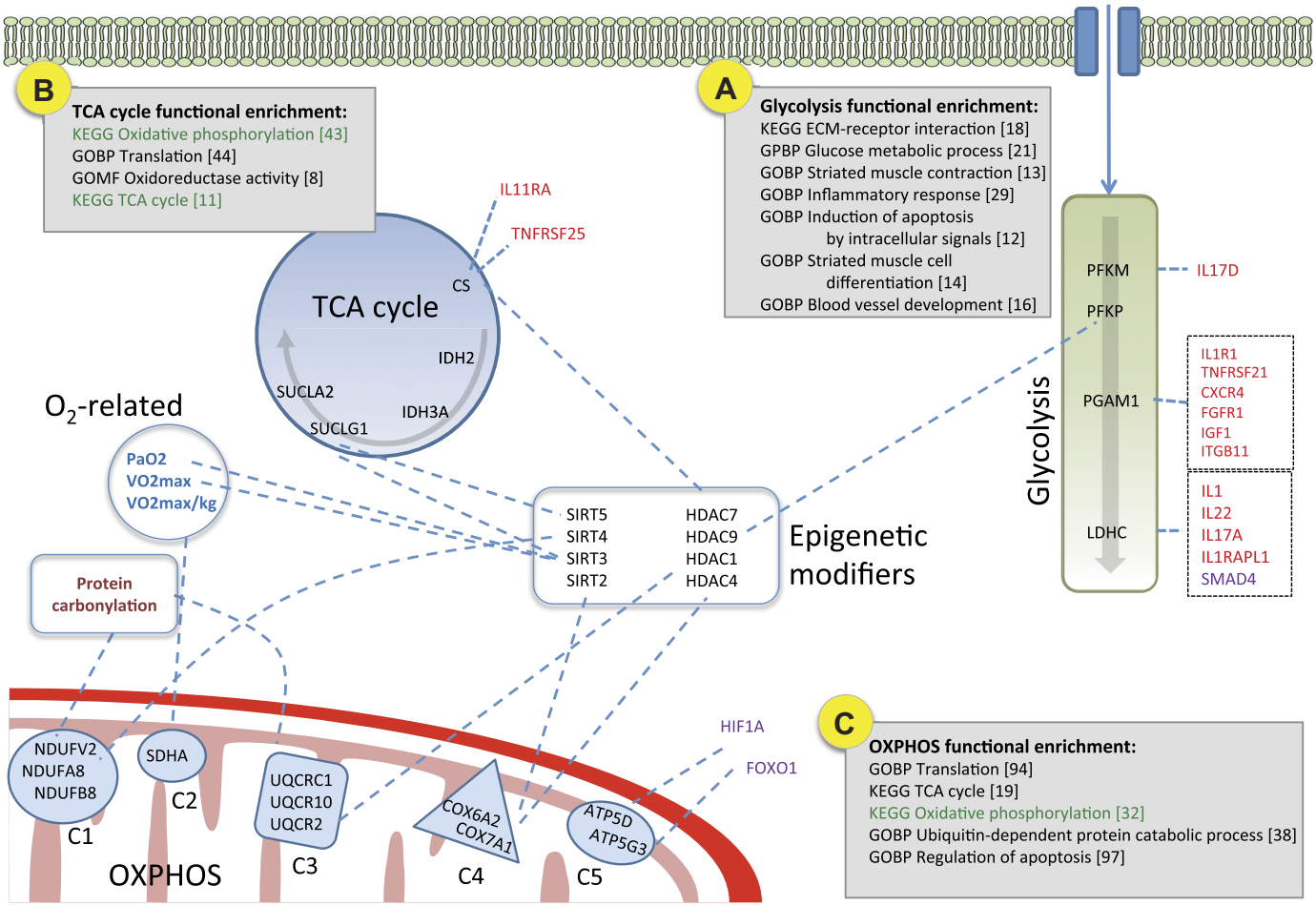

Fig. 3. Graphical representation highlighting putative regulatory associations (significant correlation between two factors is shown as a dashed line) that likely represent robust interactions, based on high mutual information values. The focus is on central metabolism pathways [i.e., glycolysis, TCA, and oxidative phosphorylation (OXPHOS), respectively] and their immediate neighbors. The gray boxes define functional enrichment of the different bioenergetic compartments based on direct neighbors. Individual genes of relevance are grouped into modules with others of related function, as are physiological readouts that may be treated in a similar manner for statistical analysis. C1–C5: the different complexes in the electron transport chain. The value of such an approach is in providing a detailed overview of a complex interaction network, reducing the huge number of potential factors into groups of defined function, and offering a limited number of candidates whose utility as biomarkers or therapeutic targets may be experimentally verified. KEGG, Kyoto Encyclopedia of Genes and Genomes; GOBP, Gene Ontology Biological Process; GPBP, Goodpasture antigen-binding protein; GOMF, Gene Ontology Molecular Function; Pa_{O_2}, arterial oxygen tension; SIRT, sirtuin; HDAC, histone deacetylase.

tone deacetylase (HDAC) enzymes [i.e., HDAC and sirtuin (SIRT) mRNAs]. This observation is consistent with previous studies that have highlighted the importance of SIRTs in regulating metabolism (15, 22, 28). Furthermore, the protein deacetylase *SIRT3* that primarily is localized in the mitochondrial matrix was also significantly positively correlated to both Pa_{O_2} and $\dot{V}O_{2max}$. In support of deacetylation being an important control point, it was recently shown that *Sirt3* knockout mice exhibit decreased oxygen consumption, thus affecting cellular respiration (28). Hence, besides the obvious oxygen-driven effect on aerobic pathways (as indirect measures of oxygen availability such as $\dot{V}O_{2max}$ are linked to key genes in oxidative phosphorylation), the present network-based systems biology approach points to tissue hypoxia as being a potentially important player in modifying expression of deacetylase modifying enzymes in severe COPD patients with a muscle-wasting phenotype. Our systems biology approach also negatively links protein carbonylation [an established proxy measure for oxidative stress (58)] to complexes 1 and 3 in the electron transport chain (Fig. 3, *bottom left*). The validity of such an association is further strengthened via functional enrichment analysis using DAVID, as a significant fraction of direct neighboring genes to protein carbonylation is statistically associated to GO terms representing cellular respiration.

If we then focus on the genes in the glycolytic pathway (Fig. 3, *top right*), a high proportion of proinflammatory mediators/receptors (e.g., *IL1B*, *IL1R1*, and *TNFRSF21*) are among the direct neighbors, as indicated by the enrichment of the "inflammatory response" GO term (Fig. 3*A* box). Hence, hypoxia is proinflammatory, as seen by more traditional observation methods (20).

Multiscale network inference approaches, similar to that illustrated in Fig. 3, have proven very effective in generating robust hypotheses (e.g., Ref. 45). However, statistical associations may not represent causality, particularly when the inferred associations stem from steady-state measures. Thus, to validate our hypothesis that varying oxygen levels (represented by $\dot{V}O_{2max}$ and Pa_{O_2}) control the expression of epigenetic

modifiers, we used a more sophisticated network inference algorithm that can learn the structure of networks from time-course data. We applied this dynamic inference approach to a murine model of hypoxia (*step 2*).

Step 2. Gene Expression Dynamics in Response to Tissue Hypoxia

Animal models are commonly used for studying the in vivo effects of hypoxia, for ethical reasons, where severe or prolonged hypoxemia is induced and invasive samples are required to explore mechanisms. Importantly, hindlimb skeletal muscles have been reported to alter metabolic phenotype and reduce fiber size in response to prolonged hypoxic stress in mice (53, 63), highlighting their potential relevance as a preclinical model of muscle wasting in COPD patients. To experimentally test the hypothesis derived from the clinical COPD network presented in Fig. 3, we, therefore, exposed adult male C57/Bl6 mice to chronic systemic hypoxia for up to 2 wk, to simulate levels of hypoxemia reported in COPD patients with advanced respiratory insufficiency. To capture the temporal effect of reduced oxygen tension on gene regulation, we sampled and gene profiled the soleus muscle ($n = 4$) at three different time points (*days 3*, *7*, and *14*) following initiation of the gradual hypoxic insult (i.e., the O_2 level was gradually lowered to 10% over the first week and kept stable during the second week) (Fig. 2, *bottom*).

First, a high-level representation of the temporal transcriptional changes was performed using a variable reduction technique called principal component analysis (PCA) (Fig. 4*B*). When plotting replicates of two variables against each other, it is relatively easy to see which is a better discriminating factor. Visual inspection becomes increasingly difficult as the number of variables increase, hence the need for PCA. In essence, this method aims at "tilting" the axes through the multidimensional data space, such that the first principal component accounts for as much of the variation in the original dataset as possible (the assumption is that the most important dynamics in the dataset are the ones with the largest variation). Our PCA revealed that the early dynamics of hypoxia are captured by the first principal component, whereas the second most important principal

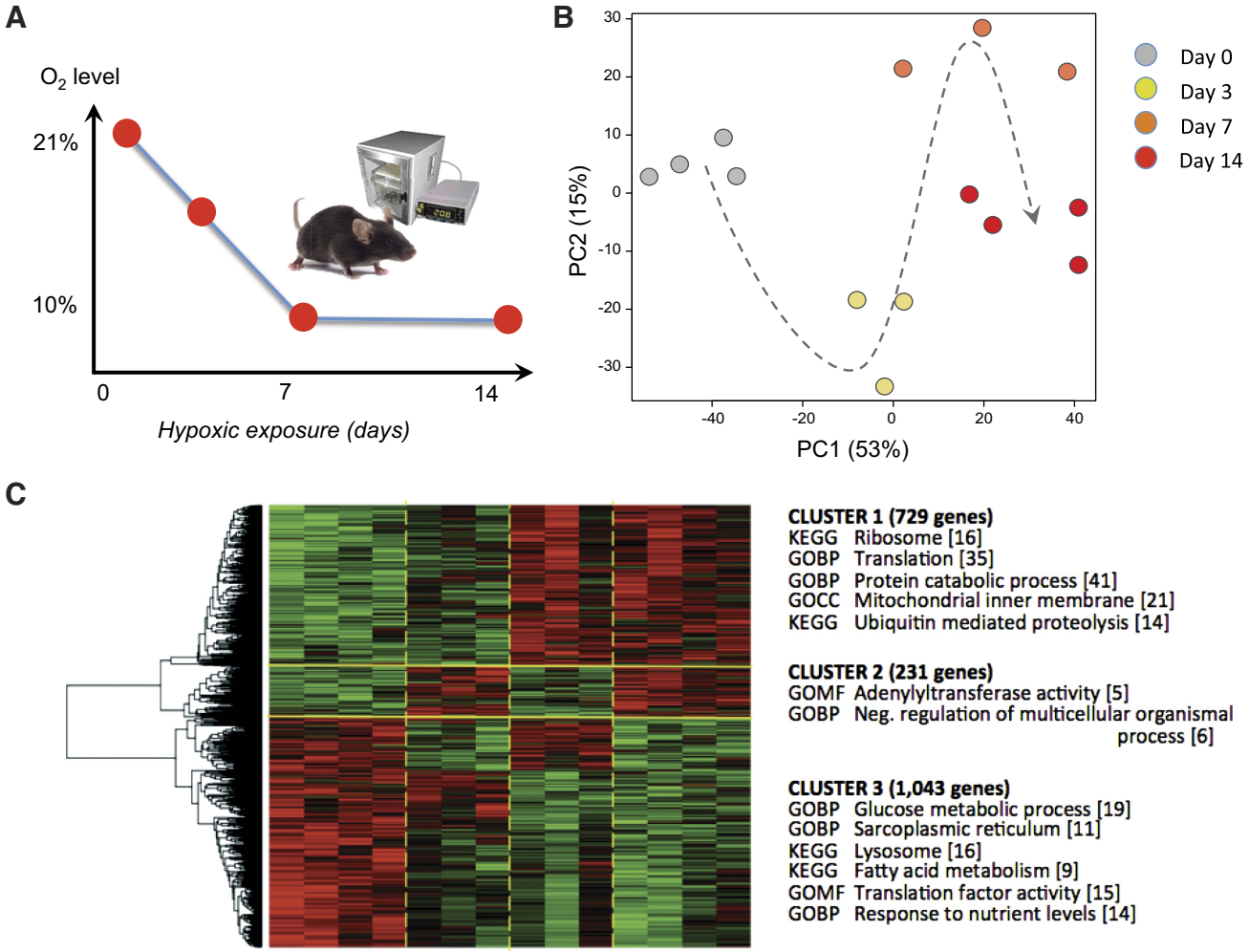

Fig. 4. High-level representation of temporal transcriptional changes in the murine model of hypoxia. *A*: graphical representation of the preclinical experimental design. The oxygen level was gradually decreased from 21% to 10% during the first week, and mice were housed for another week at this oxygen concentration. *B*: principal component (PC) plot highlighting the transcriptional dynamics caused by the hypoxic challenge. *C*: hierarchical clustering using mRNA expression levels of genes modulated by hypoxia ($P < 0.05$). Each row represents a transcript, and each column represents a sample. Red and green colors indicate expression levels above and below the median value of the distribution of signal, respectively. Using solid yellow lines, we have subdivided genes into overall trends to help the reader. Enriched functional terms within these are listed next to the heatmap. GOCC, Gene Ontology Cellular Component.

component (in terms of variance captured) separated the later time points. Furthermore, functional enrichment analysis of the differentially expressed genes (ANOVA, $P < 0.05$) using DAVID (Fig. 4*A*) highlighted several important pathways/ontologies. Most striking was the enrichment of protein catabolic process and ubiquitin-mediated proteolysis among genes upregulated at *days 7* and *14*, clearly suggestive of a transcriptionally regulated muscle wasting phenotype driven by the experimentally induced hypoxemic state.

State space models (SSMs) are a class of probabilistic graphical models (33). SSM provides a general framework for analyzing deterministic and stochastic dynamic systems that can be measured/observed through a stochastic process. The SSM framework has been successfully used for the analysis of gene expression data (23, 51). In its simpler application, the model formalizes the effect of hidden, unmeasurable factors in specifying observed gene expression changes over time. The inclusion of these hidden factors is important, since we cannot hope to measure all possible factors contributing to genetic regulatory interactions (e.g., levels of regulatory proteins as well as effects of mRNA and protein degradation).

The next step was to apply state-space modeling to reverse engineer transcriptional network modules (i.e., representing discrete temporal dimensions) from our replicated murine time course dataset. Such module-based reduction in complexity allows analysis of hundreds or even thousands of genes, as those with a similar temporal expression profile are aggregated into a transcriptional module. To allow construction of a near genome-level model, we took advantage of a newer approach that incorporates this concept of modularization (23).

A SSM can reconstruct the topology of a network representing the systems dynamics, despite a relatively small number of time points, by using biological replicates for each time point (23). To reduce complexity, variables that do not change significantly are excluded from the modeling process. In this case study, genes deemed to be significant by ANOVA at a 1% significance level, as well as all hub genes, were included (931 variables in total) (see http://pcwww.liv.ac.uk/~herberjm/JAPreview/Table_S3.pdf for

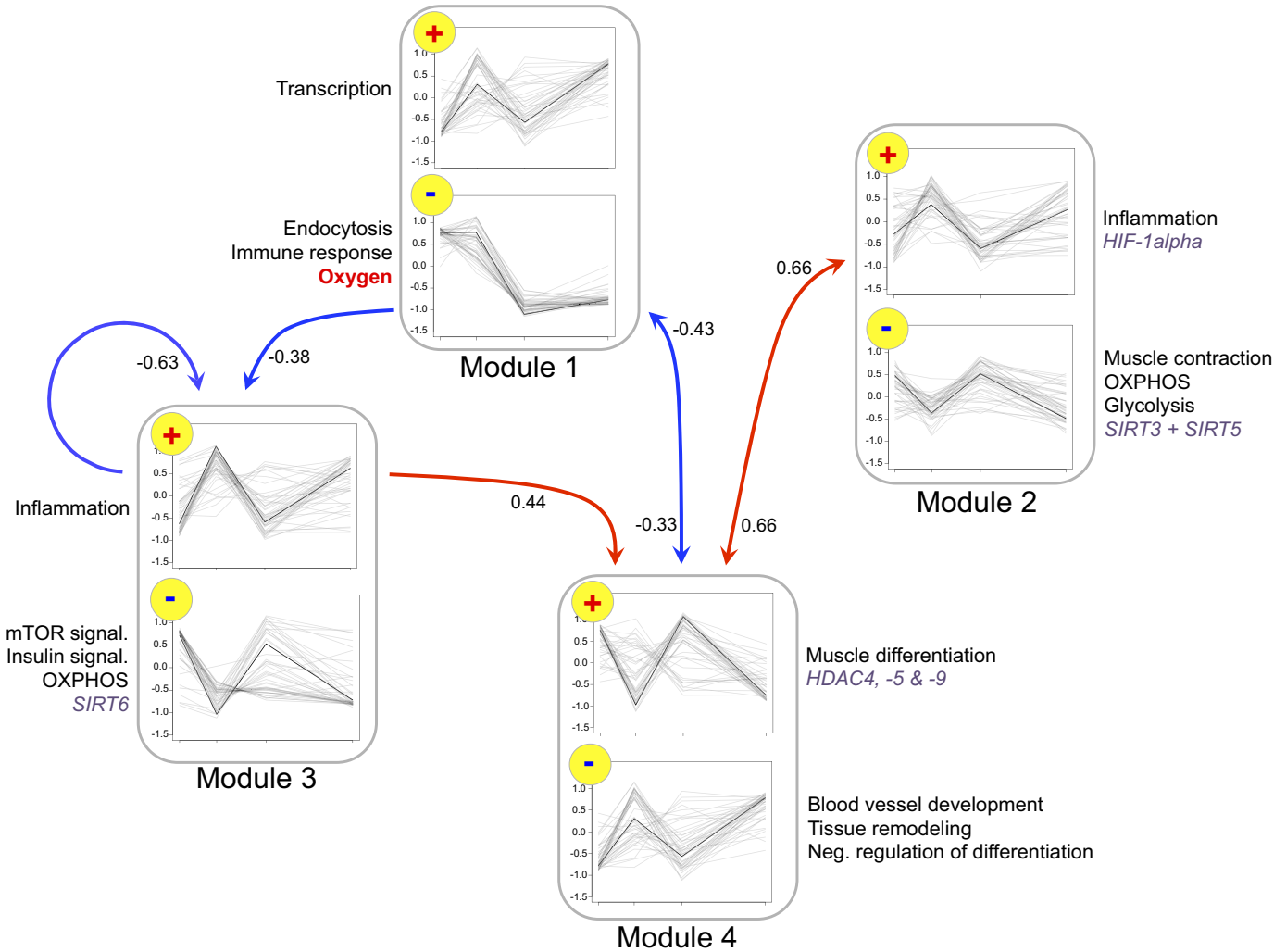

Fig. 5. The hierarchical dynamic state-space model identified four modules (*x*-axes define length of hypoxic exposure), each characterized by two separate transcriptional profiles: plus and minus, representing up- and downregulation, respectively. The hierarchical position of the modules represents the estimated temporal structure of the network. Functionally enriched gene ontology (GO) terms (regular text) as well as key genes (italics) are identified next to the relevant module. Blue arrows represent temporal repression, whereas red arrows represent temporal induction. The numerical value next to each arrow represents the estimated coefficient. mTOR, mammalian target of rapamycin; HIF-1α, hypoxia-inducible factor-1α.

additional tables). The hub genes were chosen to represent the different components in our interpretative model derived from the clinical COPD dataset (Fig. 3). Finally, the experimentally set oxygen level was used as an independent variable.

Based on unsupervised clustering using HOPACH within the software programming environment R (65), we identified eight distinct gene clusters with similar expression profiles. Hence, to model the effect of hypoxemia on the skeletal muscle transcriptome, the hidden state dimension was set to 4, as each inferred module contains both a positive (+) and a negative (−) component.

The hierarchical dynamic model in four temporal dimensions shows that *modules 1* and *2*, which sit on the highest level of hierarchy (i.e., precede others in time), were enriched in GO terms related to muscle contraction, bioenergetic pathways, and inflammation, among others (Fig. 5). Interestingly, the experimental oxygen concentration was represented in *module 1*(−), whereas two deacetylases *SIRT3* and *SIRT5* were found in *module 2*(−). A negative influence is observed of *module 1* on *module 3*, which is located further down the temporal hierarchy. *Module 3*(+) is highly enriched in inflammatory processes, whereas its negative counterpart mainly represents two key signaling pathways (mammalian target of rapamycin and insulin). At the lowest temporal level we find *module 4*, which is enriched in GO terms related to muscle differentiation, tissue remodeling, and blood vessel development. Interestingly, three HDACs are represented in *module 4*(+) (Fig. 5). Figure 6 represents a more focused version of Fig. 5, highlighting the most significant interactions between components in the four inferred modules from Fig. 5.

We, therefore, conclude that the inferred dynamic model using a SSM approach appropriately recapitulates the interpretative model advanced in Fig. 3. In addition, it identifies oxygen at the highest level of hierarchy, whereas key effector functions controlled by oxygen, such as inflammation and muscle differentiation, are downstream in the temporal hierarchy.

CONCLUSIONS

The aim of this brief review is to provide an intuitive overview on data-driven "learning" of biological pathways, linking molecular and physiological readouts. We used a case study to make it easier for experimental biologists to see the potential of computational biology to provide interpretative models of complex patterns, and stress that the identification of general properties of a system from a genomewide analysis of a molecular state of a system is a very powerful approach.

The ability to generate omics data with relatively accessible technologies offers an unprecedented opportunity to study how

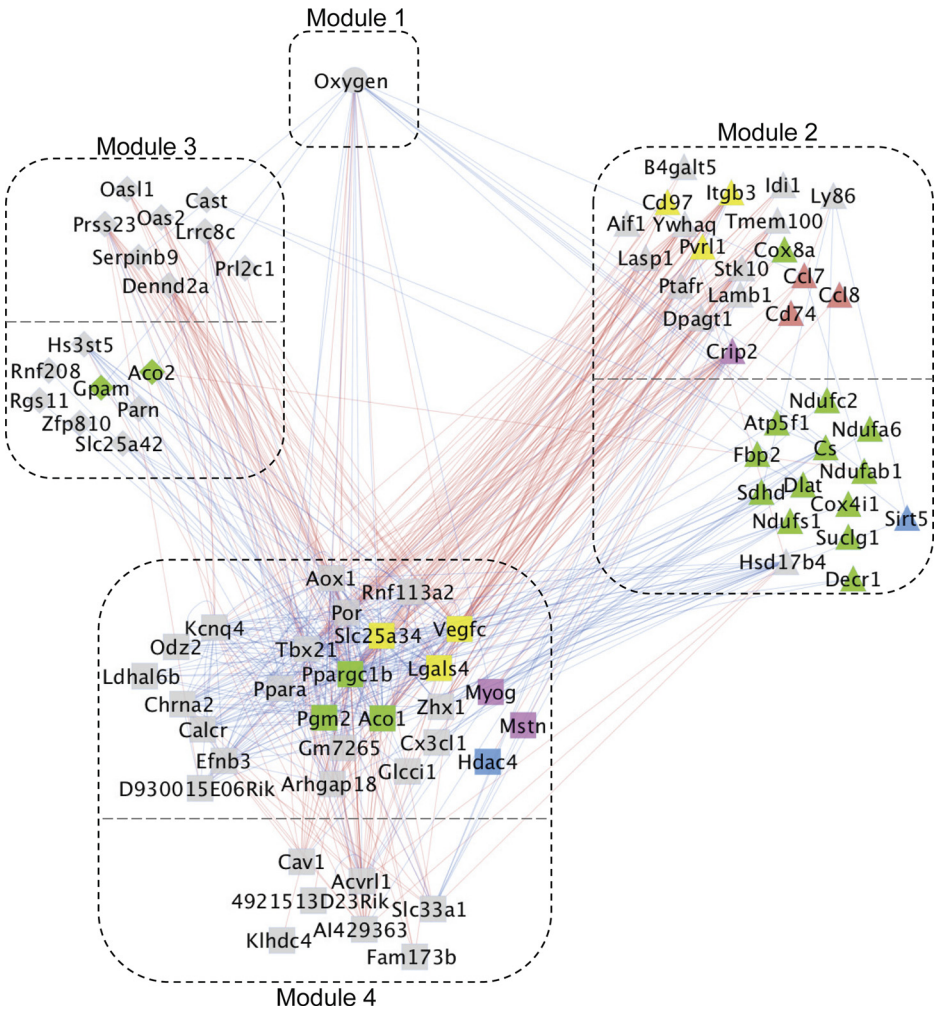

Fig. 6. A higher resolution representation of Fig. 5, highlighting the most significant gene interactions between components in the four inferred modules, is shown. Lines represent factor interactions based on mutual information (blue represents temporal repression, red represents temporal induction). Genes are color coded for broad functional categories (red, cytokines; blue, epigenetic modifiers; green, aerobic metabolism; purple, muscle differentiation; yellow, cell interaction).

genetic information is used to control complex biological processes and their interaction. Until now we have only been able to understand a fraction of that complexity. The computational methods described in this review are designed to support this effort in the measure that they help isolate from these large datasets molecular signatures that correlate to phenotypic outcome.

With the help of computational biology, we are, therefore, able to develop hypotheses, which can be experimentally validated. In this context data-driven biology is not in contraposition with hypothesis-driven research. Instead it is a tool that supports hypothesis generation in the event that the data are too complex to be interpreted solely using common sense. This approach is well developed in other areas of science, such as cancer biology, where there is a vast literature showing that important hypotheses can be generated from modeling of these large datasets (12, 62).

In this paper, we demonstrate the development of an integrative workflow that incorporates measurements from different levels of cellular and molecular organization using a case study representing muscle wasting in COPD. The outline provides an exemplar where individual steps can be modified according to the type of data at hand, and additional data types added. For example, in contrast to established gene expression microarrays, techniques for proteomics and especially metabolomics are still under development. Once it is possible to measure the whole proteome and metabolome of a sample, systems identification pipelines will clearly benefit from these omics techniques.

The specific findings in the case study relate to the definition of an oxygen-dependent signature in COPD. Such signature (exemplified in Fig. 3) is static and entirely based on statistical inference. The model is, therefore, based only on correlation between a series of patient biopsy snapshots and, therefore, does not allow any inference of causality. The use of a mouse model of gradual hypoxia allowed us to demonstrate that a signature inferred from the clinical cohort is indeed modulated by experimental reduction in oxygen levels. Moreover, the development of a mathematical model identifies oxygen as the most upstream event as an emergent property. This may appear as an obvious finding, but, from a methodological perspective, validates the analytic approach.

The data we have used in this case study are gene expression profiling and as such are representative of available datasets. This has several limitations. The first is that models, including multiple levels in the expression of genetics information (e.g., epigenetics, microRNA, proteomics, metabolomics, etc.) may better represent biological complexity. However, current computational methods are inadequate to represent properly the interaction between these levels. Moreover, time course data that rely on disruptive sampling strategies are not true time course experiments. As the new functional genomics technologies develop further, as well as novel approaches to model the interaction between different layer of biological organization, we expect that the efficacy of data-driven approaches will increase further.

ACKNOWLEDGMENTS

At the request of the author(s), readers are herein alerted to the fact that additional materials related to this manuscript may be found at the institutional website of one of the authors, which is: http://pcwww.liv.ac.uk/~herberjm/JAPreview/Table_S2.pdf and http://pcwww.liv.ac.uk/~herberjm/JAPreview/Table_S3.pdf. These materials are not a part of this manuscript and have not undergone peer review by the American Physiological Society (APS). APS and the journal editors take no responsibility for these materials, for the website address, or for any links to or from it.

DISCLOSURES

No conflicts of interest, financial or otherwise, are declared by the author(s).

AUTHOR CONTRIBUTIONS

Author contributions: P.K.D. and F.F. conception and design of research; P.K.D., S.E., and F.F. performed experiments; P.K.D. and F.F. analyzed data; P.K.D. and F.F. interpreted results of experiments; P.K.D., N.T., and F.F. prepared figures; P.K.D., S.E., and F.F. drafted manuscript; P.K.D., S.E., and F.F. edited and revised manuscript; P.K.D., S.E., and F.F. approved final version of manuscript.

REFERENCES

1. **Alderson D, Doyle JC, Li L, Willinger W.** Towards a theory of scale-free graphs: definition, properties, and implications. *Internet Math* 2: 431–523, 2005.
2. **Ashburner M, Ball CA, Blake JA, Botstein D, Butler H, Cherry JM, Davis AP, Dolinski K, Dwight SS, Eppig JT, Harris MA, Hill DP, Issel-Tarver L, Kasarskis A, Lewis S, Matese JC, Richardson JE, Ringwald M, Rubin GM, Sherlock G.** Gene ontology: tool for the unification of biology. The Gene Ontology Consortium. *Nat Genet* 25: 25–29, 2000.
3. **Bansal M, Della Gatta G, di Bernardo D.** Inference of gene regulatory networks and compound mode of action from time course gene expression profiles. *Bioinformatics* 22: 815–822, 2006.
4. **Barabasi A, Albert R.** Emergence of scaling in random networks. *Science* 286: 509–512, 1999.
5. **Barrett T, Suzek TO, Troup DB, Wilhite SE, Ngau WC, Ledoux P, Rudnev D, Lash AE, Fujibuchi W, Edgar R.** NCBI GEO: mining millions of expression profiles–database and tools. *Nucleic Acids Res* 33: D562–D566, 2005.
6. **Batagelj V, Mrvar A.** Pajek–program for large network analysis. *Connect (Tor)* 21: 47–57, 1998.
7. **Brazma A, Parkinson H, Sarkans U, Shojatalab M, Vilo J, Abeygunawardena N, Holloway E, Kapushesky M, Kemmeren P, Lara GG, Oezcimen A, Rocca-Serra P, Sansone SA.** ArrayExpress–a public repository for microarray gene expression data at the EBI. *Nucleic Acids Res* 31: 68–71, 2003.
8. **Butte AJ, Kohane IS.** Mutual information relevance networks: functional genomic clustering using pairwise entropy measurements. *Pac Symp Biocomput* 2000: 418–429, 2000.
9. **Cassese A, Guindani M, Tadesse MG, Falciani F, Vannucci M.** A hierarchical Bayesian model for inference of copy number variants and their association to gene expression. *Ann Appl Stat* 8: 148–175, 2014.
10. **Davidsen PK, Herbert JM, Antczak P, Clarke K, Ferrer E, Peinado VI, Gonzalez C, Roca J, Egginton S, Falciani F.** A systems biology approach reveals a link between systemic cytokines and skeletal muscle energy metabolism in a rodent smoking model and human COPD. *Genome Med* 6: 59, 2014.

10a. **De Smet R, Marchal K.** Advantages and limitations of current network inference methods. *Nat Rev Microbiol* 8: 717–729, 2010.

11. **Dennis G, Sherman BT, Hosack DA, Yang J, Gao W, Lane HC, Lempicki RA.** DAVID: Database for Annotation, Visualization, and Integrated Discovery. *Genome Biol* 4: P3, 2003.
12. **Du W, Elemento O.** Cancer systems biology: embracing complexity to develop better anticancer therapeutic strategies. *Oncogene* 34: 3215–3225, 2015.
13. **Faith JJ, Hayete B, Thaden JT, Mogno I, Wierzbowski J, Cottarel G, Kasif S, Collins JJ, Gardner TS.** Large-scale mapping and validation of *Escherichia coli* transcriptional regulation from a compendium of expression profiles. *PLoS Biol* 5: e8, 2007.
14. **Falati S, Gross P, Merrill-Skoloff G, Furie BC, Furie B.** Real-time in vivo imaging of platelets, tissue factor and fibrin during arterial thrombus formation in the mouse. *Nat Med* 8: 1175–1180, 2002.
15. **Finkel T, Deng CX, Mostoslavsky R.** Recent progress in the biology and physiology of sirtuins. *Nature* 460: 587–591, 2009.
16. **Gavaghan D, Garny A, Maini PK, Kohl P.** Mathematical models in physiology. *Philos Trans A Math Phys Eng Sci* 364: 1099–1106, 2006.

17. **Gehlenborg N, O'Donoghue SI, Baliga NS, Goesmann A, Hibbs MA, Kitano H, Kohlbacher O, Neuweger H, Schneider R, Tenenbaum D, Gavin AC.** Visualization of omics data for systems biology. *Nat Methods* 7: S56–S68, 2010.
18. **Goldovsky L, Cases I, Enright AJ, Ouzounis CA.** BioLayout (Java): versatile network visualisation of structural and functional relationships. *Appl Bioinformatics* 4: 71–74, 2005.
19. **Gomez-Cabrero D, Compte A, Tegner J.** Workflow for generating competing hypothesis from models with parameter uncertainty. *Interface Focus* 1: 438–449, 2011.
20. **Gonzalez NC, Wood JG.** Alveolar hypoxia-induced systemic inflammation: what low PO(2) does and does not do. *Adv Exp Med Biol* 662: 27–32, 2010.
21. **Gupta R, Stincone A, Antczak P, Durant S, Bicknell R, Bikfalvi A, Falciani F.** A computational framework for gene regulatory network inference that combines multiple methods and datasets. *BMC Syst Biol* 5: 52, 2011.
22. **He W, Newman JC, Wang MZ, Ho L, Verdin E.** Mitochondrial sirtuins: regulators of protein acylation and metabolism. *Trends Endocrinol Metab* 23: 467–476, 2012.
23. **Hirose O, Yoshida R, Imoto S, Yamaguchi R, Higuchi T, Charnock-Jones DS, Print C, Miyano S.** Statistical inference of transcriptional module-based gene networks from time course gene expression profiles by using state space models. *Bioinformatics* 24: 932–942, 2008.
24. **Holloway KV, O'Gorman M, Woods P, Morton JP, Evans L, Cable NT, Goldspink DF, Burniston JG.** Proteomic investigation of changes in human vastus lateralis muscle in response to interval-exercise training. *Proteomics* 9: 5155–5174, 2009.
25. **Huang DW, Sherman BT, Lempicki RA.** Bioinformatics enrichment tools: paths toward the comprehensive functional analysis of large gene lists. *Nucleic Acids Res* 37: 1–13, 2009.
26. **Huxley AF.** Muscle structure and theories of contraction. *Prog Biophys Biophys Chem* 7: 255–318, 1957.
27. **Ideker T, Ozier O, Schwikowski B, Siegel AF.** Discovering regulatory and signalling circuits in molecular interaction networks. *Bioinformatics* 18, *Suppl* 1: S233–S240, 2002.
28. **Jing E, Emanuelli B, Hirschey MD, Boucher J, Lee KY, Lombard D, Verdin EM, Kahn CR.** Sirtuin-3 (Sirt3) regulates skeletal muscle metabolism and insulin signaling via altered mitochondrial oxidation and reactive oxygen species production. *Proc Natl Acad Sci U S A* 108: 14608–14613, 2011.
29. **Jones P, Côté RG, Martens L, Quinn AF, Taylor CF, Derache W, Hermjakob H, Apweiler R.** PRIDE: a public repository of protein and peptide identifications for the proteomics community. *Nucleic Acids Res* 34: D659–D663, 2006.
30. **Joyner MJ, Pedersen BK.** Ten questions about systems biology. *J Physiol* 589: 1017–1030, 2011.
31. **Keller P, Vollaard NBJ, Gustafsson T, Gallagher IJ, Sundberg CJ, Rankinen T, Britton SL, Bouchard C, Koch LG, Timmons JA.** A transcriptional map of the impact of endurance exercise training on skeletal muscle phenotype. *J Appl Physiol* 110: 46–59, 2011.
32. **Kohl P, Noble D.** Systems biology and the virtual physiological human. *Mol Syst Biol* 5: 292, 2009.
33. **Koller D, Friedman N.** *Probabilistic Graphical Models*. Cambridge, MA: MIT Press, 2009.
34. **Krogh A.** The number and distribution of capillaries in muscles with calculations of the oxygen pressure head necessary for supplying the tissue. *J Physiol* 52: 409–415, 1919.
35. **Kupershmidt I, Su QJ, Grewal A, Sundaresh S, Halperin I, Flynn J, Shekar M, Wang H, Park J, Cui W, Wall GD, Wisotzkey R, Alag S, Akhtari S, Ronaghi M.** Ontology-based meta-analysis of global collections of high-throughput public data. *PLoS One* 5: e13066, 2010.
36. **Maere S, Heymans K, Kuiper M.** BiNGO: a Cytoscape plugin to assess overrepresentation of gene ontology categories in biological networks. *Bioinformatics* 21: 3448–3449, 2005.
37. **Mah N.** A comparison of oligonucleotide and cDNA-based microarray systems. *Physiol Genomics* 16: 361–370, 2004.
38. **Margolin AA, Nemenman I, Basso K, Wiggins C, Stolovitzky G, Dalla Favera R, Califano A.** ARACNE: an algorithm for the reconstruction of gene regulatory networks in a mammalian cellular context. *BMC Bioinformatics* 7, *Suppl* 1: S7, 2006.
39. **Mattson DL.** Functional genomics. In: *Integrative Physiology in the Proteomics and Post-Genomics Age*, edited by Walz W. New York: Humana, 2005, p. 7–26.
40. **Merico D, Gfeller D, Bader GD.** How to visually interpret biological data using networks. *Nat Biotechnol* 27: 921–924, 2009.
41. **Meyer PE, Kontos K, Lafitte F, Bontempi G.** Information-theoretic inference of large transcriptional regulatory networks. *EURASIP J Bioinform Syst Biol* 2007: 79879, 2007.
42. **Neapolitan RE.** *Learning Bayesian Networks*. Upper Saddle River, NJ: Pearson Prentice Hall, 2004.
43. **Noble D.** *The Music of Life: Biology Beyond Genes*. Oxford, UK: Oxford University Press, 2008.
44. **Noble D.** Computational models of the heart and their use in assessing the actions of drugs. *J Pharm Sci* 107: 107–117, 2008.
45. **Ogata H, Goto S, Sato K, Fujibuchi W, Bono H, Kanehisa M.** KEGG: Kyoto Encyclopedia of Genes and Genomes. *Nucleic Acids Res* 27: 29–34, 1999.
46. **Opgen-Rhein R, Strimmer K.** Learning causal networks from systems biology time course data: an effective model selection procedure for the vector autoregressive process. *BMC Bioinformatics* 8, *Suppl* 2: S3, 2007.
47. **Ortega F, Sameith K, Turan N, Compton R, Trevino V, Vannucci M, Falciani F.** Models and computational strategies linking physiological response to molecular networks from large-scale data. *Philos Trans A Math Phys Eng Sci* 366: 3067–3089, 2008.
48. **Perrin BE, Ralaivola L, Mazurie A, Bottani S, Mallet J, d'Alché-Buc F.** Gene networks inference using dynamic Bayesian networks. *Bioinformatics* 19, *Suppl* 2: ii138–ii148, 2003.
49. **Poultney CS, Greenfield A, Bonneau R.** Integrated inference and analysis of regulatory networks from multi-level measurements. *Methods Cell Biol* 110: 19–56, 2012.
50. **Rabinovich RA, Bastos R, Ardite E, Llinàs L, Orozco-Levi M, Gea J, Vilaró J, Barberà JA, Rodríguez-Roisin R, Fernández-Checa JC, Roca J.** Mitochondrial dysfunction in COPD patients with low body mass index. *Eur Respir J* 29: 643–650, 2007.
51. **Rangel C, Angus J, Ghahramani Z, Lioumi M, Sotheran E, Gaiba A, Wild DL, Falciani F.** Modeling T-cell activation using gene expression profiling and state-space models. *Bioinformatics* 20: 1361–1372, 2004.
52. **Ravasz E, Somera AL, Mongru DA, Oltvai ZN, Barabási AL.** Hierarchical organization of modularity in metabolic networks. *Science* 297: 1551–1555, 2002.
53. **Reinke C, Bevans-Fonti S, Drager LF, Shin MK, Polotsky VY.** Effects of different acute hypoxic regimens on tissue oxygen profiles and metabolic outcomes. *J Appl Physiol* 111: 881–890, 2011.
54. **Segal E, Shapira M, Regev A, Pe'er D, Botstein D, Koller D, Friedman N.** Module networks: identifying regulatory modules and their condition-specific regulators from gene expression data. *Nat Genet* 34: 166–176, 2003.
55. **Shannon P, Markiel A, Ozier O, Baliga NS, Wang JT, Ramage D, Amin N, Schwikowski B, Ideker T.** Cytoscape: a software environment for integrated models of biomolecular interaction networks. *Genome Res* 13: 2498–2504, 2003.
57. **Su G, Kuchinsky A, Morris JH, States DJ, Meng F.** GLay: community structure analysis of biological networks. *Bioinformatics* 26: 3135–3137, 2010.
58. **Suzuki YJ, Carini M, Butterfield DA.** Protein carbonylation. *Antioxid Redox Signal* 12: 323–325, 2010.
59. **Timmons JA, Knudsen S, Rankinen T, Koch LG, Sarzynski M, Jensen T, Keller P, Scheele C, Vollaard NBJ, Nielsen S, Akerström T, MacDougald OA, Jansson E, Greenhaff PL, Tarnopolsky MA, van Loon LJC, Pedersen BK, Sundberg CJ, Wahlestedt C, Britton SL, Bouchard C.** Using molecular classification to predict gains in maximal aerobic capacity following endurance exercise training in humans. *J Appl Physiol* 108: 1487–1496, 2010.
60. **Trevino V, Falciani F.** GALGO: an R package for multivariate variable selection using genetic algorithms. *Bioinformatics* 22: 1154–1156, 2006.
61. **Turan N, Kalko S, Stincone A, Clarke K, Sabah A, Howlett K, Curnow SJ, Rodriguez DA, Cascante M, O'Neill L, Egginton S, Roca J, Falciani F.** A systems biology approach identifies molecular networks defining skeletal muscle abnormalities in chronic obstructive pulmonary disease. *PLoS Comput Biol* 7: e1002129, 2011.
62. **Werner HMJ, Mills GB, Ram PT.** Cancer systems biology: a peek into the future of patient care? *Nat Rev Clin Oncol* 11: 167–176, 2014.
63. **Willmann G.** *Transcriptional Regulation after Chronic Hypoxia Exposure in Skeletal Muscle*. Cologne, Germany: University of Cologne, 2013.
64. **Yu J, Smith VA, Wang PP, Hartemink AJ, Jarvis ED.** Advances to Bayesian network inference for generating causal networks from observational biological data. *Bioinformatics* 20: 3594–3603, 2004.
65. **van der Laan MJ, Pollard KS.** Hybrid clustering of gene expression data with visualization and the bootstrap. *J Stat Plan Inference* 117: 275–303, 2003.

ARTICLE

doi:10.1038/nature11247

An integrated encyclopedia of DNA elements in the human genome

The ENCODE Project Consortium*

The human genome encodes the blueprint of life, but the function of the vast majority of its nearly three billion bases is unknown. The Encyclopedia of DNA Elements (ENCODE) project has systematically mapped regions of transcription, transcription factor association, chromatin structure and histone modification. These data enabled us to assign biochemical functions for 80% of the genome, in particular outside of the well-studied protein-coding regions. Many discovered candidate regulatory elements are physically associated with one another and with expressed genes, providing new insights into the mechanisms of gene regulation. The newly identified elements also show a statistical correspondence to sequence variants linked to human disease, and can thereby guide interpretation of this variation. Overall, the project provides new insights into the organization and regulation of our genes and genome, and is an expansive resource of functional annotations for biomedical research.

The human genome sequence provides the underlying code for human biology. Despite intensive study, especially in identifying protein-coding genes, our understanding of the genome is far from complete, particularly with regard to non-coding RNAs, alternatively spliced transcripts and regulatory sequences. Systematic analyses of transcripts and regulatory information are essential for the identification of genes and regulatory regions, and are an important resource for the study of human biology and disease. Such analyses can also provide comprehensive views of the organization and variability of genes and regulatory information across cellular contexts, species and individuals.

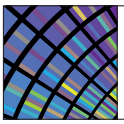

The Encyclopedia of DNA Elements (ENCODE) project aims to delineate all functional elements encoded in the human genome[1–3]. Operationally, we define a functional element as a discrete genome segment that encodes a defined product (for example, protein or non-coding RNA) or displays a reproducible biochemical signature (for example, protein binding, or a specific chromatin structure). Comparative genomic studies suggest that 3–8% of bases are under purifying (negative) selection[4–8] and therefore may be functional, although other analyses have suggested much higher estimates[9–11]. In a pilot phase covering 1% of the genome, the ENCODE project annotated 60% of mammalian evolutionarily constrained bases, but also identified many additional putative functional elements without evidence of constraint[2]. The advent of more powerful DNA sequencing technologies now enables whole-genome and more precise analyses with a broad repertoire of functional assays.

Here we describe the production and initial analysis of 1,640 data sets designed to annotate functional elements in the entire human genome. We integrate results from diverse experiments within cell types, related experiments involving 147 different cell types, and all ENCODE data with other resources, such as candidate regions from genome-wide association studies (GWAS) and evolutionarily constrained regions. Together, these efforts reveal important features about the organization and function of the human genome, summarized below.

- The vast majority (80.4%) of the human genome participates in at least one biochemical RNA- and/or chromatin-associated event in at least one cell type. Much of the genome lies close to a regulatory event: 95% of the genome lies within 8 kilobases (kb) of a DNA–protein interaction (as assayed by bound ChIP-seq motifs or DNase I footprints), and 99% is within 1.7 kb of at least one of the biochemical events measured by ENCODE.
- Primate-specific elements as well as elements without detectable mammalian constraint show, in aggregate, evidence of negative selection; thus, some of them are expected to be functional.
- Classifying the genome into seven chromatin states indicates an initial set of 399,124 regions with enhancer-like features and 70,292 regions with promoter-like features, as well as hundreds of thousands of quiescent regions. High-resolution analyses further subdivide the genome into thousands of narrow states with distinct functional properties.
- It is possible to correlate quantitatively RNA sequence production and processing with both chromatin marks and transcription factor binding at promoters, indicating that promoter functionality can explain most of the variation in RNA expression.
- Many non-coding variants in individual genome sequences lie in ENCODE-annotated functional regions; this number is at least as large as those that lie in protein-coding genes.
- Single nucleotide polymorphisms (SNPs) associated with disease by GWAS are enriched within non-coding functional elements, with a majority residing in or near ENCODE-defined regions that are outside of protein-coding genes. In many cases, the disease phenotypes can be associated with a specific cell type or transcription factor.

ENCODE data production and initial analyses

Since 2007, ENCODE has developed methods and performed a large number of sequence-based studies to map functional elements across the human genome[3]. The elements mapped (and approaches used) include RNA transcribed regions (RNA-seq, CAGE, RNA-PET and manual annotation), protein-coding regions (mass spectrometry), transcription-factor-binding sites (ChIP-seq and DNase-seq), chromatin structure (DNase-seq, FAIRE-seq, histone ChIP-seq and MNase-seq), and DNA methylation sites (RRBS assay) (Box 1 lists methods and abbreviations; Supplementary Table 1, section P, details production statistics)[3]. To compare and integrate results across the different laboratories, data production efforts focused on two selected

*Lists of participants and their affiliations appear at the end of the paper.

BOX 1

ENCODE abbreviations

RNA-seq. Isolation of RNA sequences, often with different purification techniques to isolate different fractions of RNA followed by high-throughput sequencing.

CAGE. Capture of the methylated cap at the 5′ end of RNA, followed by high-throughput sequencing of a small tag adjacent to the 5′ methylated caps. 5′ methylated caps are formed at the initiation of transcription, although other mechanisms also methylate 5′ ends of RNA.

RNA-PET. Simultaneous capture of RNAs with both a 5′ methyl cap and a poly(A) tail, which is indicative of a full-length RNA. This is then followed by sequencing a short tag from each end by high-throughput sequencing.

ChIP-seq. Chromatin immunoprecipitation followed by sequencing. Specific regions of crosslinked chromatin, which is genomic DNA in complex with its bound proteins, are selected by using an antibody to a specific epitope. The enriched sample is then subjected to high-throughput sequencing to determine the regions in the genome most often bound by the protein to which the antibody was directed. Most often used are antibodies to any chromatin-associated epitope, including transcription factors, chromatin binding proteins and specific chemical modifications on histone proteins.

DNase-seq. Adaption of established regulatory sequence assay to modern techniques. The DNase I enzyme will preferentially cut live chromatin preparations at sites where nearby there are specific (non-histone) proteins. The resulting cut points are then sequenced using high-throughput sequencing to determine those sites 'hypersensitive' to DNase I, corresponding to open chromatin.

FAIRE-seq. Formaldehyde assisted isolation of regulatory elements. FAIRE isolates nucleosome-depleted genomic regions by exploiting the difference in crosslinking efficiency between nucleosomes (high) and sequence-specific regulatory factors (low). FAIRE consists of crosslinking, phenol extraction, and sequencing the DNA fragments in the aqueous phase.

RRBS. Reduced representation bisulphite sequencing. Bisulphite treatment of DNA sequence converts unmethylated cytosines to uracil. To focus the assay and save costs, specific restriction enzymes that cut around CpG dinucleotides can reduce the genome to a portion specifically enriched in CpGs. This enriched sample is then sequenced to determine the methylation status of individual cytosines quantitatively.

Tier 1. Tier 1 cell types were the highest-priority set and comprised three widely studied cell lines: K562 erythroleukaemia cells; GM12878, a B-lymphoblastoid cell line that is also part of the 1000 Genomes project (http://1000genomes.org)[55]; and the H1 embryonic stem cell (H1 hESC) line.

Tier 2. The second-priority set of cell types in the ENCODE project which included HeLa-S3 cervical carcinoma cells, HepG2 hepatoblastoma cells and primary (non-transformed) human umbilical vein endothelial cells (HUVECs).

Tier 3. Any other ENCODE cell types not in tier 1 or tier 2.

sets of cell lines, designated 'tier 1' and 'tier 2' (Box 1). To capture a broader spectrum of biological diversity, selected assays were also executed on a third tier comprising more than 100 cell types including primary cells. All data and protocol descriptions are available at http://www.encodeproject.org/, and a User's Guide including details of cell-type choice and limitations was published recently[3].

Integration methodology

For consistency, data were generated and processed using standardized guidelines, and for some assays, new quality-control measures were designed (see refs 3, 12 and http://encodeproject.org/ENCODE/dataStandards.html; A. Kundaje, personal communication). Uniform data-processing methods were developed for each assay (see Supplementary Information; A. Kundaje, personal communication), and most assay results can be represented both as signal information (a per-base estimate across the genome) and as discrete elements (regions computationally identified as enriched for signal). Extensive processing pipelines were developed to generate each representation (M. M. Hoffman *et al.*, manuscript in preparation and A. Kundaje, personal communication). In addition, we developed the irreproducible discovery rate (IDR)[13] measure to provide a robust and conservative estimate of the threshold where two ranked lists of results from biological replicates no longer agree (that is, are irreproducible), and we applied this to defining sets of discrete elements. We identified, and excluded from most analyses, regions yielding untrustworthy signals likely to be artefactual (for example, multicopy regions). Together, these regions comprise 0.39% of the genome (see Supplementary Information). The poster accompanying this issue represents different ENCODE-identified elements and their genome coverage.

Transcribed and protein-coding regions

We used manual and automated annotation to produce a comprehensive catalogue of human protein-coding and non-coding RNAs as well as pseudogenes, referred to as the GENCODE reference gene set[14,15] (Supplementary Table 1, section U). This includes 20,687 protein-coding genes (GENCODE annotation, v7) with, on average, 6.3 alternatively spliced transcripts (3.9 different protein-coding transcripts) per locus. In total, GENCODE-annotated exons of protein-coding genes cover 2.94% of the genome or 1.22% for protein-coding exons. Protein-coding genes span 33.45% from the outermost start to stop codons, or 39.54% from promoter to poly(A) site. Analysis of mass spectrometry data from K562 and GM12878 cell lines yielded 57 confidently identified unique peptide sequences in intergenic regions relative to GENCODE annotation. Taken together with evidence of pervasive genome transcription[16], these data indicate that additional protein-coding genes remain to be found.

In addition, we annotated 8,801 automatically derived small RNAs and 9,640 manually curated long non-coding RNA (lncRNA) loci[17]. Comparing lncRNAs to other ENCODE data indicates that lncRNAs are generated through a pathway similar to that for protein-coding genes[17]. The GENCODE project also annotated 11,224 pseudogenes, of which 863 were transcribed and associated with active chromatin[18].

RNA

We sequenced RNA[16] from different cell lines and multiple subcellular fractions to develop an extensive RNA expression catalogue. Using a conservative threshold to identify regions of RNA activity, 62% of genomic bases are reproducibly represented in sequenced long (>200 nucleotides) RNA molecules or GENCODE exons. Of these bases, only 5.5% are explained by GENCODE exons. Most transcribed bases are within or overlapping annotated gene boundaries (that is, intronic), and only 31% of bases in sequenced transcripts were intergenic[16].

We used CAGE-seq (5′ cap-targeted RNA isolation and sequencing) to identify 62,403 transcription start sites (TSSs) at high confidence (IDR of 0.01) in tier 1 and 2 cell types. Of these, 27,362 (44%) are within 100 base pairs (bp) of the 5′ end of a GENCODE-annotated transcript or previously reported full-length messenger RNA. The remaining regions predominantly lie across exons and 3′ untranslated regions (UTRs), and some exhibit cell-type-restricted expression; these may represent the start sites of novel, cell-type-specific transcripts.

Finally, we saw a significant proportion of coding and non-coding transcripts processed into steady-state stable RNAs shorter than 200 nucleotides. These precursors include transfer RNA, microRNA, small nuclear RNA and small nucleolar RNA (tRNA, miRNA, snRNA and snoRNA, respectively) and the 5′ termini of these processed products align with the capped 5′ end tags[16].

Table 1 | Summary of transcription factor classes analysed in ENCODE

Acronym	Description	Factors analysed
ChromRem	ATP-dependent chromatin complexes	5
DNARep	DNA repair	3
HISase	Histone acetylation, deacetylation or methylation complexes	8
Other	Cyclin kinase associated with transcription	1
Pol2	Pol II subunit	1 (2 forms)
Pol3	Pol III-associated	6
TFNS	General Pol II-associated factor, not site-specific	8
TFSS	Pol II transcription factor with sequence-specific DNA binding	87

Protein bound regions

To identify regulatory regions directly, we mapped the binding locations of 119 different DNA-binding proteins and a number of RNA polymerase components in 72 cell types using ChIP-seq (Table 1, Supplementary Table 1, section N, and ref. 19); 87 (73%) were sequence-specific transcription factors. Overall, 636,336 binding regions covering 231 megabases (Mb; 8.1%) of the genome are enriched for regions bound by DNA-binding proteins across all cell types. We assessed each protein-binding site for enrichment of known DNA-binding motifs and the presence of novel motifs. Overall, 86% of the DNA segments occupied by sequence-specific transcription factors contained a strong DNA-binding motif, and in most (55%) cases the known motif was most enriched (P. Kheradpour and M. Kellis, manuscript in preparation).

Protein-binding regions lacking high or moderate affinity cognate recognition sites have 21% lower median scores by rank than regions with recognition sequences (Wilcoxon rank sum P value $<10^{-16}$). Eighty-two per cent of the low-signal regions have high-affinity recognition sequences for other factors. In addition, when ChIP-seq peaks are ranked by their concordance with their known recognition sequence, the median DNase I accessibility is twofold higher in the bottom 20% of peaks than in the upper 80% (genome structure correction (GSC)[20] P value $<10^{-16}$), consistent with previous observations[21–24]. We speculate that low signal regions are either lower-affinity sites[21] or indirect transcription-factor target regions associated through interactions with other factors (see also refs 25, 26).

We organized all the information associated with each transcription factor—including the ChIP-seq peaks, discovered motifs and associated histone modification patterns—in FactorBook (http://www.factorbook.org; ref. 26), a public resource that will be updated as the project proceeds.

DNase I hypersensitive sites and footprints

Chromatin accessibility characterized by DNase I hypersensitivity is the hallmark of regulatory DNA regions[27,28]. We mapped 2.89 million unique, non-overlapping DNase I hypersensitive sites (DHSs) by DNase-seq in 125 cell types, the overwhelming majority of which lie distal to TSSs[29]. We also mapped 4.8 million sites across 25 cell types that displayed reduced nucleosomal crosslinking by FAIRE, many of which coincide with DHSs. In addition, we used micrococcal nuclease to map nucleosome occupancy in GM12878 and K562 cells[30].

In tier 1 and tier 2 cell types, we identified a mean of 205,109 DHSs per cell type (at false discovery rate (FDR) 1%), encompassing an average of 1.0% of the genomic sequence in each cell type, and 3.9% in aggregate. On average, 98.5% of the occupancy sites of transcription factors mapped by ENCODE ChIP-seq (and, collectively, 94.4% of all 1.1 million transcription factor ChIP-seq peaks in K562 cells) lie within accessible chromatin defined by DNase I hotspots[29]. However, a small number of factors, most prominently heterochromatin-bound repressive complexes (for example, the TRIM28–SETDB1–ZNF274 complex[31,32] encoded by the *TRIM28*, *SETDB1* and *ZNF274* genes), seem to occupy a significant fraction of nucleosomal sites.

Using genomic DNase I footprinting[33,34] on 41 cell types we identified 8.4 million distinct DNase I footprints (FDR 1%)[25]. Our *de novo* motif discovery on DNase I footprints recovered ~90% of known transcription factor motifs, together with hundreds of novel evolutionarily conserved motifs, many displaying highly cell-selective occupancy patterns similar to major developmental and tissue-specific regulators.

Regions of histone modification

We assayed chromosomal locations for up to 12 histone modifications and variants in 46 cell types, including a complete matrix of eight modifications across tier 1 and tier 2. Because modification states may span multiple nucleosomes, which themselves can vary in position across cell populations, we used a continuous signal measure of histone modifications in downstream analysis, rather than calling regions (M. M. Hoffman *et al.*, manuscript in preparation; see http://code.google.com/p/align2rawsignal/). For the strongest, 'peak-like' histone modifications, we used MACS[35] to characterize enriched sites. Table 2 describes the different histone modifications, their peak characteristics, and a summary of their known roles (reviewed in refs 36–39).

Our data show that global patterns of modification are highly variable across cell types, in accordance with changes in transcriptional activity. Consistent with previous studies[40,41], we find that integration of the different histone modification information can be used systematically to assign functional attributes to genomic regions (see below).

DNA methylation

Methylation of cytosine, usually at CpG dinucleotides, is involved in epigenetic regulation of gene expression. Promoter methylation is typically associated with repression, whereas genic methylation correlates with transcriptional activity[42]. We used reduced representation bisulphite sequencing (RRBS) to profile DNA methylation quantitatively for an average of 1.2 million CpGs in each of 82 cell lines and tissues (8.6% of non-repetitive genomic CpGs), including CpGs in intergenic regions, proximal promoters and intragenic regions (gene bodies)[43], although it should be noted that the RRBS method preferentially targets CpG-rich islands. We found that 96% of CpGs exhibited differential methylation in at least one cell type or tissue

Table 2 | Summary of ENCODE histone modifications and variants

Histone modification or variant	Signal characteristics	Putative functions
H2A.Z	Peak	Histone protein variant (H2A.Z) associated with regulatory elements with dynamic chromatin
H3K4me1	Peak/region	Mark of regulatory elements associated with enhancers and other distal elements, but also enriched downstream of transcription starts
H3K4me2	Peak	Mark of regulatory elements associated with promoters and enhancers
H3K4me3	Peak	Mark of regulatory elements primarily associated with promoters/transcription starts
H3K9ac	Peak	Mark of active regulatory elements with preference for promoters
H3K9me1	Region	Preference for the 5′ end of genes
H3K9me3	Peak/region	Repressive mark associated with constitutive heterochromatin and repetitive elements
H3K27ac	Peak	Mark of active regulatory elements; may distinguish active enhancers and promoters from their inactive counterparts
H3K27me3	Region	Repressive mark established by polycomb complex activity associated with repressive domains and silent developmental genes
H3K36me3	Region	Elongation mark associated with transcribed portions of genes, with preference for 3′ regions after intron 1
H3K79me2	Region	Transcription-associated mark, with preference for 5′ end of genes
H4K20me1	Region	Preference for 5′ end of genes

assayed (K. Varley *et al.*, personal communication), and levels of DNA methylation correlated with chromatin accessibility. The most variably methylated CpGs are found more often in gene bodies and intergenic regions, rather than in promoters and upstream regulatory regions. In addition, we identified an unexpected correspondence between unmethylated genic CpG islands and binding by P300, a histone acetyltransferase linked to enhancer activity[44].

Because RRBS is a sequence-based assay with single-base resolution, we were able to identify CpGs with allele-specific methylation consistent with genomic imprinting, and determined that these loci exhibit aberrant methylation in cancer cell lines (K. Varley *et al.*, personal communication). Furthermore, we detected reproducible cytosine methylation outside CpG dinucleotides in adult tissues[45], providing further support that this non-canonical methylation event may have important roles in human biology (K. Varley *et al.*, personal communication).

Chromosome-interacting regions

Physical interaction between distinct chromosome regions that can be separated by hundreds of kilobases is thought to be important in the regulation of gene expression[46]. We used two complementary chromosome conformation capture (3C)-based technologies to probe these long-range physical interactions.

A 3C-carbon copy (5C) approach[47,48] provided unbiased detection of long-range interactions with TSSs in a targeted 1% of the genome (the 44 ENCODE pilot regions) in four cell types (GM12878, K562, HeLa-S3 and H1 hESC)[49]. We discovered hundreds of statistically significant long-range interactions in each cell type after accounting for chromatin polymer behaviour and experimental variation. Pairs of interacting loci showed strong correlation between the gene expression level of the TSS and the presence of specific functional element classes such as enhancers. The average number of distal elements interacting with a TSS was 3.9, and the average number of TSSs interacting with a distal element was 2.5, indicating a complex network of interconnected chromatin. Such interwoven long-range architecture was also uncovered genome-wide using chromatin interaction analysis with paired-end tag sequencing (ChIA-PET)[50] applied to identify interactions in chromatin enriched by RNA polymerase II (Pol II) ChIP from five cell types[51]. In K562 cells, we identified 127,417 promoter-centred chromatin interactions using ChIA-PET, 98% of which were intra-chromosomal. Whereas promoter regions of 2,324 genes were involved in 'single-gene' enhancer–promoter interactions, those of 19,813 genes were involved in 'multi-gene' interaction complexes spanning up to several megabases, including promoter–promoter and enhancer–promoter interactions[51].

These analyses portray a complex landscape of long-range gene–element connectivity across ranges of hundreds of kilobases to several megabases, including interactions among unrelated genes (Supplementary Fig. 1, section Y). Furthermore, in the 5C results, 50–60% of long-range interactions occurred in only one of the four cell lines, indicative of a high degree of tissue specificity for gene–element connectivity[49].

Summary of ENCODE-identified elements

Accounting for all these elements, a surprisingly large amount of the human genome, 80.4%, is covered by at least one ENCODE-identified element (detailed in Supplementary Table 1, section Q). The broadest element class represents the different RNA types, covering 62% of the genome (although the majority is inside of introns or near genes). Regions highly enriched for histone modifications form the next largest class (56.1%). Excluding RNA elements and broad histone elements, 44.2% of the genome is covered. Smaller proportions of the genome are occupied by regions of open chromatin (15.2%) or sites of transcription factor binding (8.1%), with 19.4% covered by at least one DHS or transcription factor ChIP-seq peak across all cell lines. Using our most conservative assessment, 8.5% of bases are covered by either a transcription-factor-binding-site motif (4.6%) or a DHS footprint (5.7%). This, however, is still about 4.5-fold higher than the amount of protein-coding exons, and about twofold higher than the estimated amount of pan-mammalian constraint.

Given that the ENCODE project did not assay all cell types, or all transcription factors, and in particular has sampled few specialized or developmentally restricted cell lineages, these proportions must be underestimates of the total amount of functional bases. However, many assays were performed on more than one cell type, allowing assessment of the rate of discovery of new elements. For both DHSs and CTCF-bound sites, the number of new elements initially increases rapidly with a steep gradient for the saturation curve and then slows with increasing number of cell types (Supplementary Figs 1 and 2, section R). With the current data, at the flattest part of the saturation curve each new cell type adds, on average, 9,500 DHS elements (across 106 cell types) and 500 CTCF-binding elements (across 49 cell types), representing 0.45% of the total element number. We modelled saturation for the DHSs and CTCF-binding sites using a Weibull distribution ($r^2 > 0.999$) and predict saturation at approximately 4.1 million (standard error (s.e.) = 108,000) and 185,100 (s.e. = 18,020) sites, respectively, indicating that we have discovered around half of the estimated total DHSs. These estimates represent a lower bound, but reinforce the observation that there is more non-coding functional DNA than either coding sequence or mammalian evolutionarily constrained bases.

The impact of selection on functional elements

From comparative genomic studies, at least 3–8% of bases are under purifying (negative) selection[4–11], indicating that these bases may potentially be functional. We previously found that 60% of mammalian evolutionarily constrained bases were annotated in the ENCODE pilot project, but also observed that many functional elements lacked evidence of constraint[2], a conclusion substantiated by others[52–54]. The diversity and genome-wide occurrence of functional elements now identified provides an unprecedented opportunity to examine further the forces of negative selection on human functional sequences.

We examined negative selection using two measures that highlight different periods of selection in the human genome. The first measure, inter-species, pan-mammalian constraint (GERP-based scores; 24 mammals[8]), addresses selection during mammalian evolution. The second measure is intra-species constraint estimated from the numbers of variants discovered in human populations using data from the 1000 Genomes project[55], and covers selection over human evolution. In Fig. 1, we plot both these measures of constraint for different classes of identified functional elements, excluding features overlapping exons and promoters that are known to be constrained. Each graph also shows genomic background levels and measures of coding-gene constraint for comparison. Because we plot human population diversity on an inverted scale, elements that are more constrained by negative selection will tend to lie in the upper and right-hand regions of the plot.

For DNase I elements (Fig. 1b) and bound motifs (Fig. 1c), most sets of elements show enrichment in pan-mammalian constraint and decreased human population diversity, although for some cell types the DNase I sites do not seem overall to be subject to pan-mammalian constraint. Bound transcription factor motifs have a natural control from the set of transcription factor motifs with equal sequence potential for binding but without binding evidence from ChIP-seq experiments—in all cases, the bound motifs show both more mammalian constraint and higher suppression of human diversity.

Consistent with previous findings, we do not observe genome-wide evidence for pan-mammalian selection of novel RNA sequences (Fig. 1d). There are also a large number of elements without mammalian constraint, between 17% and 90% for transcription-factor-binding regions as well as DHSs and FAIRE regions. Previous studies could not determine whether these sequences are either biochemically active, but with little overall impact on the organism, or under lineage-specific selection. By isolating sequences preferentially inserted into

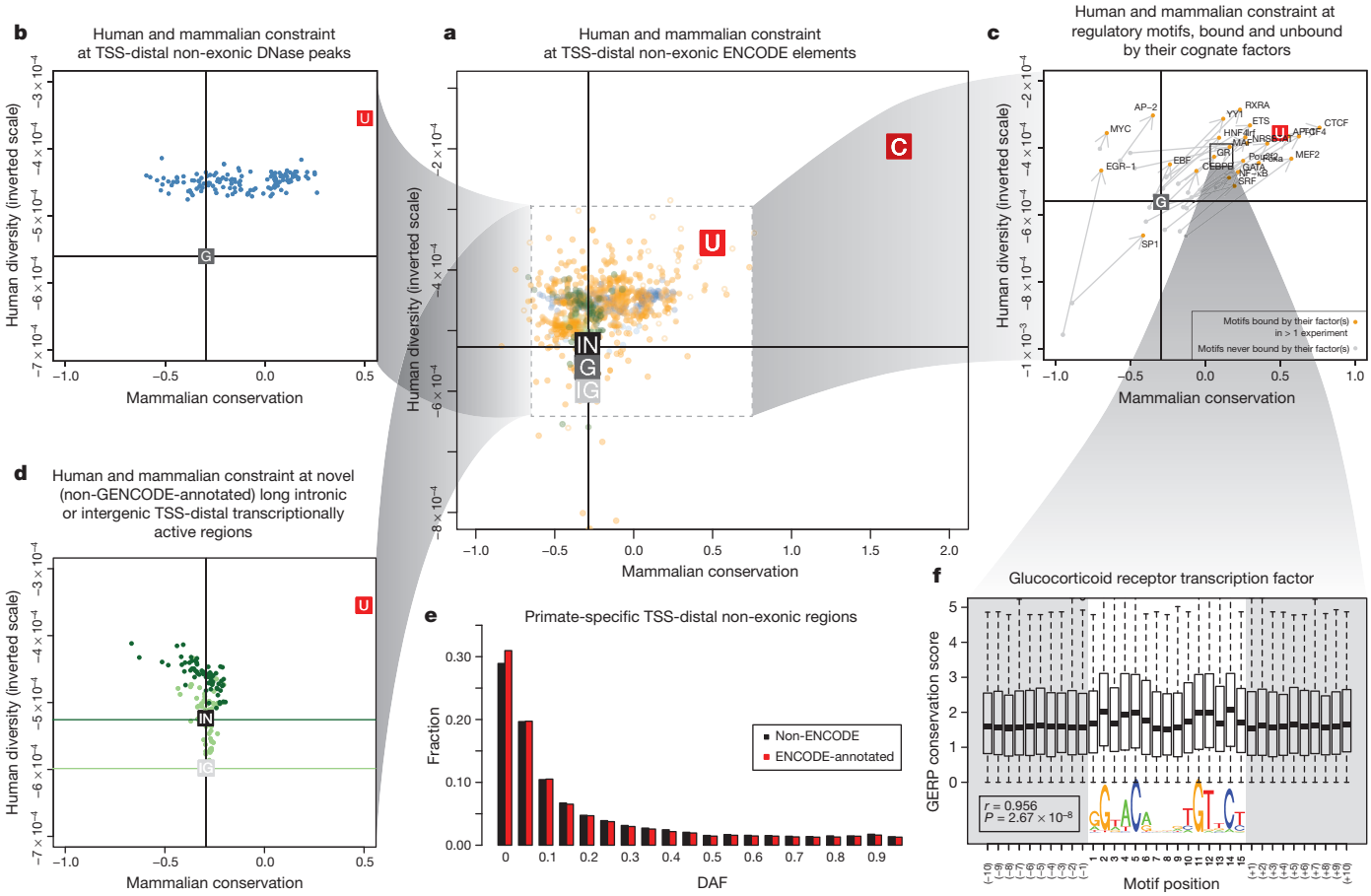

Figure 1 | Impact of selection on ENCODE functional elements in mammals and human populations. **a**, Levels of pan-mammalian constraint (mean GERP score; 24 mammals[8], *x* axis) compared to diversity, a measure of negative selection in the human population (mean expected heterozygosity, inverted scale, *y* axis) for ENCODE data sets. Each point is an average for a single data set. The top-right corners have the strongest evolutionary constraint and lowest diversity. Coding (C), UTR (U), genomic (G), intergenic (IG) and intronic (IN) averages are shown as filled squares. In each case the vertical and horizontal cross hairs show representative levels for the neutral expectation for mammalian conservation and human population diversity, respectively. The spread over all non-exonic ENCODE elements greater than 2.5 kb from TSSs is shown. The inner dashed box indicates that parts of the plot have been magnified for the surrounding outer panels, although the scales in the outer plots provide the exact regions and dimensions magnified. The spread for DHS sites (**b**) and RNA elements (**d**) is shown in the plots on the left. RNA elements are either long novel intronic (dark green) or long intergenic (light green) RNAs. The horizontal cross hairs are colour-coded to the relevant data set in **d**. **c**, Spread of transcription factor motif instances either in regions bound by the transcription factor (orange points) or in the corresponding unbound motif matches in grey, with bound and unbound points connected with an arrow in each case showing that bound sites are generally more constrained and less diverse. **e**, Derived allele frequency spectrum for primate-specific elements, with variations outside ENCODE elements in black and variations covered by ENCODE elements in red. The increase in low-frequency alleles compared to background is indicative of negative selection occurring in the set of variants annotated by the ENCODE data. **f**, Aggregation of mammalian constraint scores over the glucocorticoid receptor (GR) transcription factor motif in bound sites, showing the expected correlation with the information content of bases in the motif. An interactive version of this figure is available in the online version of the paper.

the primate lineage, which is only feasible given the genome-wide scale of this data, we are able to examine this issue specifically. Most primate-specific sequence is due to retrotransposon activity, but an appreciable proportion is non-repetitive primate-specific sequence. Of 104,343,413 primate-specific bases (excluding repetitive elements), 67,769,372 (65%) are found within ENCODE-identified elements. Examination of 227,688 variants segregating in these primate-specific regions revealed that all classes of elements (RNA and regulatory) show depressed derived allele frequencies, consistent with recent negative selection occurring in at least some of these regions (Fig. 1e). An alternative approach examining sequences that are not clearly under pan-mammalian constraint showed a similar result (L. Ward and M. Kellis, manuscript submitted). This indicates that an appreciable proportion of the unconstrained elements are lineage-specific elements required for organismal function, consistent with long-standing views of recent evolution[56], and the remainder are probably 'neutral' elements[2] that are not currently under selection but may still affect cellular or larger scale phenotypes without an effect on fitness.

The binding patterns of transcription factors are not uniform, and we can correlate both inter- and intra-species measures of negative selection with the overall information content of motif positions. The selection on some motif positions is as high as protein-coding exons (Fig. 1f; L. Ward and M. Kellis, manuscript submitted). These aggregate measures across motifs show that the binding preferences found in the population of sites are also relevant to the per-site behaviour. By developing a per-site metric of population effect on bound motifs, we found that highly constrained bound instances across mammals are able to buffer the impact of individual variation[57].

ENCODE data integration with known genomic features

Promoter-anchored integration

Many of the ENCODE assays directly or indirectly provide information about the action of promoters. Focusing on the TSSs of protein-coding transcripts, we investigated the relationships between different ENCODE assays, in particular testing the hypothesis that RNA expression (output) can be effectively predicted from patterns of

chromatin modification or transcription factor binding (input). Consistent with previous reports[58], we observe two relatively distinct types of promoter: (1) broad, mainly (C+G)-rich, TATA-less promoters; and (2) narrow, TATA-box-containing promoters. These promoters have distinct patterns of histone modifications, and transcription-factor-binding sites are selectively enriched in each class (Supplementary Fig. 1, section Z).

We developed predictive models to explore the interaction between histone modifications and measures of transcription at promoters, distinguishing between modifications known to be added as a consequence of transcription (such as H3K36me3 and H3K79me2) and other categories of histone marks[59]. In our analyses, the best models had two components: an initial classification component (on/off) and a second quantitative model component. Our models showed that activating acetylation marks (H3K27ac and H3K9ac) are roughly as informative as activating methylation marks (H3K4me3 and H3K4me2) (Fig. 2a). Although repressive marks, such as H3K27me3 or H3K9me3, show negative correlation both individually and in the model, removing these marks produces only a small reduction in model performance. However, for a subset of promoters in each cell line, repressive histone marks (H3K27me3 or H3K9me3) must be used to predict their expression accurately. We also examined the interplay between the H3K79me2 and H3K36me3 marks, both of which mark gene bodies, probably reflecting recruitment of modification enzymes by polymerase isoforms. As described previously, H3K79me2 occurs preferentially at the 5′ ends of gene bodies and H3K36me3 occurs more 3′, and our analyses support the previous model in which the H3K79me2 to H3K36me3 transition occurs at the first 3′ splice site[60].

Few previous studies have attempted to build qualitative or quantitative models of transcription genome-wide from transcription factor levels because of the paucity of documented transcription-factor-binding regions and the lack of coordination around a single cell line. We thus examined the predictive capacity of transcription-factor-binding signals for the expression levels of promoters (Fig. 2b).

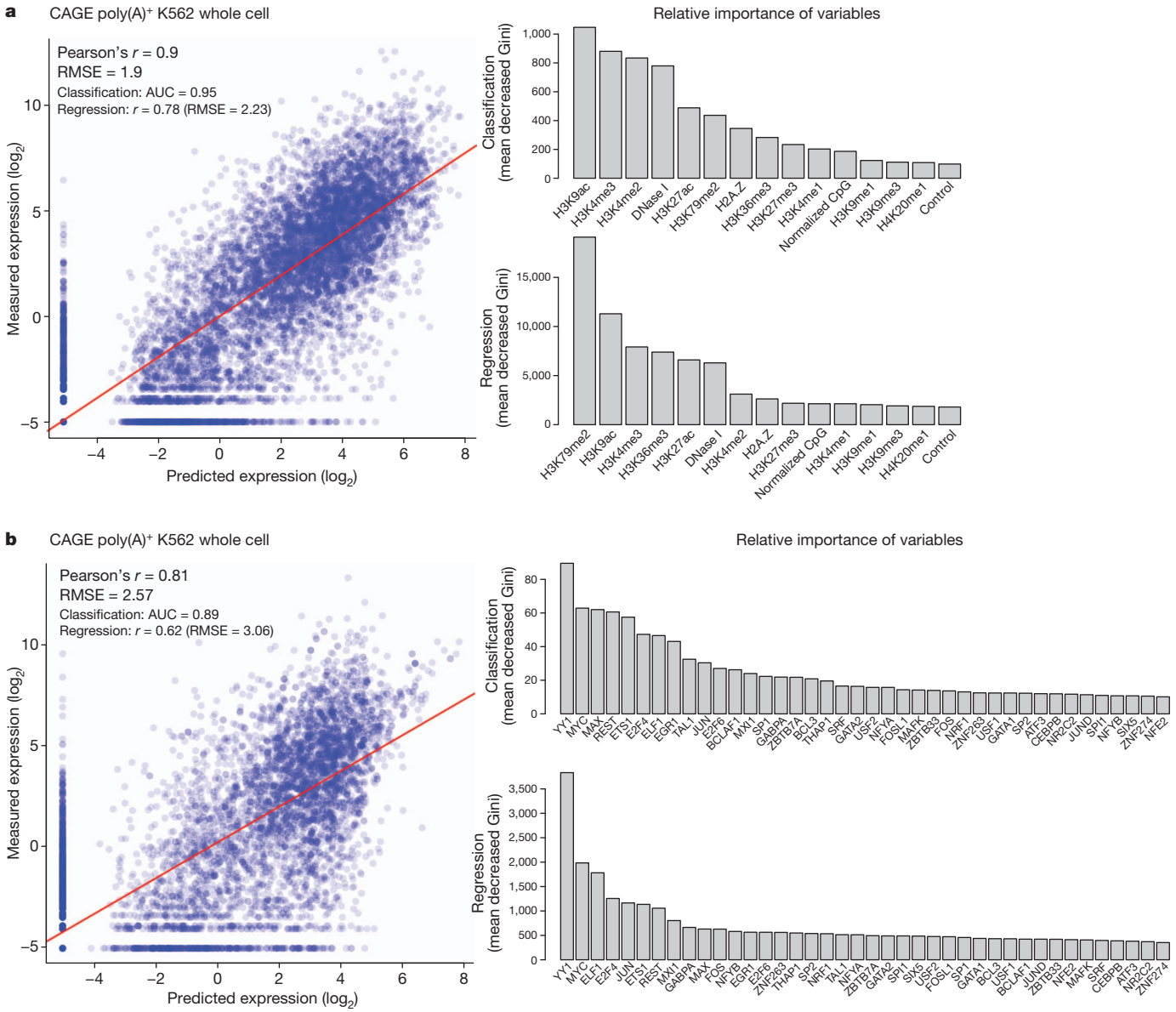

Figure 2 | Modelling transcription levels from histone modification and transcription-factor-binding patterns. **a**, **b**, Correlative models between either histone modifications or transcription factors, respectively, and RNA production as measured by CAGE tag density at TSSs in K562 cells. In each case the scatter plot shows the output of the correlation models (*x* axis) compared to observed values (*y* axis). The bar graphs show the most important histone modifications (**a**) or transcription factors (**b**) in both the initial classification phase (top bar graph) or the quantitative regression phase (bottom bar graph), with larger values indicating increasing importance of the variable in the model. Further analysis of other cell lines and RNA measurement types is reported elsewhere[59,79]. AUC, area under curve; Gini, Gini coefficient; RMSE, root mean square error.

In contrast to the profiles of histone modifications, most transcription factors show enriched binding signals in a narrow DNA region near the TSS, with relatively higher binding signals in promoters with higher CpG content. Most of this correlation could be recapitulated by looking at the aggregate binding of transcription factors without specific transcription factor terms. Together, these correlation models indicate both that a limited set of chromatin marks are sufficient to 'explain' transcription and that a variety of transcription factors might have broad roles in general transcription levels across many genes. It is important to note that this is an inherently observational study of correlation patterns, and is consistent with a variety of mechanistic models with different causal links between the chromatin, transcription factor and RNA assays. However, it does indicate that there is enough information present at the promoter regions of genes to explain most of the variation in RNA expression.

We developed predictive models similar to those used to model transcriptional activity to explore the relationship between levels of histone modification and inclusion of exons in alternately spliced transcripts. Even accounting for expression level, H3K36me3 has a positive contribution to exon inclusion, whereas H3K79me2 has a negative contribution (H. Tilgner *et al.*, manuscript in preparation). By monitoring the RNA populations in the subcellular fractions of K562 cells, we found that essentially all splicing is co-transcriptional[61], further supporting a link between chromatin structure and splicing.

Transcription-factor-binding site-anchored integration

Transcription-factor-binding sites provide a natural focus around which to explore chromatin properties. Transcription factors are often multifunctional and can bind a variety of genomic loci with different combinations and patterns of chromatin marks and nucleosome organization. Hence, rather than averaging chromatin mark profiles across all binding sites of a transcription factor, we developed a clustering procedure, termed the Clustered Aggregation Tool (CAGT), to identify subsets of binding sites sharing similar but distinct patterns of chromatin mark signal magnitude, shape and hidden directionality[30]. For example, the average profile of the repressive histone mark H3K27me3 over all 55,782 CTCF-binding sites in H1 hESCs shows poor signal enrichment (Fig. 3a). However, after grouping profiles by signal magnitude we found a subset of 9,840 (17.6%) CTCF-binding sites that exhibit significant flanking H3K27me3 signal. Shape and orientation analysis further revealed that the predominant signal profile for H3K27me3 around CTCF peak summits is asymmetric, consistent with a boundary role for some CTCF sites between active and polycomb-silenced domains. Further examples are provided in Supplementary Figs 5 and 6 of section E. For TAF1, predominantly found near TSSs, the asymmetric sites are orientated with the direction of transcription. However, for distal sites, such as those bound by GATA1 and CTCF, we also observed a high proportion of asymmetric histone patterns, although independent of motif directionality. In fact, all transcription-factor-binding data sets in all cell lines show predominantly asymmetric patterns (asymmetry ratio >0.6) for all chromatin marks but not for DNase I signal (Fig. 3b). This indicates that most transcription-factor-bound chromatin events correlate with structured, directional patterns of histone modifications, and that promoter directionality is not the only source of orientation at these sites.

We also examined nucleosome occupancy relative to the symmetry properties of chromatin marks around transcription-factor-binding sites. Around TSSs, there is usually strong asymmetric nucleosome occupancy, often accounting for most of the histone modification signal (for instance, see Supplementary Fig. 4, section E). However, away from TSSs, there is far less concordance. For example, CTCF-binding sites typically show arrays of well-positioned nucleosomes on either side of the peak summit (Supplementary Fig. 1, section E)[62]. Where the flanking chromatin mark signal is high, the signals are often asymmetric, indicating differential marking with histone modifications (Supplementary Figs 2 and 3, section E). Thus, we

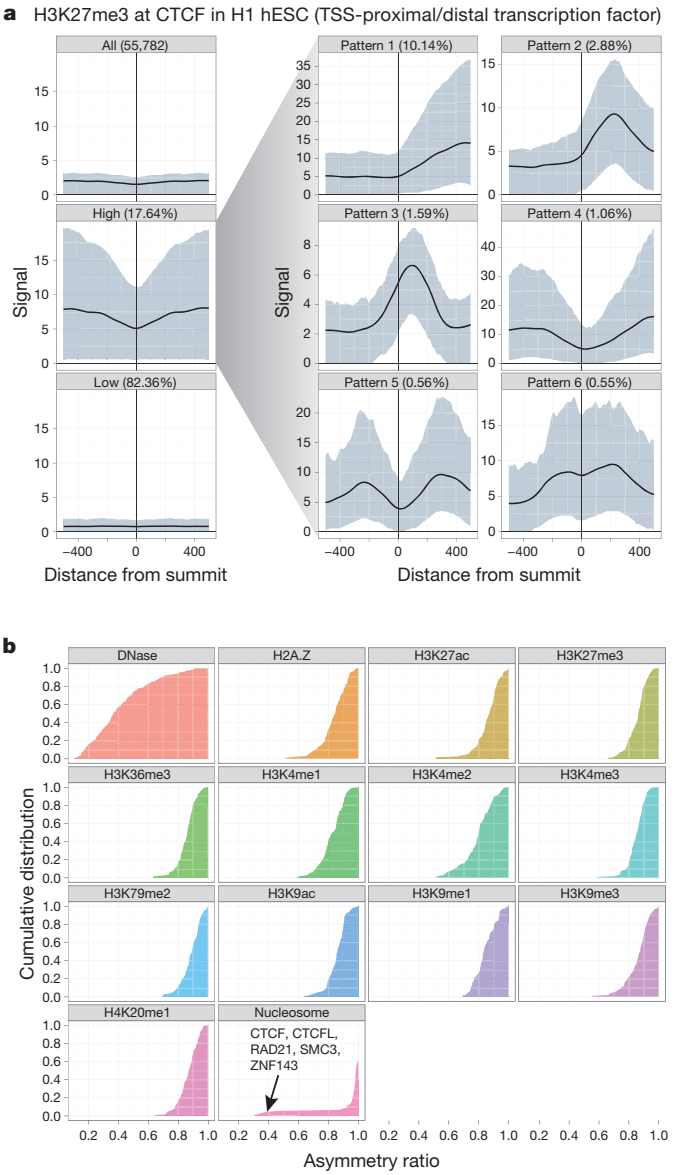

Figure 3 | Patterns and asymmetry of chromatin modification at transcription-factor-binding sites. **a**, Results of clustered aggregation of H3K27me3 modification signal around CTCF-binding sites (a multifunctional protein involved with chromatin structure). The first three plots (left column) show the signal behaviour of the histone modification over all sites (top) and then split into the high and low signal components. The solid lines show the mean signal distribution by relative position with the blue shaded area delimiting the tenth and ninetieth percentile range. The high signal component is then decomposed further into six different shape classes on the right (see ref. 30 for details). The shape decomposition process is strand aware. **b**, Summary of shape asymmetry for DNase I, nucleosome and histone modification signals by plotting an asymmetry ratio for each signal over all transcription-factor-binding sites. All histone modifications measured in this study show predominantly asymmetric patterns at transcription-factor-binding sites. An interactive version of this figure is available in the online version of the paper.

confirm on a genome-wide scale that transcription factors can form barriers around which nucleosomes and histone modifications are arranged in a variety of configurations[62–65]. This is explored in further detail in refs 25, 26 and 30.

Transcription factor co-associations

Transcription-factor-binding regions are nonrandomly distributed across the genome, with respect to both other features (for example, promoters) and other transcription-factor-binding regions. Within the

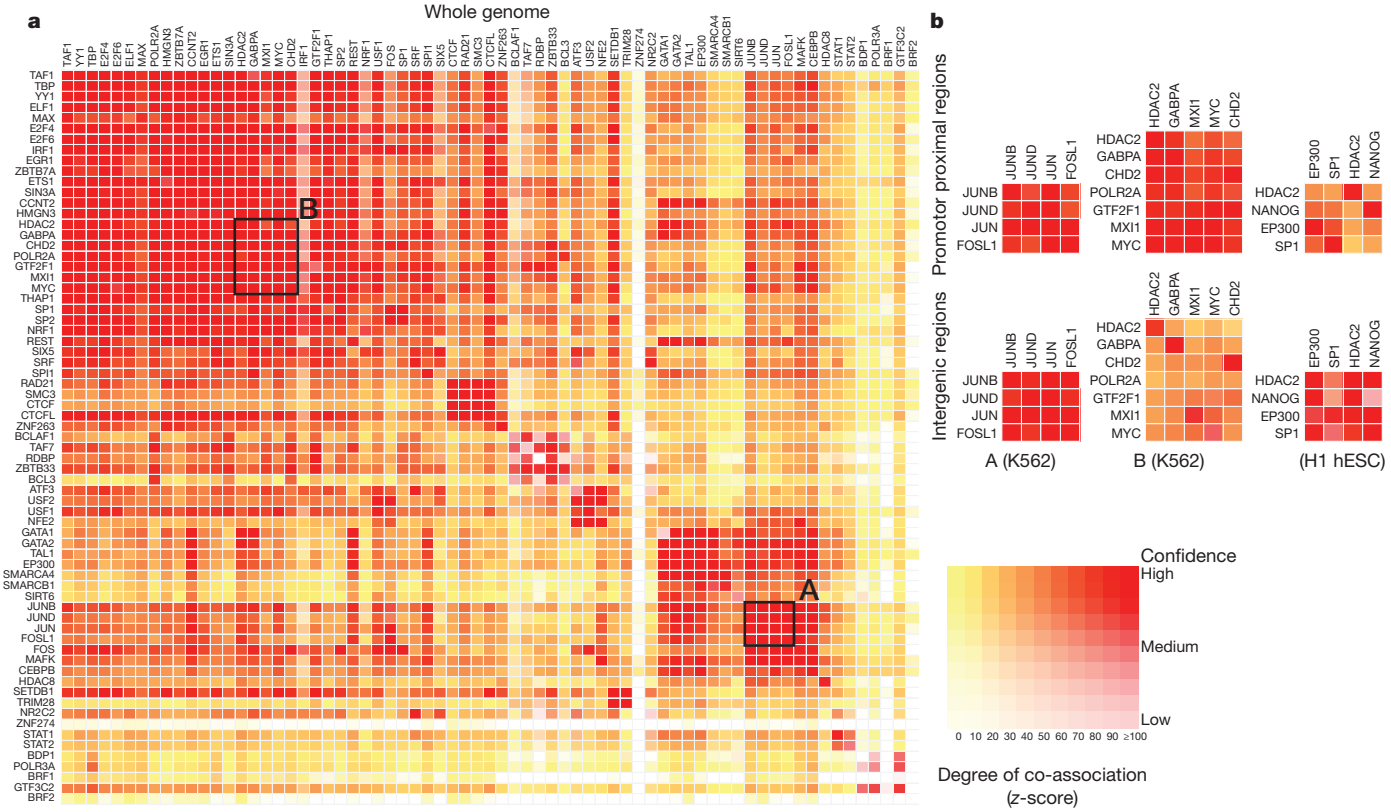

Figure 4 | Co-association between transcription factors. **a**, Significant co-associations of transcription factor pairs using the GSC statistic across the entire genome in K562 cells. The colour strength represents the extent of association (from red (strongest), orange, to yellow (weakest)), whereas the depth of colour represents the fit to the GSC[20] model (where white indicates that the statistical model is not appropriate) as indicated by the key. Most transcription factors have a nonrandom association to other transcription factors, and these associations are dependent on the genomic context, meaning that once the genome is separated into promoter proximal and distal regions, the overall levels of co-association decrease, but more specific relationships are uncovered. **b**, Three classes of behaviour are shown. The first column shows a set of associations for which strength is independent of location in promoter and distal regions, whereas the second column shows a set of transcription factors that have stronger associations in promoter-proximal regions. Both of these examples are from data in K562 cells and are highlighted on the genome-wide co-association matrix (**a**) by the labelled boxes A and B, respectively. The third column shows a set of transcription factors that show stronger association in distal regions (in the H1 hESC line). An interactive version of this figure is available in the online version of the paper.

tier 1 and 2 cell lines, we found 3,307 pairs of statistically co-associated factors ($P < 1 \times 10^{-16}$, GSC) involving 114 out of a possible 117 factors (97%) (Fig. 4a). These include expected associations, such as Jun and Fos, and some less expected novel associations, such as TCF7L2 with HNF4-α and FOXA2 (ref. 66; a full listing is given in Supplementary Table 1, section F). When one considers promoter and intergenic

Table 3 | Summary of the combined state types

Label	Description	Details*	Colour
CTCF	CTCF-enriched element	Sites of CTCF signal lacking histone modifications, often associated with open chromatin. Many probably have a function in insulator assays, but because of the multifunctional nature of CTCF, we are conservative in our description. Also enriched for the cohesin components RAD21 and SMC3; CTCF is known to recruit the cohesin complex.	Turquoise
E	Predicted enhancer	Regions of open chromatin associated with H3K4me1 signal. Enriched for other enhancer-associated marks, including transcription factors known to act at enhancers. In enhancer assays, many of these (>50%) function as enhancers. A more conservative alternative would be *cis*-regulatory regions. Enriched for sites for the proteins encoded by *EP300*, *FOS*, *FOSL1*, *GATA2*, *HDAC8*, *JUNB*, *JUND*, *NFE2*, *SMARCA4*, *SMARCB1*, *SIRT6* and *TAL1* genes in K562 cells. Have nuclear and whole-cell RNA signal, particularly poly(A)− fraction.	Orange
PF	Predicted promoter flanking region	Regions that generally surround TSS segments (see below).	Light red
R	Predicted repressed or low-activity region	This is a merged state that includes H3K27me3 polycomb-enriched regions, along with regions that are silent in terms of observed signal for the input assays to the segmentations (low or no signal). They may have other signals (for example, RNA, not in the segmentation input data). Enriched for sites for the proteins encoded by *REST* and some other factors (for example, proteins encoded by *BRF2*, *CEBPB*, *MAFK*, *TRIM28*, *ZNF274* and *SETDB1* genes in K562 cells).	Grey
TSS	Predicted promoter region including TSS	Found close to or overlapping GENCODE TSS sites. High precision/recall for TSSs. Enriched for H3K4me3. Sites of open chromatin. Enriched for transcription factors known to act close to promoters and polymerases Pol II and Pol III. Short RNAs are most enriched in these segments.	Bright red
T	Predicted transcribed region	Overlap gene bodies with H3K36me3 transcriptional elongation signal. Enriched for phosphorylated form of Pol II signal (elongating polymerase) and poly(A)$^+$ RNA, especially cytoplasmic.	Dark green
WE	Predicted weak enhancer or open chromatin *cis*-regulatory element	Similar to the E state, but weaker signals and weaker enrichments.	Yellow

* Where specific enrichments or overlaps are identified, these are derived from analysis in GM12878 and/or K562 cells where the data for comparison is richest. The colours indicated are used in Figs 5 and 7 and in display of these tracks from the ENCODE data hub.

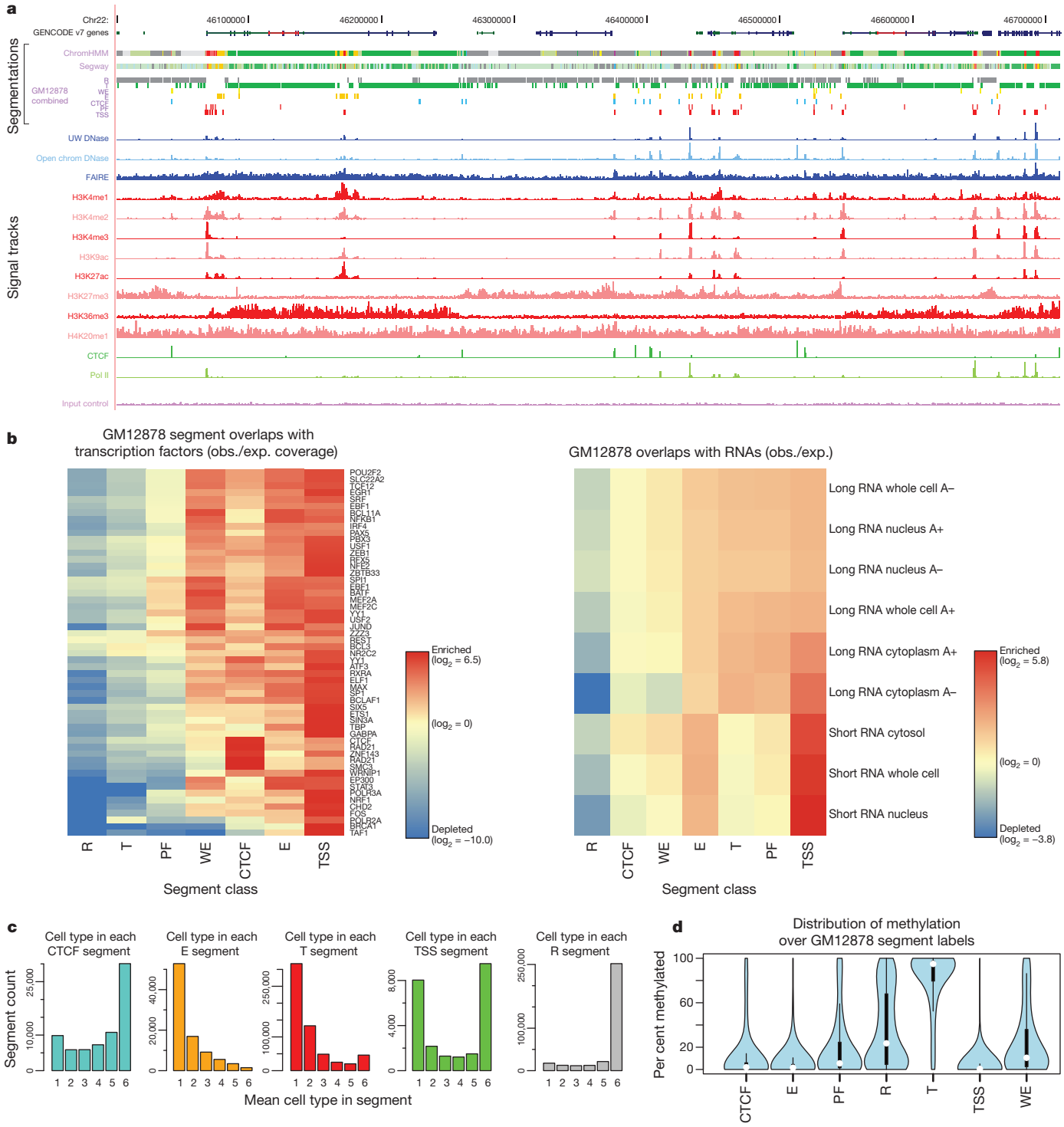

Figure 5 | Integration of ENCODE data by genome-wide segmentation. **a**, Illustrative region with the two segmentation methods (ChromHMM and Segway) in a dense view and the combined segmentation expanded to show each state in GM12878 cells, beneath a compressed view of the GENCODE gene annotations. Note that at this level of zoom and genome browser resolution, some segments appear to overlap although they do not. Segmentation classes are named and coloured according to the scheme in Table 3. Beneath the segmentations are shown each of the normalized signals that were used as the input data for the segmentations. Open chromatin signals from DNase-seq from the University of Washington group (UW DNase) or the ENCODE open chromatin group (Openchrom DNase) and FAIRE assays are shown in blue; signal from histone modification ChIP-seq in red; and transcription factor ChIP-seq signal for Pol II and CTCF in green. The mauve ChIP-seq control signal (input control) at the bottom was also included as an input to the segmentation. **b**, Association of selected transcription factor (left) and RNA (right) elements in the combined segmentation states (*x* axis) expressed as an observed/expected ratio (obs./exp.) for each combination of transcription factor or RNA element and segmentation class using the heat-map scale shown in the key besides each heat map. **c**, Variability of states between cell lines, showing the distribution of occurrences of the state in the six cell lines at specific genome locations: from unique to one cell line to ubiquitous in all six cell lines for five states (CTCF, E, T, TSS and R). **d**, Distribution of methylation level at individual sites from RRBS analysis in GM12878 cells across the different states, showing the expected hypomethylation at TSSs and hypermethylation of genes bodies (T state) and repressed (R) regions.

regions separately, this changes to 3,201 pairs (116 factors, 99%) for promoters and 1,564 pairs (108 factors, 92%) for intergenic regions, with some associations more specific to these genomic contexts (for example, the cluster of HDAC2, GABPA, CHD2, GTF2F1, MXI1 and MYC in promoter regions and SP1, EP300, HDAC2 and NANOG in intergenic regions (Fig. 4b)). These general and context-dependent associations lead to a network representation of the co-binding with many interesting properties, explored in refs 19, 25 and 26. In addition, we also identified a set of regions bound by multiple factors representing high occupancy of transcription factor (HOT) regions[67].

Genome-wide integration

To identify functional regions genome-wide, we next integrated elements independent of genomic landmarks using either discriminative training methods, where a subset of known elements of a particular class were used to train a model that was then used to discover more instances of this class, or using methods in which only data from ENCODE assays were used without explicit knowledge of any annotation.

For discriminative training, we used a three-step process to predict potential enhancers, described in Supplementary Information and ref. 67. Two alternative discriminative models converged on a set of ~13,000 putative enhancers in K562 cells[67]. In the second approach, two methodologically distinct unbiased approaches (see refs 40, 68 and M. M. Hoffman *et al.*, manuscript in preparation) converged on a concordant set of histone modification and chromatin-accessibility patterns that can be used to segment the genome in each of the tier 1 and tier 2 cell lines, although the individual loci in each state in each cell line are different. With the exception of RNA polymerase II and CTCF, the addition of transcription factor data did not substantially alter these patterns. At this stage, we deliberately excluded RNA and methylation assays, reserving these data as a means to validate the segmentations.

Our integration of the two segmentation methods (M. M. Hoffman *et al.*, manuscript in preparation) established a consensus set of seven major classes of genome states, described in Table 3. The standard view of active promoters, with a distinct core promoter region (TSS and PF states), leading to active gene bodies (T, transcribed state), is rediscovered in this model (Fig. 5a, b). There are three 'active' distal states. We tentatively labelled two as enhancers (predicted enhancers, E, and predicted weak enhancers, WE) due to their occurrence in regions of open chromatin with high H3K4me1, although they differ in the levels of marks such as H3K27ac, currently thought to distinguish active from inactive enhancers. The other active state (CTCF) has high CTCF binding and includes sequences that function as insulators in a transfection assay. The remaining repressed state (R) summarizes sequences split between different classes of actively repressed or inactive, quiescent chromatin. We found that the CTCF-binding-associated state is relatively invariant across cell types, with individual regions frequently occupying the CTCF state across all six cell types (Fig. 5c). Conversely, the E and T states have substantial cell-specific behaviour, whereas the TSS state has a bimodal behaviour with similar numbers of cell-invariant and cell-specific occurrences. It is important to note that the consensus summary classes do not capture all the detail discovered in the individual segmentations containing more states.

The distribution of RNA species across segments is quite distinct, indicating that underlying biological activities are captured in the segmentation. Polyadenylated RNA is heavily enriched in gene bodies. Around promoters, there are short RNA species previously identified as promoter-associated short RNAs (Fig. 5b)[16,69]. Similarly, DNA methylation shows marked distinctions between segments, recapitulating the known biology of predominantly unmethylated active promoters (TSS states) followed by methylated gene bodies[42] (T state, Fig. 5d). The two enhancer-enriched states show distinct patterns of DNA methylation, with the less active enhancer state (by H3K27ac/H3K4me1 levels) showing higher methylation. These states also have an excess of RNA elements without poly(A) tails and methyl-cap RNA, as assayed by CAGE sequences, compared to matched intergenic controls, indicating a specific transcriptional mode associated with active enhancers[70]. Transcription factors also showed distinct distributions across the segments (Fig. 5b). A striking pattern is the concentration of transcription factors in the TSS-associated state. The enhancers contain a different set of transcription factors. For example, in K562 cells, the E state is enriched for binding by the proteins encoded by the *EP300*, *FOS*, *FOSL1*, *GATA2*, *HDAC8*, *JUNB*, *JUND*, *NFE2*, *SMARCA4*, *SMARCB1*, *SIRT6* and *TAL1* genes. We tested a subset of these predicted enhancers in both mouse and fish transgenic models (examples in Fig. 6), with over half of the elements showing activity, often in the corresponding tissue type.

The segmentation provides a linear determination of functional state across the genome, but not an association of particular distal regions with genes. By using the variation of DNase I signal across cell lines, 39% of E (enhancer associated) states could be linked to a proposed regulated gene[29] concordant with physical proximity patterns determined by 5C[49] or ChIA-PET.

To provide a fine-grained regional classification, we turned to a self organizing map (SOM) to cluster genome segmentation regions based on their assay signal characteristics (Fig. 7). The segmentation regions were initially randomly assigned to a 1,350-state map in a two-dimensional toroidal space (Fig. 7a). This map can be visualized as a two-dimensional rectangular plane onto which the various signal distributions can be plotted. For instance, the rectangle at the bottom left of Fig. 7a shows the distribution of the genome in the initial randomized map. The SOM was then trained using the twelve different ChIP-seq and DNase-seq assays in the six cell types previously analysed in the large-scale segmentations (that is, over 72-dimensional space). After training, the SOM clustering was again visualized in two dimensions, now showing the organized distribution of genome segments (lower right of panel, Fig. 7a). Individual data sets associated with the genome segments in each SOM map unit (hexagonal cells) can then be visualized in the same framework to learn how each additional kind of data is distributed on the chromatin state map. Figure 7b shows CAGE/TSS expression data overlaid on the randomly initialized (left) and trained map (right) panels. In this way the trained SOM highlighted cell-type-specific TSS clusters (bottom panels of Fig. 7b), indicating that there are sets of tissue-specific TSSs that are distinguished from each other by subtle combinations of ENCODE

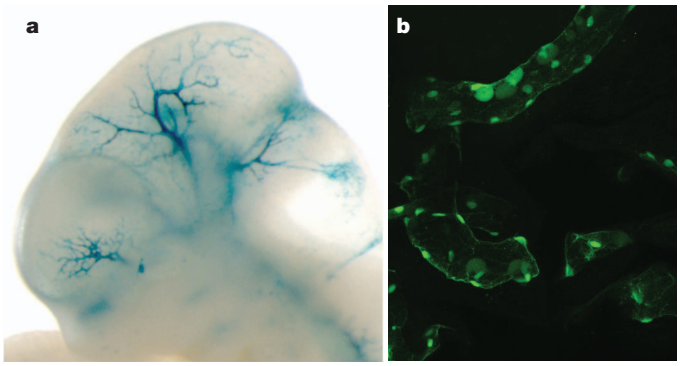

Figure 6 | Experimental characterization of segmentations. Randomly sampled E state segments (see Table 3) from the K562 segmentation were cloned for mouse- and fish-based transgenic enhancer assays. **a**, Representative LacZ-stained transgenic embryonic day (E)11.5 mouse embryo obtained with construct hs2065 (EN167, chr10: 46052882–46055670, GRCh37). Highly reproducible staining in the blood vessels was observed in 9 out of 9 embryos resulting from independent transgenic integration events. **b**, Representative green fluorescent protein reporter transgenic medaka fish obtained from a construct with a basal *hsp70* promoter on meganuclease-based transfection. Reproducible transgenic expression in the circulating nucleated blood cells and the endothelial cell walls was seen in 81 out of 100 transgenic tests of this construct.

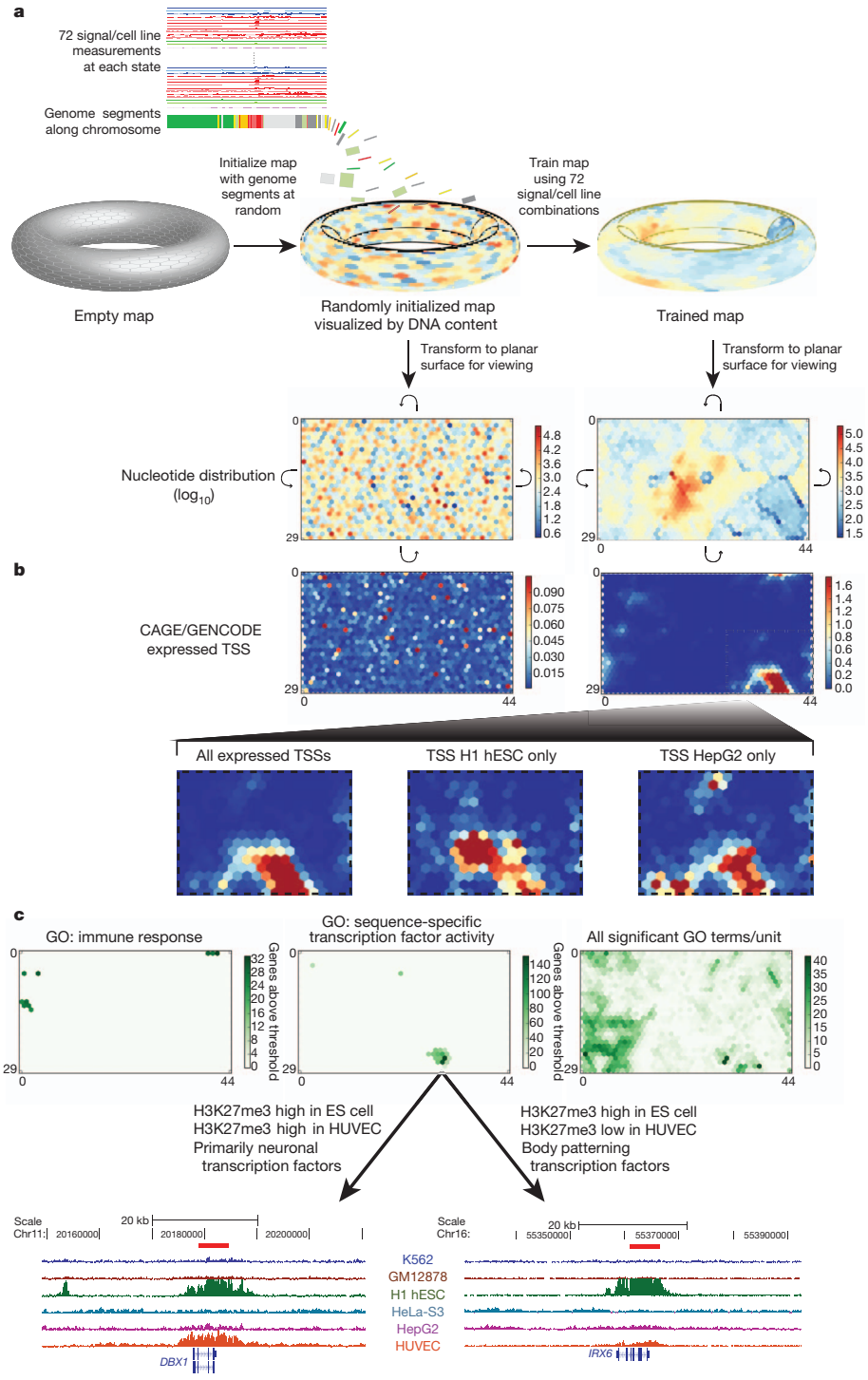

Figure 7 | High-resolution segmentation of ENCODE data by self-organizing maps (SOM). **a**–**c**, The training of the SOM (**a**) and analysis of the results (**b**, **c**) are shown. Initially we arbitrarily placed genomic segments from the ChromHMM segmentation on to the toroidal map surface, although the SOM does not use the ChromHMM state assignments (**a**). We then trained the map using the signal of the 12 different ChIP-seq and DNase-seq assays in the six cell types analysed. Each unit of the SOM is represented here by a hexagonal cell in a planar two-dimensional view of the toroidal map. Curved arrows indicate that traversing the edges of two dimensional view leads back to the opposite edge. The resulting map can be overlaid with any class of ENCODE or other data to view the distribution of that data within this high-resolution segmentation. In panel **a** the distributions of genome bases across the untrained and trained map (left and right, respectively) are shown using heat-map colours for $\log_{10}$ values. **b**, The distribution of TSSs from CAGE experiments of GENCODE annotation on the planar representations of either the initial random organization (left) or the final trained SOM (right) using heat maps coloured according to the accompanying scales. The bottom half of **b** expands the different distributions in the SOM for all expressed TSSs (left) or TSSs specifically expressed in two example cell lines, H1 hESC (centre) and HepG2 (right). **c**, The association of Gene Ontology (GO) terms on the same representation of the same trained SOM. We assigned genes that are within 20 kb of a genomic segment in a SOM unit to that unit, and then associated this set of genes with GO terms using a hypergeometric distribution after correcting for multiple testing. Map units that are significantly associated to GO terms are coloured green, with increasing strength of colour reflecting increasing numbers of genes significantly associated with the GO terms for either immune response (left) or sequence-specific transcription factor activity (centre). In each case, specific SOM units show association with these terms. The right-hand panel shows the distribution on the same SOM of all significantly associated GO terms, now colouring by GO term count per SOM unit. For sequence-specific transcription factor activity, two example genomic regions are extracted at the bottom of panel **c** from neighbouring SOM units. These are regions around the *DBX1* (from SOM unit 26,31, left panel) and *IRX6* (SOM unit 27,30, right panel) genes, respectively, along with their H3K27me3 ChIP-seq signal for each of the tier 1 and 2 cell types. For *DBX1*, representative of a set of primarily neuronal transcription factors associated with unit 26,31, there is a repressive H3K27me3 signal in both H1 hESCs and HUVECs; for *IRX6*, representative of a set of body patterning transcription factors associated with SOM unit 27,30, the repressive mark is restricted largely to the embryonic stem (ES) cell. An interactive version of this figure is available in the online version of the paper.

chromatin data. Many of the ultra-fine-grained state classifications revealed in the SOM are associated with specific gene ontology (GO) terms (right panel of Fig. 7c). For instance, the left panel of Fig. 7c identifies ten SOM map units enriched with genomic regions associated with genes associated with the GO term 'immune response'. The central panel identifies a different set of map units enriched for the GO term 'sequence-specific transcription factor activity'. The two map units most enriched for this GO term, indicated by the darkest green colouring, contain genes with segments that are high in H3K27me3 in H1 hESCs, but that differ in H3K27me3 levels in HUVECs. Gene function analysis with the GO ontology tool (GREAT[71]) reveals that the map unit with high H3K27me3 levels in both cell types is enriched in transcription factor genes with known neuronal functions, whereas the neighbouring map unit is enriched in genes involved in body patterning. The genome browser shots at the bottom of Fig. 7c pick out an example region for each of the two SOM map units illustrating the difference in H3K27me3 signal. Overall, we have 228 distinct GO terms associated with specific segments across

one or more states (A. Mortazavi, personal communication), and can assign over one-third of genes to a GO annotation solely on the basis of its multicellular histone patterns. Thus, the SOM analysis provides a fine-grained map of chromatin data across multiple cell types, which can then be used to relate chromatin structure to other data types at differing levels of resolution (for instance, the large cluster of units containing any active TSS, its subclusters composed of units enriched in TSSs active in only one cell type, or individual map units significantly enriched for specific GO terms).

The classifications presented here are necessarily limited by the assays and cell lines studied, and probably contain a number of heterogeneous classes of elements. Nonetheless, robust classifications can be made, allowing a systematic view of the human genome.

Insights into human genomic variation

We next explored the potential impact of sequence variation on ENCODE functional elements. We examined allele-specific variation using results from the GM12878 cells that are derived from an individual (NA12878) sequenced in the 1000 Genomes project, along with her parents. Because ENCODE assays are predominantly sequence-based, the trio design allows each GM12878 data set to be divided by the specific parental contributions at heterozygous sites, producing aggregate haplotypic signals from multiple genomic sites. We examined 193 ENCODE assays for allele-specific biases using 1,409,992 phased, heterozygous SNPs and 167,096 insertions/deletions (indels) (Fig. 8). Alignment biases towards alleles present in the reference genome sequence were avoided using a sequence specifically tailored to the variants and haplotypes present in NA12878 (a 'personalized genome')[72]. We found instances of preferential binding towards each parental allele. For example, comparison of the results from the POLR2A, H3K79me2 and H3K27me3 assays in the region of *NACC2* (Fig. 8a) shows a strong paternal bias for H3K79me2 and POL2RA and a strong maternal bias for H3K27me3, indicating differential activity for the maternal and paternal alleles.

Figure 8b shows the correlation of selected allele-specific signals across the whole genome. For instance, we found a strong allelic correlation between POL2RA and BCLAF1 binding, as well as negative correlation between H3K79me2 and H3K27me3, both at genes (Fig. 8b, below the diagonal, bottom left) and chromosomal segments (top right). Overall, we found that positive allelic correlations among the 193 ENCODE assays are stronger and more frequent than negative correlations. This may be due to preferential capture of accessible alleles and/or the specific histone modification and transcription factor, assays used in the project.

Rare variants, individual genomes and somatic variants

We further investigated the potential functional effects of individual variation in the context of ENCODE annotations. We divided NA12878 variants into common and rare classes, and partitioned these into those overlapping ENCODE annotation (Fig. 9a and Supplementary Tables 1 and 2, section K). We also predicted potential functional effects: for protein-coding genes, these are either non-synonymous SNPs or variants likely to induce loss of function by frame-shift, premature stop, or splice-site disruption; for other regions, these are variants that overlap a transcription-factor-binding site. We found similar numbers of potentially functional variants affecting protein-coding genes or affecting other ENCODE annotations, indicating that many functional variants within individual genomes lie outside exons of protein-coding genes. A more detailed analysis of regulatory variant annotation is described in ref. 73.

To study further the potential effects of NA12878 genome variants on transcription-factor-binding regions, we performed peak calling using a constructed personal diploid genome sequence for NA12878 (ref. 72). We aligned ChIP-seq sequences from GM12878 separately against the maternal and paternal haplotypes. As expected, a greater

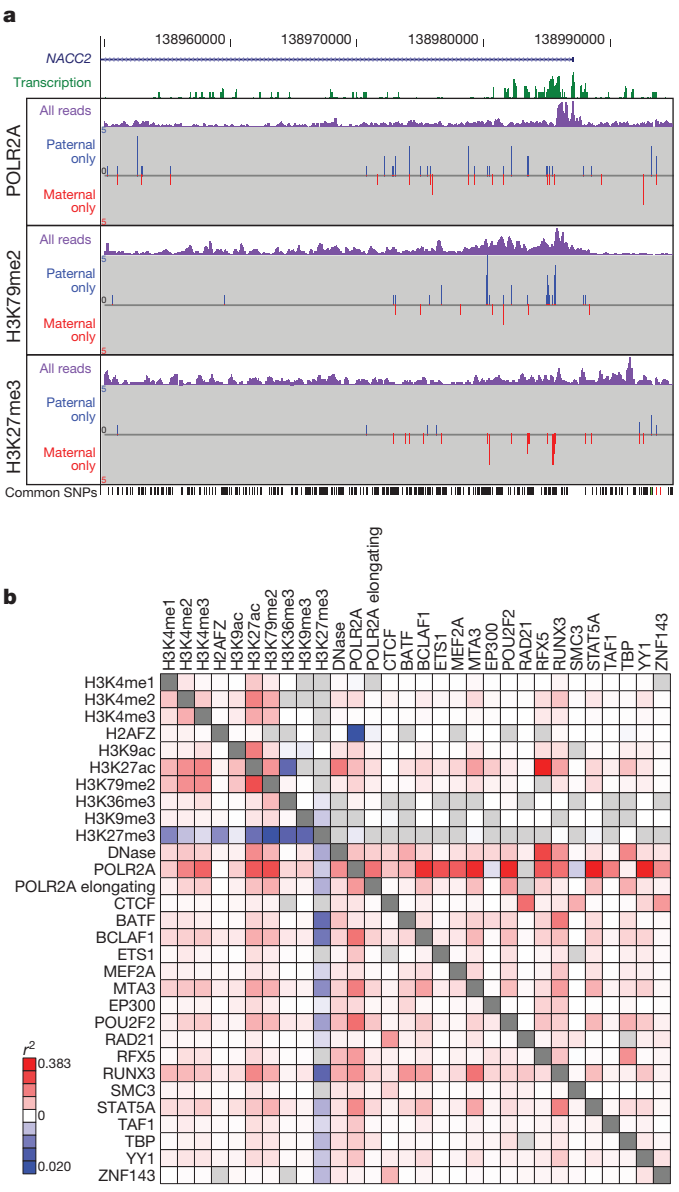

Figure 8 | Allele-specific ENCODE elements. a, Representative allele-specific information from GM12878 cells for selected assays around the first exon of the *NACC2* gene (genomic region Chr9: 138950000–138995000, GRCh37). Transcription signal is shown in green, and the three sections show allele-specific data for three data sets (POLR2A, H3K79me2 and H3K27me3 ChIP-seq). In each case the purple signal is the processed signal for all sequence reads for the assay, whereas the blue and red signals show sequence reads specifically assigned to either the paternal or maternal copies of the genome, respectively. The set of common SNPs from dbSNP, including the phased, heterozygous SNPs used to provide the assignment, are shown at the bottom of the panel. *NACC2* has a statistically significant paternal bias for POLR2A and the transcription-associated mark H3K79me2, and has a significant maternal bias for the repressive mark H3K27me3. **b**, Pair-wise correlations of allele-specific signal within single genes (below the diagonal) or within individual ChromHMM segments across the whole genome for selected DNase-seq and histone modification and transcription factor ChIP-seq assays. The extent of correlation is coloured according to the heat-map scale indicated from positive correlation (red) through to anti-correlation (blue). An interactive version of this figure is available in the online version of the paper.

fraction of reads were aligned than to the reference genome (see Supplementary Information, Supplementary Fig. 1, section K). On average, approximately 1% of transcription-factor-binding sites in GM12878 cells are detected in a haplotype-specific fashion. For instance, Fig. 9b shows a CTCF-binding site not detected using the

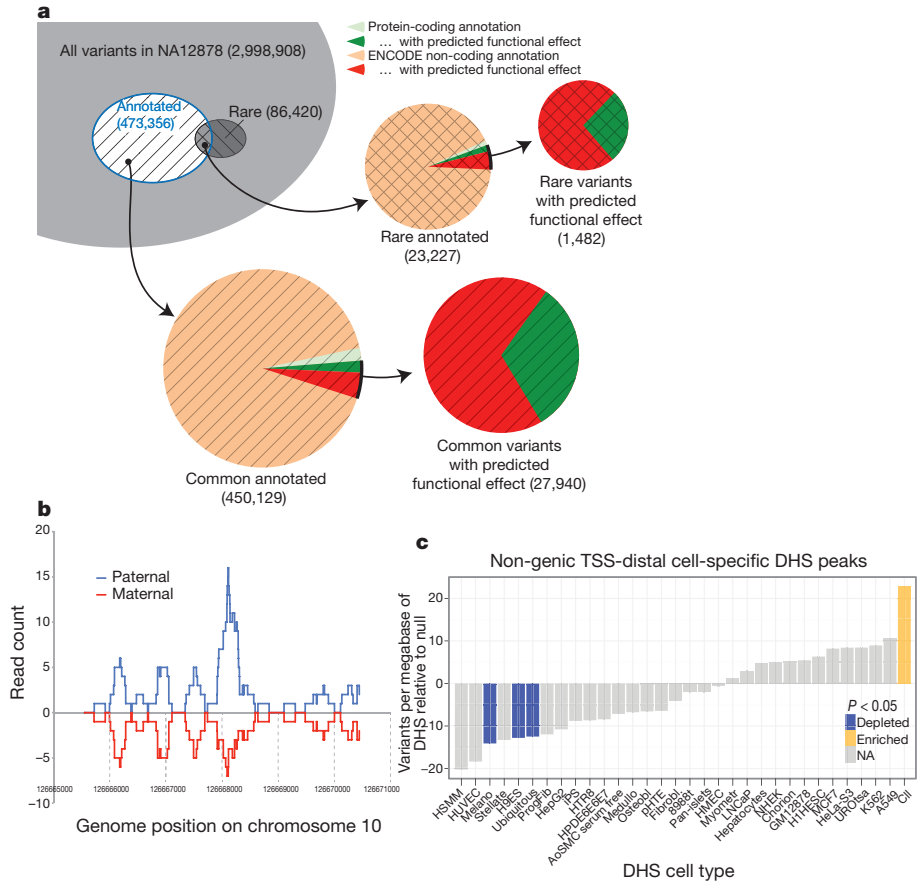

Figure 9 | Examining ENCODE elements on a per individual basis in the normal and cancer genome. **a**, Breakdown of variants in a single genome (NA12878) by both frequency (common or rare (that is, variants not present in the low-coverage sequencing of 179 individuals in the pilot 1 European panel of the 1000 Genomes project[55])) and by ENCODE annotation, including protein-coding gene and non-coding elements (GENCODE annotations for protein-coding genes, pseudogenes and other ncRNAs, as well as transcription-factor-binding sites from ChIP-seq data sets, excluding broad annotations such as histone modifications, segmentations and RNA-seq). Annotation status is further subdivided by predicted functional effect, being non-synonymous and missense mutations for protein-coding regions and variants overlapping bound transcription factor motifs for non-coding element annotations. A substantial proportion of variants are annotated as having predicted functional effects in the non-coding category. **b**, One of several relatively rare occurrences, where alignment to an individual genome sequence (paternal and maternal panels) shows a different readout from the reference genome. In this case, a paternal-haplotype-specific CTCF peak is identified. **c**, Relative level of somatic variants from a whole-genome melanoma sample that occur in DHSs unique to different cell lines. The coloured bars show cases that are significantly enriched or suppressed in somatic mutations. Details of ENCODE cell types can be found at http://encodeproject.org/ENCODE/cellTypes.html. An interactive version of this figure is available in the online version of the paper.

reference sequence that is only present on the paternal haplotype due to a 1-bp deletion (see also Supplementary Fig. 2, section K). As costs of DNA sequencing decrease further, optimized analysis of ENCODE-type data should use the genome sequence of the individual or cell being analysed when possible.

Most analyses of cancer genomes so far have focused on characterizing somatic variants in protein-coding regions. We intersected four available whole-genome cancer data sets with ENCODE annotations (Fig. 9c and Supplementary Fig. 2, section L). Overall, somatic variation is relatively depleted from ENCODE annotated regions, particularly for elements specific to a cell type matching the putative tumour source (for example, skin melanocytes for melanoma). Examining the mutational spectrum of elements in introns for cases where a strand-specific mutation assignment could be made reveals that there are mutational spectrum differences between DHSs and unannotated regions (0.06 Fisher's exact test, Supplementary Fig. 3, section L). The suppression of somatic mutation is consistent with important functional roles of these elements within tumour cells, highlighting a potential alternative set of targets for examination in cancer.

Common variants associated with disease

In recent years, GWAS have greatly extended our knowledge of genetic loci associated with human disease risk and other phenotypes. The output of these studies is a series of SNPs (GWAS SNPs) correlated with a phenotype, although not necessarily the functional variants. Notably, 88% of associated SNPs are either intronic or intergenic[74]. We examined 4,860 SNP–phenotype associations for 4,492 SNPs curated in the National Human Genome Research Institute (NHGRI) GWAS catalogue[74]. We found that 12% of these SNPs overlap transcription-factor-occupied regions whereas 34% overlap DHSs (Fig. 10a). Both figures reflect significant enrichments relative to the overall proportions of 1000 Genomes project SNPs (about 6% and 23%, respectively). Even after accounting for biases introduced by selection of SNPs for the standard genotyping arrays, GWAS SNPs show consistently higher overlap with ENCODE annotations (Fig. 10a, see Supplementary Information). Furthermore, after partitioning the genome by density of different classes of functional elements, GWAS SNPs were consistently enriched beyond all the genotyping SNPs in function-rich partitions, and depleted in function-poor partitions (see Supplementary Fig. 1, section M). GWAS SNPs are particularly enriched in the segmentation classes associated with enhancers and TSSs across several cell types (see Supplementary Fig. 2, section M).

Examining the SOM of integrated ENCODE annotations (see above), we found 19 SOM map units showing significant enrichment for GWAS SNPs, including many SOM units previously associated with specific gene functions, such as the immune response regions.

Thus, an appreciable proportion of SNPs identified in initial GWAS scans are either functional or lie within the length of an ENCODE annotation (~500 bp on average) and represent plausible candidates for the functional variant. Expanding the set of feasible functional SNPs to those in reasonable linkage disequilibrium, up to 71% of GWAS SNPs have a potential causative SNP overlapping a DNase I site, and 31% of loci have a candidate SNP that overlaps a binding site occupied by a transcription factor (see also refs 73, 75).

The GWAS catalogue provides a rich functional categorization from the precise phenotypes being studied. These phenotypic categorizations are nonrandomly associated with ENCODE annotations and there is marked correspondence between the phenotype and the identity of the cell type or transcription factor used in the ENCODE assay (Fig. 10b). For example, five SNPs associated with Crohn's disease overlap GATA2-binding sites (*P* value 0.003 by random permutation or 0.001 by an empirical approach comparing to the GWAS-matched SNPs; see Supplementary Information), and fourteen are located in DHSs found in immunologically relevant cell types. A notable example is a gene desert on chromosome 5p13.1 containing eight SNPs associated with inflammatory diseases. Several are close to or within DHSs in T-helper type 1 (T_H1) and T_H2 cells as well as peaks of binding by transcription factors in HUVECs (Fig. 10c). The latter cell line is not immunological, but factor occupancy detected there could be a proxy for binding of a more relevant factor, such as GATA3, in T cells. Genetic variants in this region also affect expression levels of *PTGER4* (ref. 76), encoding the prostaglandin receptor EP4. Thus, the ENCODE data reinforce the hypothesis that genetic variants in 5p13.1 modulate the expression of flanking genes, and furthermore provide the specific hypothesis that the variants affect occupancy of a GATA factor in an allele-specific manner, thereby influencing susceptibility to Crohn's disease.

Nonrandom association of phenotypes with ENCODE cell types strengthens the argument that at least some of the GWAS lead SNPs are functional or extremely close to functional variants. Each of the associations between a lead SNP and an ENCODE annotation remains a credible hypothesis of a particular functional element

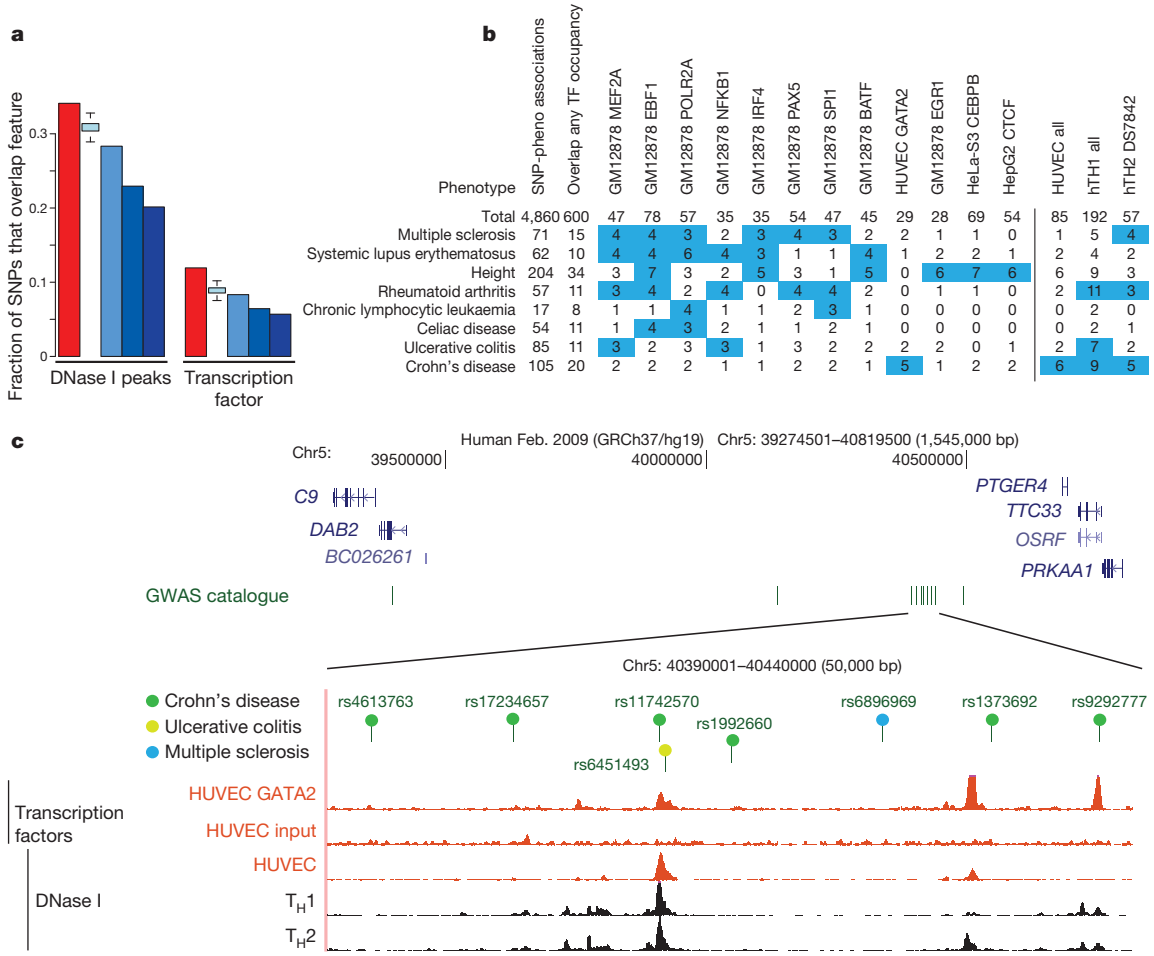

Figure 10 | Comparison of genome-wide-association-study-identified loci with ENCODE data. **a**, Overlap of lead SNPs in the NHGRI GWAS SNP catalogue (June 2011) with DHSs (left) or transcription-factor-binding sites (right) as red bars compared with various control SNP sets in blue. The control SNP sets are (from left to right): SNPs on the Illumina 2.5M chip as an example of a widely used GWAS SNP typing panel; SNPs from the 1000 Genomes project; SNPs extracted from 24 personal genomes (see personal genome variants track at http://main.genome-browser.bx.psu.edu (ref. 80)), all shown as blue bars. In addition, a further control used 1,000 randomizations from the genotyping SNP panel, matching the SNPs with each NHGRI catalogue SNP for allele frequency and distance to the nearest TSS (light blue bars with bounds at 1.5 times the interquartile range). For both DHSs and transcription-factor-binding regions, a larger proportion of overlaps with GWAS-implicated SNPs is found compared to any of the controls sets. **b**, Aggregate overlap of phenotypes to selected transcription-factor-binding sites (left matrix) or DHSs in selected cell lines (right matrix), with a count of overlaps between the phenotype and the cell line/factor. Values in blue squares pass an empirical *P*-value threshold ≤0.01 (based on the same analysis of overlaps between randomly chosen, GWAS-matched SNPs and these epigenetic features) and have at least a count of three overlaps. The *P* value for the total number of phenotype–transcription factor associations is <0.001. **c**, Several SNPs associated with Crohn's disease and other inflammatory diseases that reside in a large gene desert on chromosome 5, along with some epigenetic features indicative of function. The SNP (rs11742570) strongly associated to Crohn's disease overlaps a GATA2 transcription-factor-binding signal determined in HUVECs. This region is also DNase I hypersensitive in HUVECs and T-helper T_H1 and T_H2 cells. An interactive version of this figure is available in the online version of the paper.

class or cell type to explore with future experiments. Supplementary Tables 1–3, section M, list all 14,885 pairwise associations across the ENCODE annotations. The accompanying papers have a more detailed examination of common variants with other regulatory information[19,25,29,73,75,77].

Concluding remarks

The unprecedented number of functional elements identified in this study provides a valuable resource to the scientific community as well as significantly enhances our understanding of the human genome. Our analyses have revealed many novel aspects of gene expression and regulation as well as the organization of such information, as illustrated by the accompanying papers (see http://www.encodeproject.org/ENCODE/pubs.html for collected ENCODE publications). However, there are still many specific details, particularly about the mechanistic processes that generate these elements and how and where they function, that require additional experiments to elucidate.

The large spread of coverage—from our highest resolution, most conservative set of bases implicated in GENCODE protein-coding gene exons (2.9%) or specific protein DNA binding (8.5%) to the broadest, most general set of marks covering the genome (approximately 80%), with many gradations in between—presents a spectrum of elements with different functional properties discovered by ENCODE. A total of 99% of the known bases in the genome are within 1.7 kb of any ENCODE element, whereas 95% of bases are within 8 kb of a bound transcription factor motif or DNase I footprint. Interestingly, even using the most conservative estimates, the fraction of bases likely to be involved in direct gene regulation, even though incomplete, is significantly higher than that ascribed to protein-coding exons (1.2%), raising the possibility that more information in the human genome may be important for gene regulation than for biochemical function. Many of the regulatory elements are not constrained across mammalian evolution, which so far has been one of the most reliable indications of an important biochemical event for the organism. Thus, our data provide orthologous indicators for suggesting possible functional elements.

Importantly, for the first time we have sufficient statistical power to assess the impact of negative selection on primate-specific elements, and all ENCODE classes display evidence of negative selection in these unique-to-primate elements. Furthermore, even with our most conservative estimate of functional elements (8.5% of putative DNA/protein binding regions) and assuming that we have already sampled half of the elements from our transcription factor and cell-type diversity, one would estimate that at a minimum 20% (17% from protein binding and 2.9% protein coding gene exons) of the genome participates in these specific functions, with the likely figure significantly higher.

The broad coverage of ENCODE annotations enhances our understanding of common diseases with a genetic component, rare genetic diseases, and cancer, as shown by our ability to link otherwise anonymous associations to a functional element. ENCODE and similar studies provide a first step towards interpreting the rest of the genome—beyond protein-coding genes—thereby augmenting common disease genetic studies with testable hypotheses. Such information justifies performing whole-genome sequencing (rather than exome only, 1.2% of the genome) on rare diseases and investigating somatic variants in non-coding functional elements, for instance, in cancer. Furthermore, as GWAS analyses typically associate disease to SNPs in large regions, comparison to ENCODE non-coding functional elements can help pinpoint putative causal variants in addition to refinement of location by fine-mapping techniques[78]. Combining ENCODE data with allele-specific information derived from individual genome sequences provides specific insight on the impact of a genetic variant. Indeed, we believe that a significant goal would be to use functional data such as that derived from this project to assign every genomic variant to its possible impact on human phenotypes.

So far, ENCODE has sampled 119 of 1,800 known transcription factors and general components of the transcriptional machinery on a limited number of cell types, and 13 of more than 60 currently known histone or DNA modifications across 147 cell types. DNase I, FAIRE and extensive RNA assays across subcellular fractionations have been undertaken on many cell types, but overall these data reflect a minor fraction of the potential functional information encoded in the human genome. An important future goal will be to enlarge this data set to additional factors, modifications and cell types, complementing the other related projects in this area (for example, Roadmap Epigenomics Project, http://www.roadmapepigenomics.org/, and International Human Epigenome Consortium, http://www.ihec-epigenomes.org/). These projects will constitute foundational resources for human genomics, allowing a deeper interpretation of the organization of gene and regulatory information and the mechanisms of regulation, and thereby provide important insights into human health and disease. Co-published ENCODE-related papers can be explored online via the *Nature* ENCODE explorer (http://www.nature.com/ENCODE), a specially designed visualization tool that allows users to access the linked papers and investigate topics that are discussed in multiple papers via thematically organized threads.

METHODS SUMMARY

For full details of Methods, see Supplementary Information.

Received 24 November 2011; accepted 29 May 2012.

1. ENCODE Project Consortium. The ENCODE (ENCyclopedia Of DNA Elements) Project. *Science* **306,** 636–640 (2004).
2. Birney, E. *et al.* Identification and analysis of functional elements in 1% of the human genome by the ENCODE pilot project. *Nature* **447,** 799–816 (2007).
3. The ENCODE Project Consortium. A user's guide to the encyclopedia of DNA elements (ENCODE). *PLoS Biol.* **9,** e1001046 (2011).
4. Mouse Genome Sequencing Consortium. Initial sequencing and comparative analysis of the mouse genome. *Nature* **420,** 520–562 (2002).
5. Chiaromonte, F. *et al.* The share of human genomic DNA under selection estimated from human-mouse genomic alignments. *Cold Spring Harb. Symp. Quant. Biol.* **68,** 245–254 (2003).
6. Cooper, G. M. *et al.* Distribution and intensity of constraint in mammalian genomic sequence. *Genome Res.* **15,** 901–913 (2005).
7. Parker, S. C., Hansen, L., Abaan, H. O., Tullius, T. D. & Margulies, E. H. Local DNA topography correlates with functional noncoding regions of the human genome. *Science* **324,** 389–392 (2009).
8. Lindblad-Toh, K. *et al.* A high-resolution map of human evolutionary constraint using 29 mammals. *Nature* **478,** 476–482 (2011).
9. Pheasant, M. & Mattick, J. S. Raising the estimate of functional human sequences. *Genome Res.* **17,** 1245–1253 (2007).
10. Ponting, C. P. & Hardison, R. C. What fraction of the human genome is functional? *Genome Res.* **21,** 1769–1776 (2011).
11. Asthana, S. *et al.* Widely distributed noncoding purifying selection in the human genome. *Proc. Natl Acad. Sci. USA* **104,** 12410–12415 (2007).
12. Landt, S. G. *et al.* ChIP-seq guidelines and practices used by the ENCODE and modENCODE consortia. *Genome Res.* http://dx.doi.org/10.1101/gr.136184.111 (2012).
13. Li, Q., Brown, J. B., Huang, H. & Bickel, P. J. Measuring reproducibility of high-throughput experiments. *Ann. Appl. Stat.* **5,** 1752–1779 (2011).
14. Harrow, J. *et al.* GENCODE: The reference human genome annotation for the ENCODE project. *Genome Res.* http://dx.doi.org/10.1101/gr.135350.111 (2012).
15. Howald, C. *et al.* Combining RT-PCR-seq and RNA-seq to catalog all genic elements encoded in the human genome. *Genome Res.* http://dx.doi.org/10.1101/gr.134478.111 (2012).
16. Djebali, S. *et al.* Landscape of transcription in human cells. *Nature* http://dx.doi.org/10.1038/nature11233 (this issue).
17. Derrien, T. *et al.* The GENCODE v7 catalog of human long noncoding RNAs: Analysis of their gene structure, evolution, and expression. *Genome Res.* http://dx.doi.org/10.1101/gr.132159.111 (2012).
18. Pei, B. *et al.* The GENCODE pseudogene resource. *Genome Biol.* **13,** R51 (2012).
19. Gerstein, M. B. *et al.* Architecture of the human regulatory network derived from ENCODE data. *Nature* http://dx.doi.org/10.1038/nature11245 (this issue).
20. Bickel, P. J., Boley, N., Brown, J. B., Huang, H. Y. & Zhang, N. R. Subsampling methods for genomic inference. *Ann. Appl. Stat.* **4,** 1660–1697 (2010).
21. Kaplan, T. *et al.* Quantitative models of the mechanisms that control genome-wide patterns of transcription factor binding during early *Drosophila* development. *PLoS Genet.* **7,** e1001290 (2011).
22. Li, X. Y. *et al.* The role of chromatin accessibility in directing the widespread, overlapping patterns of *Drosophila* transcription factor binding. *Genome Biol.* **12,** R34 (2011).

23. Pique-Regi, R. *et al.* Accurate inference of transcription factor binding from DNA sequence and chromatin accessibility data. *Genome Res.* **21,** 447–455 (2011).
24. Zhang, Y. *et al.* Primary sequence and epigenetic determinants of *in vivo* occupancy of genomic DNA by GATA1. *Nucleic Acids Res.* **37,** 7024–7038 (2009).
25. Neph, S. *et al.* An expansive human regulatory lexicon encoded in transcription factor footprints. *Nature* http://dx.doi.org/10.1038/nature11212 (this issue).
26. Whitfield, T. W. *et al.* Functional analysis of transcription factor binding sites in human promoters. *Genome Biol.* **13,** R50 (2012).
27. Gross, D. S. & Garrard, W. T. Nuclease hypersensitive sites in chromatin. *Annu. Rev. Biochem.* **57,** 159–197 (1988).
28. Urnov, F. D. Chromatin remodeling as a guide to transcriptional regulatory networks in mammals. *J. Cell. Biochem.* **88,** 684–694 (2003).
29. Thurman, R. E. *et al.* The accessible chromatin landscape of the human genome. *Nature* http://dx.doi.org/10.1038/nature11232 (this issue).
30. Kundaje, A. *et al.* Ubiquitous heterogeneity and asymmetry of the chromatin environment at regulatory elements. *Genome Res.* http://dx.doi.org/10.1101/gr.136366.111 (2012).
31. Schultz, D. C., Ayyanathan, K., Negorev, D., Maul, G. G. & Rauscher, F. J. III. SETDB1: a novel KAP-1-associated histone H3, lysine 9-specific methyltransferase that contributes to HP1-mediated silencing of euchromatic genes by KRAB zinc-finger proteins. *Genes Dev.* **16,** 919–932 (2002).
32. Frietze, S., O'Geen, H., Blahnik, K. R., Jin, V. X. & Farnham, P. J. ZNF274 recruits the histone methyltransferase SETDB1 to the 3′ ends of ZNF genes. *PLoS ONE* **5,** e15082 (2010).
33. Boyle, A. P. *et al.* High-resolution genome-wide *in vivo* footprinting of diverse transcription factors in human cells. *Genome Res.* **21,** 456–464 (2011).
34. Hesselberth, J. R. *et al.* Global mapping of protein-DNA interactions *in vivo* by digital genomic footprinting. *Nature Methods* **6,** 283–289 (2009).
35. Zhang, Y. *et al.* Model-based analysis of ChIP-Seq (MACS). *Genome Biol.* **9,** R137 (2008).
36. Kouzarides, T. Chromatin modifications and their function. *Cell* **128,** 693–705 (2007).
37. Li, B., Carey, M. & Workman, J. L. The role of chromatin during transcription. *Cell* **128,** 707–719 (2007).
38. Hon, G. C., Hawkins, R. D. & Ren, B. Predictive chromatin signatures in the mammalian genome. *Hum. Mol. Genet.* **18,** R195–R201 (2009).
39. Zhou, V. W., Goren, A. & Bernstein, B. E. Charting histone modifications and the functional organization of mammalian genomes. *Nature Rev. Genet.* **12,** 7–18 (2011).
40. Ernst, J. *et al.* Mapping and analysis of chromatin state dynamics in nine human cell types. *Nature* **473,** 43–49 (2011).
41. Hon, G., Wang, W. & Ren, B. Discovery and annotation of functional chromatin signatures in the human genome. *PLoS Comput. Biol.* **5,** e1000566 (2009).
42. Ball, M. P. *et al.* Targeted and genome-scale strategies reveal gene-body methylation signatures in human cells. *Nature Biotechnol.* **27,** 361–368 (2009).
43. Meissner, A. *et al.* Genome-scale DNA methylation maps of pluripotent and differentiated cells. *Nature* **454,** 766–770 (2008).
44. Ogryzko, V. V., Schiltz, R. L., Russanova, V., Howard, B. H. & Nakatani, Y. The transcriptional coactivators p300 and CBP are histone acetyltransferases. *Cell* **87,** 953–959 (1996).
45. Lister, R. *et al.* Human DNA methylomes at base resolution show widespread epigenomic differences. *Nature* **462,** 315–322 (2009).
46. Dekker, J. Gene regulation in the third dimension. *Science* **319,** 1793–1794 (2008).
47. Dostie, J. *et al.* Chromosome Conformation Capture Carbon Copy (5C): a massively parallel solution for mapping interactions between genomic elements. *Genome Res.* **16,** 1299–1309 (2006).
48. Lajoie, B. R., van Berkum, N. L., Sanyal, A. & Dekker, J. My5C: web tools for chromosome conformation capture studies. *Nature Methods* **6,** 690–691 (2009).
49. Sanyal, A., Lajoie, B., Jain, G. & Dekker, J. The long-range interaction landscape of gene promoters. *Nature* http://dx.doi.org/10.1038/nature11279 (this issue).
50. Fullwood, M. J. *et al.* An oestrogen-receptor-alpha-bound human chromatin interactome. *Nature* **462,** 58–64 (2009).
51. Li, G. *et al.* Extensive promoter-centered chromatin interactions provide a topological basis for transcription regulation. *Cell* **148,** 84–98 (2012).
52. Borneman, A. R. *et al.* Divergence of transcription factor binding sites across related yeast species. *Science* **317,** 815–819 (2007).
53. Odom, D. T. *et al.* Tissue-specific transcriptional regulation has diverged significantly between human and mouse. *Nature Genet.* **39,** 730–732 (2007).
54. Schmidt, D. *et al.* Five-vertebrate ChIP-seq reveals the evolutionary dynamics of transcription factor binding. *Science* **328,** 1036–1040 (2010).
55. A map of human genome variation from population-scale sequencing. *Nature* **467,** 1061–1073 (2010).
56. King, M. C. & Wilson, A. C. Evolution at two levels in humans and chimpanzees. *Science* **188,** 107–116 (1975).
57. Spivakov, M. *et al.* Analysis of variation at transcription factor binding sites in *Drosophila* and humans. *Genome Biol.* **13,** R49 (2012).
58. Sandelin, A. *et al.* Mammalian RNA polymerase II core promoters: insights from genome-wide studies. *Nature Rev. Genet.* **8,** 424–436 (2007).
59. Dong, X. *et al.* Modeling gene expression using chromatin features in various cellular contexts. *Genome Biol.* **13,** R53 (2012).
60. Huff, J. T., Plocik, A. M., Guthrie, C. & Yamamoto, K. R. Reciprocal intronic and exonic histone modification regions in humans. *Nature Struct. Mol. Biol.* **17,** 1495–1499 (2010).
61. Tilgner, H. *et al.* Deep sequencing of subcellular RNA fractions shows splicing to be predominantly co-transcriptional in the human genome but inefficient for lncRNAs. *Genome Res.* http://dx.doi.org/10.1101/gr.134445.111 (2012).
62. Fu, Y., Sinha, M., Peterson, C. L. & Weng, Z. The insulator binding protein CTCF positions 20 nucleosomes around its binding sites across the human genome. *PLoS Genet.* **4,** e1000138 (2008).
63. Kornberg, R. D. & Stryer, L. Statistical distributions of nucleosomes: nonrandom locations by a stochastic mechanism. *Nucleic Acids Res.* **16,** 6677–6690 (1988).
64. Schones, D. E. *et al.* Dynamic regulation of nucleosome positioning in the human genome. *Cell* **132,** 887–898 (2008).
65. Valouev, A. *et al.* Determinants of nucleosome organization in primary human cells. *Nature* **474,** 516–520 (2011).
66. Frietze, S. *et al.* Cell type-specific binding patterns reveal that TCF7L2 can be tethered to the genome by association with GATA3. *Genome Biol.* **13,** R52 (2012).
67. Yip, K. Y. *et al.* Classification of human genomic regions based on experimentally-determined binding sites of more than 100 transcription-related factors. *Genome Biol.* **13,** R48 (2012).
68. Hoffman, M. M. *et al.* Unsupervised pattern discovery in human chromatin structure through genomic segmentation. *Nature Methods* **9,** 473–476 (2012).
69. Kapranov, P. *et al.* RNA maps reveal new RNA classes and a possible function for pervasive transcription. *Science* **316,** 1484–1488 (2007).
70. Koch, F. *et al.* Transcription initiation platforms and GTF recruitment at tissue-specific enhancers and promoters. *Nature Struct. Mol. Biol.* **18,** 956–963 (2011).
71. McLean, C. Y. *et al.* GREAT improves functional interpretation of cis-regulatory regions. *Nature Biotechnol.* **28,** 495–501 (2010).
72. Rozowsky, J. *et al.* AlleleSeq: analysis of allele-specific expression and binding in a network framework. *Mol. Syst. Biol.* **7,** 522 (2011).
73. Boyle, A. P. *et al.* Annotation of functional variation in personal genomes using RegulomeDB. *Genome Res.* http://dx.doi.org/10.1101/gr.137323.112 (2012).
74. Hindorff, L. A. *et al.* Potential etiologic and functional implications of genome-wide association loci for human diseases and traits. *Proc. Natl Acad. Sci. USA* **106,** 9362–9367 (2009).
75. Schaub, M. A., Boyle, A. P., Kundaje, A., Batzoglou, S. & Snyder, M. Linking disease associations with regulatory information in the human genome. *Genome Res.* http://dx.doi.org/10.1101/gr.136127.111 (2012).
76. Libioulle, C. *et al.* Novel Crohn disease locus identified by genome-wide association maps to a gene desert on 5p13.1 and modulates expression of PTGER4. *PLoS Genet.* **3,** e58 (2007).
77. Vernot, B. *et al.* Personal and population genomics of human regulatory variation. *Genome Res.* http://dx.doi.org/10.1101/gr.134890.111 (2012).
78. Harismendy, O. *et al.* 9p21 DNA variants associated with coronary artery disease impair interferon-γ signalling response. *Nature* **470,** 264–268 (2011).
79. Cheng, C. *et al.* Understanding transcriptional regulation by integrative analysis of transcription factor binding data. *Genome Res.* http://dx.doi.org/10.1101/gr.136838.111 (2012).
80. Schuster, S. C. *et al.* Complete Khoisan and Bantu genomes from southern Africa. *Nature* **463,** 943–947 (2010).

Supplementary Information is available in the online version of the paper.

Acknowledgements We thank additional members of our laboratories and institutions who have contributed to the experimental and analytical components of this project. We thank D. Leja for assistance with production of the figures. The Consortium is funded by grants from the NHGRI as follows: production grants: U54HG004570 (B. E. Bernstein); U01HG004695 (E. Birney); U54HG004563 (G. E. Crawford); U54HG004557 (T. R. Gingeras); U54HG004555 (T. J. Hubbard); U41HG004568 (W. J. Kent); U54HG004576 (R. M. Myers); U54HG004558 (M. Snyder); U54HG004592 (J. A. Stamatoyannopoulos). Pilot grants: R01HG003143 (J. Dekker); RC2HG005591 and R01HG003700 (M. C. Giddings); R01HG004456-03 (Y. Ruan); U01HG004571 (S. A. Tenenbaum); U01HG004561 (Z. Weng); RC2HG005679 (K. P. White). This project was supported in part by American Recovery and Reinvestment Act (ARRA) funds from the NHGRI through grants U54HG004570, U54HG004563, U41HG004568, U54HG004592, R01HG003143, RC2HG005591, R01HG003541, U01HG004561, RC2HG005679 and R01HG003988 (L. Pennacchio). In addition, work from NHGRI Groups was supported by the Intramural Research Program of the NHGRI (L. Elnitski, ZIAHG200323; E. H. Margulies, ZIAHG200341). Research in the Pennachio laboratory was performed at Lawrence Berkeley National Laboratory and at the United States Department of Energy Joint Genome Institute, Department of Energy Contract DE-AC02-05CH11231, University of California.

Author Contributions See the consortium author list for details of author contributions.

Author Information The Supplementary Information is accompanied by a Virtual Machine (VM) containing the functioning analysis data and code. Further details of the VM are available from http://encodeproject.org/ENCODE/integrativeAnalysis/VM. Correspondence and requests for materials should be addressed to E.B. (birney@ebi.ac.uk).

The ENCODE Project Consortium

Overall coordination (data analysis coordination) Ian Dunham[1], Anshul Kundaje[2]†; **Data production leads (data production)** Shelley F. Aldred[3], Patrick J. Collins[3], Carrie A. Davis[4], Francis Doyle[5], Charles B. Epstein[6], Seth Frietze[7], Jennifer Harrow[8], Rajinder Kaul[9], Jainab Khatun[10], Bryan R. Lajoie[11], Stephen G. Landt[12], Bum-Kyu Lee[13],

Florencia Pauli[14], Kate R. Rosenbloom[15], Peter Sabo[16], Alexias Safi[17], Amartya Sanyal[11], Noam Shoresh[6], Jeremy M. Simon[18], Lingyun Song[17], Nathan D. Trinklein[3]; **Lead analysts (data analysis)** Robert C. Altshuler[19], Ewan Birney[1], James B. Brown[20], Chao Cheng[21], Sarah Djebali[22], Xianjun Dong[23], Ian Dunham[1], Jason Ernst[19]†, Terrence S. Furey[24], Mark Gerstein[21], Belinda Giardine[25], Melissa Greven[23], Ross C. Hardison[25,26], Robert S. Harris[25], Javier Herrero[1], Michael M. Hoffman[16], Sowmya Iyer[27], Manolis Kellis[19], Jainab Khatun[10], Pouya Kheradpour[19], Anshul Kundaje[2]†, Timo Lassmann[28], Qunhua Li[20]†, Xinying Lin[23], Georgi K. Marinov[29], Angelika Merkel[22], Ali Mortazavi[30], Stephen C. J. Parker[31], Timothy E. Reddy[14]†, Joel Rozowsky[21], Felix Schlesinger[4], Robert E. Thurman[16], Jie Wang[23], Lucas D. Ward[19], Troy W. Whitfield[23], Steven P. Wilder[1], Weisheng Wu[25], Hualin S. Xi[32], Kevin Y. Yip[21]†, Jiali Zhuang[23]; **Writing group** Bradley E. Bernstein[6,33], Ewan Birney[1], Ian Dunham[1], Eric D. Green[34], Chris Gunter[14], Michael Snyder[12]; **NHGRI project management (scientific management)** Michael J. Pazin[35], Rebecca F. Lowdon[35]†, Laura A. L. Dillon[35]†, Leslie B. Adams[35], Caroline J. Kelly[35], Julia Zhang[35]†, Judith R. Wexler[35]†, Eric D. Green[34], Peter J. Good[35], Elise A. Feingold[35]; **Principal investigators (steering committee)** Bradley E. Bernstein[6,33], Ewan Birney[1], Gregory E. Crawford[17,36], Job Dekker[11], Laura Elnitski[37], Peggy J. Farnham[7], Mark Gerstein[21], Morgan C. Giddings[10], Thomas R. Gingeras[4,38], Eric D. Green[34], Roderic Guigó[22,39], Ross C. Hardison[25,26], Timothy J. Hubbard[8], Manolis Kellis[19], W. James Kent[15], Jason D. Lieb[18], Elliott H. Margulies[31]†, Richard M. Myers[14], Michael Snyder[12], John A. Stamatoyannopoulos[40], Scott A. Tenenbaum[5], Zhiping Weng[23], Kevin P. White[41], Barbara Wold[29,42]; **Boise State University and University of North Carolina at Chapel Hill Proteomics groups (data production and analysis)** Jainab Khatun[10], Yanbao Yu[43], John Wrobel[10], Brian A. Risk[10], Harsha P. Gunawardena[43], Heather C. Kuiper[43], Christopher W. Maier[43], Ling Xie[43], Xian Chen[43], Morgan C. Giddings[10]; **Broad Institute Group (data production and analysis)** Bradley E. Bernstein[6,33], Charles B. Epstein[6], Noam Shoresh[6], Jason Ernst[19]†, Pouya Kheradpour[19], Tarjei S. Mikkelsen[6], Shawn Gillespie[33], Alon Goren[6,33], Oren Ram[6,33], Xiaolan Zhang[6], Li Wang[6], Robbyn Issner[6], Michael J. Coyne[6], Timothy Durham[6], Manching Ku[6,33], Thanh Truong[6], Lucas D. Ward[19], Robert C. Altshuler[19], Matthew L. Eaton[19], Manolis Kellis[19]; **Cold Spring Harbor, University of Geneva, Center for Genomic Regulation, Barcelona, RIKEN, Sanger Institute, University of Lausanne, Genome Institute of Singapore group (data production and analysis)** Sarah Djebali[22], Carrie A. Davis[4], Angelika Merkel[22], Alex Dobin[4], Timo Lassmann[28], Ali Mortazavi[30], Andrea Tanzer[22], Julien Lagarde[22], Wei Lin[4], Felix Schlesinger[4], Chenghai Xue[4], Georgi K. Marinov[29], Jainab Khatun[10], Brian A. Williams[29], Chris Zaleski[4], Joel Rozowsky[21], Maik Röder[22], Felix Kokocinski[8]†, Rehab F. Abdelhamid[28], Tyler Alioto[22,44], Igor Antoshechkin[29], Michael T. Baer[4], Philippe Batut[4], Ian Bell[45], Kimberly Bell[4], Sudipto Chakrabortty[4], Xian Chen[43], Jacqueline Chrast[46], Joao Curado[22], Thomas Derrien[22]†, Jorg Drenkow[4], Erica Dumais[45], Jackie Dumais[45], Radha Duttagupta[45], Megan Fastuca[4], Kata Fejes-Toth[4]†, Pedro Ferreira[22], Sylvain Foissac[45], Melissa J. Fullwood[47]†, Hui Gao[45], David Gonzalez[22], Assaf Gordon[4], Harsha P. Gunawardena[43], Cédric Howald[46], Sonali Jha[4], Rory Johnson[22], Philipp Kapranov[45]†, Brandon King[29], Colin Kingswood[22,44], Guoliang Li[48], Oscar J. Luo[47], Eddie Park[30], Jonathan B. Preall[4], Kimberly Presaud[4], Paolo Ribeca[22,44], Brian A. Risk[10], Daniel Robyr[49], Xiaoan Ruan[47], Michael Sammeth[22,44], Kuljeet Singh Sandhu[47], Lorain Schaeffer[29], Lei-Hoon See[4], Atif Shahab[47], Jorgen Skancke[22], Ana Maria Suzuki[28], Hazuki Takahashi[28], Hagen Tilgner[22]†, Diane Trout[29], Nathalie Walters[46], Huaien Wang[4], John Wrobel[10], Yanbao Yu[43], Yoshihide Hayashizaki[28], Jennifer Harrow[8], Mark Gerstein[21], Timothy J. Hubbard[8], Alexandre Reymond[46], Stylianos E. Antonarakis[49], Gregory J. Hannon[4], Morgan C. Giddings[10], Yijun Ruan[47], Barbara Wold[29,42], Piero Carninci[28], Roderic Guigó[22,39], Thomas R. Gingeras[4,38]; **Data coordination center at UC Santa Cruz (production data coordination)** Kate R. Rosenbloom[15], Cricket A. Sloan[15], Katrina Learned[15], Venkat S. Malladi[15], Matthew C. Wong[15], Galt P. Barber[15], Melissa S. Cline[15], Timothy R. Dreszer[15], Steven G. Heitner[15], Donna Karolchik[15], W. James Kent[15], Vanessa M. Kirkup[15], Laurence R. Meyer[15], Jeffrey C. Long[15], Morgan Maddren[15], Brian J. Raney[15]; **Duke University, EBI, University of Texas, Austin, University of North Carolina-Chapel Hill group (data production and analysis)** Terrence S. Furey[24], Lingyun Song[17], Linda L. Grasfeder[18], Paul G. Giresi[18], Bum-Kyu Lee[13], Anna Battenhouse[13], Nathan C. Sheffield[17], Jeremy M. Simon[18], Kimberly A. Showers[18], Alexias Safi[17], Darin London[17], Akshay A. Bhinge[13], Christopher Shestak[18], Matthew R. Schaner[18], Seul Ki Kim[18], Zhuzhu Z. Zhang[18], Piotr A. Mieczkowski[50], Joanna O. Mieczkowska[18], Zheng Liu[13], Ryan M. McDaniell[13], Yunyun Ni[13], Naim U. Rashid[51], Min Jae Kim[18], Sheera Adar[18], Zhancheng Zhang[24], Tianyuan Wang[17], Deborah Winter[17], Damian Keefe[1], Ewan Birney[1], Vishwanath R. Iyer[13], Jason D. Lieb[18], Gregory E. Crawford[17,36]; **Genome Institute of Singapore group (data production and analysis)** Guoliang Li[48], Kuljeet Singh Sandhu[47], Meizhen Zheng[47], Ping Wang[47], Oscar J. Luo[47], Atif Shahab[47], Melissa J. Fullwood[47]†, Xiaoan Ruan[47], Yijun Ruan[47]; **HudsonAlpha Institute, Caltech, UC Irvine, Stanford group (data production and analysis)** Richard M. Myers[14], Florencia Pauli[14], Brian A. Williams[29], Jason Gertz[14], Georgi K. Marinov[29], Timothy E. Reddy[14]†, Jost Vielmetter[29,42], E. Christopher Partridge[14], Diane Trout[29], Katherine E. Varley[14], Clarke Gasper[29,42], Anita Bansal[14], Shirley Pepke[29,52], Preti Jain[14], Henry Amrhein[29], Kevin M. Bowling[14], Michael Anaya[29,42], Marie K. Cross[14], Brandon King[29], Michael A. Muratet[14], Igor Antoshechkin[29], Kimberly M. Newberry[14], Kenneth McCue[29], Amy S. Nesmith[14], Katherine I. Fisher-Aylor[29,42], Barbara Pusey[14], Gilberto DeSalvo[29,42], Stephanie L. Parker[14]†, Sreeram Balasubramanian[29,42], Nicholas S. Davis[14], Sarah K. Meadows[14], Tracy Eggleston[14], Chris Gunter[14], J. Scott Newberry[14], Shawn E. Levy[14], Devin M. Absher[14], Ali Mortazavi[30], Wing H. Wong[53], Barbara Wold[29,42]; **Lawrence Berkeley National Laboratory group (targeted experimental validation)** Matthew J. Blow[54], Axel Visel[54,55], Len A. Pennachio[54,55]; **NHGRI groups (data production and analysis)** Laura Elnitski[37], Elliott H. Margulies[31]†, Stephen C. J. Parker[31], Hanna M. Petrykowska[37]; **Sanger Institute, Washington University, Yale University, Center for Genomic Regulation, Barcelona, UCSC, MIT, University of Lausanne, CNIO group (data production and analysis)** Alexej Abyzov[21], Bronwen Aken[8], Daniel Barrell[8], Gemma Barson[8], Andrew Berry[8], Alexandra Bignell[8], Veronika Boychenko[8], Giovanni Bussotti[22], Jacqueline Chrast[46], Claire Davidson[8], Thomas Derrien[22]†, Gloria Despacio-Reyes[8], Mark Diekhans[15], Iakes Ezkurdia[56], Adam Frankish[8], James Gilbert[8], Jose Manuel Gonzalez[8], Ed Griffiths[8], Rachel Harte[15], David A. Hendrix[19], Cédric Howald[46], Toby Hunt[8], Irwin Jungreis[19], Mike Kay[8], Ekta Khurana[21], Felix Kokocinski[8]†, Jing Leng[21], Michael F. Lin[19], Jane Loveland[8], Zhi Lu[57], Deepa Manthravadi[8], Marco Mariotti[22], Jonathan Mudge[8], Gaurab Mukherjee[8], Cedric Notredame[22], Baikang Pei[21], Jose Manuel Rodriguez[56], Gary Saunders[8], Andrea Sboner[58], Stephen Searle[8], Cristina Sisu[21], Catherine Snow[8], Charlie Steward[8], Andrea Tanzer[22], Electra Tapanari[8], Michael L. Tress[56], Marijke J. van Baren[59]†, Nathalie Walters[46], Stefan Washietl[19], Laurens Wilming[8], Amonida Zadissa[8], Zhengdong Zhang[60], Michael Brent[59], David Haussler[61], Manolis Kellis[19], Alfonso Valencia[56], Mark Gerstein[21], Alexandre Reymond[46], Roderic Guigó[22,39], Jennifer Harrow[8], Timothy J. Hubbard[8]; **Stanford-Yale, Harvard, University of Massachusetts Medical School, University of Southern California/UC Davis group (data production and analysis)** Stephen G. Landt[12], Seth Frietze[7], Alexej Abyzov[21], Nick Addleman[12], Roger P. Alexander[21], Raymond K. Auerbach[21], Suganthi Balasubramanian[21], Keith Bettinger[12], Nitin Bhardwaj[21], Alan P. Boyle[12], Alina R. Cao[62], Philip Cayting[12], Alexandra Charos[63], Yong Cheng[12], Chao Cheng[21], Catharine Eastman[12], Ghia Euskirchen[12], Joseph D. Fleming[64], Fabian Grubert[12], Lukas Habegger[21], Manoj Hariharan[12], Arif Harmanci[21], Sushma Iyengar[65], Victor X. Jin[66], Konrad J. Karczewski[12], Maya Kasowski[12], Phil Lacroute[12], Hugo Lam[12], Nathan Lamarre-Vincent[64], Jing Leng[21], Jin Lian[67], Marianne Lindahl-Allen[64], Renqiang Min[21]†, Benoit Miotto[64], Hannah Monahan[63], Zarmik Moqtaderi[64], Xinmeng J. Mu[21], Henriette O'Geen[62], Zhengqing Ouyang[12], Dorrelyn Patacsil[12], Baikang Pei[21], Debasish Raha[63], Lucia Ramirez[12], Brian Reed[63], Joel Rozowsky[21], Andrea Sboner[58], Minyi Shi[12], Cristina Sisu[21], Teri Slifer[12], Heather Witt[7], Linfeng Wu[12], Xiaoqin Xu[62], Koon-Kiu Yan[21], Xinqiong Yang[12], Kevin Y. Yip[21]†, Zhengdong Zhang[60], Kevin Struhl[64], Sherman M. Weissman[67], Mark Gerstein[21], Peggy J. Farnham[7], Michael Snyder[12]; **University of Albany SUNY group (data production and analysis)** Scott A. Tenenbaum[5], Luiz O. Penalva[68], Francis Doyle[5]; **University of Chicago, Stanford group (data production and analysis)** Subhradip Karmakar[41], Stephen G. Landt[12], Raj R. Bhanvadia[41], Alina Choudhury[41], Marc Domanus[41], Lijia Ma[41], Jennifer Moran[41], Dorrelyn Patacsil[12], Teri Slifer[12], Alec Victorsen[41], Xinqiong Yang[12], Michael Snyder[12], Kevin P. White[41]; **University of Heidelberg group (targeted experimental validation)** Thomas Auer[69]†, Lazaro Centanin[69], Michael Eichenlaub[69], Franziska Gruhl[69], Stephan Heermann[69], Burkhard Hoeckendorf[69], Daigo Inoue[69], Tanja Kellner[69], Stephan Kirchmaier[69], Claudia Mueller[69], Robert Reinhardt[69], Lea Schertel[69], Stephanie Schneider[69], Rebecca Sinn[69], Beate Wittbrodt[69], Jochen Wittbrodt[69]; **University of Massachusetts Medical School Bioinformatics group (data production and analysis)** Zhiping Weng[23], Troy W. Whitfield[23], Jie Wang[23], Patrick J. Collins[3], Shelley F. Aldred[3], Nathan D. Trinklein[3], E. Christopher Partridge[14], Richard M. Myers[14]; **University of Massachusetts Medical School Genome Folding group (data production and analysis)** Job Dekker[11], Gaurav Jain[11], Bryan R. Lajoie[11], Amartya Sanyal[11]; **University of Washington, University of Massachusetts Medical Center group (data production and analysis)** Gayathri Balasundaram[70], Daniel L. Bates[16], Rachel Byron[70], Theresa K. Canfield[16], Morgan J. Diegel[16], Douglas Dunn[16], Abigail K. Ebersol[71], Tristan Frum[71], Kavita Garg[72], Erica Gist[16], R. Scott Hansen[71], Lisa Boatman[71], Eric Haugen[16], Richard Humbert[16], Gaurav Jain[11], Audra K. Johnson[16], Ericka M. Johnson[71], Tattyana V. Kutyavin[16], Bryan R. Lajoie[11], Kristen Lee[16], Dimitra Lotakis[71], Matthew T. Maurano[16], Shane J. Neph[16], Fiedencio V. Neri[16], Eric D. Nguyen[71], Hongzhu Qu[16], Alex P. Reynolds[16], Vaughn Roach[16], Eric Rynes[16], Peter Sabo[16], Minerva E. Sanchez[71], Richard S. Sandstrom[16], Amartya Sanyal[11], Anthony O. Shafer[16], Andrew B. Stergachis[16], Sean Thomas[16], Robert E. Thurman[16], Benjamin Vernot[16], Jeff Vierstra[16], Shinny Vong[16], Hao Wang[16], Molly A. Weaver[16], Yongqi Yan[71], Miaohua Zhang[70], Joshua M. Akey[16], Michael Bender[70], Michael O. Dorschner[73], Mark Groudine[70], Michael J. MacCoss[16], Patrick Navas[71], George Stamatoyannopoulos[71], Rajinder Kaul[9], Job Dekker[11], John A. Stamatoyannopoulos[40]; **Data Analysis Center (data analysis)**; Ian Dunham[1], Kathryn Beal[1], Alvis Brazma[74], Paul Flicek[1], Javier Herrero[1], Nathan Johnson[1], Damian Keefe[1], Margus Lukk[74]†, Nicholas M. Luscombe[75], Daniel Sobral[1]†, Juan M. Vaquerizas[75], Steven P. Wilder[1], Serafim Batzoglou[2], Arend Sidow[76], Nadine Hussami[2], Sofia Kyriazopoulou-Panagiotopoulou[2], Max W. Libbrecht[2]†, Marc A. Schaub[2], Anshul Kundaje[2]†, Ross C. Hardison[25,26], Webb Miller[25], Belinda Giardine[25], Robert S. Harris[25], Weisheng Wu[25], Peter J. Bickel[20], Balazs Banfai[20], Nathan P. Boley[20], James B. Brown[20], Haiyan Huang[20], Qunhua Li[20]†, Jingyi Jessica Li[20], William Stafford Noble[16,77], Jeffrey A. Bilmes[78], Orion J. Buske[16], Michael M. Hoffman[16], Avinash D. Sahu[16]†, Peter V. Kharchenko[79], Peter J. Park[79], Dannon Baker[80], James Taylor[80], Zhiping Weng[23], Sowmya Iyer[27], Xianjun Dong[23], Melissa Greven[23], Xinying Lin[23], Jie Wang[23], Hualin S. Xi[32], Jiali Zhuang[23], Mark Gerstein[21], Roger P. Alexander[21], Suganthi Balasubramanian[21], Chao Cheng[21], Arif Harmanci[21], Lucas Lochovsky[21], Renqiang Min[21]†, Xinmeng J. Mu[21], Joel Rozowsky[21], Koon-Kiu Yan[21], Kevin Y. Yip[21]† & Ewan Birney[1]

[1]Vertebrate Genomics Group, European Bioinformatics Institute (EMBL-EBI), Wellcome Trust Genome Campus, Hinxton, Cambridgeshire CB10 1SD, UK. [2]Department of Computer Science, Stanford University, 318 Campus Drive, Stanford, California 94305-5428, USA. [3]SwitchGear Genomics, 1455 Adams Drive Suite 1317, Menlo Park, California 94025, USA. [4]Functional Genomics, Cold Spring Harbor Laboratory, 1 Bungtown Road, Cold Spring Harbor, New York 11724, USA. [5]College of Nanoscale Sciences and Engineering, University ay Albany-SUNY, 257 Fuller Road, NFE 4405, Albany, New York 12203, USA. [6]Broad Institute of MIT and Harvard, 7 Cambridge Center, Cambridge, Massachusetts 02142, USA. [7]Biochemistry and Molecular Biology, USC/Norris Comprehensive Cancer Center, 1450 Biggy Street, NRT 6503, Los Angeles, California 90089, USA. [8]Informatics, Wellcome Trust Sanger Institute, Wellcome Trust Genome Campus, Hinxton, Cambridgeshire CB10 1SA, UK. [9]Department of Medicine, Division of Medical Genetics, University of Washington, 3720 15th Avenue NE, Seattle, Washington 98195, USA. [10]College of Arts and Sciences, Boise State University, 1910 University Drive, Boise, Idaho 83725, USA. [11]Program in Systems Biology, Program in Gene Function and Expression, Department of Biochemistry and Molecular

Pharmacology, University of Massachusetts Medical School, 364 Plantation Street, Worcester, Massachusetts 01605, USA. [12]Department of Genetics, Stanford University, 300 Pasteur Drive, M-344, Stanford, California 94305-5120, USA. [13]Center for Systems and Synthetic Biology, Institute for Cellular and Molecular Biology, Section of Molecular Genetics and Microbiology, The University of Texas at Austin, 1 University Station A4800, Austin, Texas 78712, USA. [14]HudsonAlpha Institute for Biotechnology, 601 Genome Way, Huntsville, Alabama 35806, USA. [15]Center for Biomolecular Science and Engineering, University of California, Santa Cruz, 1156 High Street, Santa Cruz, California 95064, USA. [16]Department of Genome Sciences, University of Washington, 3720 15th Ave NE, Seattle, Washington 98195-5065, USA. [17]Institute for Genome Sciences and Policy, Duke University, 101 Science Drive, Durham, North Carolina 27708, USA. [18]Department of Biology, Carolina Center for Genome Sciences, and Lineberger Comprehensive Cancer Center, The University of North Carolina at Chapel Hill, 408 Fordham Hall, Chapel Hill, North Carolina 27599-3280, USA. [19]Computer Science and Artificial Intelligence Laboratory, Broad Institute of MIT and Harvard, Massachusetts Institute of Technology, 32 Vassar Street, Cambridge, Massachusetts 02139, USA. [20]Department of Statistics, University of California, Berkeley, 367 Evans Hall, University of California, Berkeley, Berkeley, California 94720, USA. [21]Computational Biology and Bioinformatics Program, Yale University, 266 Whitney Avenue, New Haven, Connecticut 06520, USA. [22]Bioinformatics and Genomics, Centre for Genomic Regulation (CRG) and UPF, Doctor Aiguader, 88, Barcelona 08003, Catalonia, Spain. [23]Program in Bioinformatics and Integrative Biology, University of Massachusetts Medical School, 364 Plantation Street, Worcester, Massachusetts 01605, USA. [24]Department of Genetics, The University of North Carolina at Chapel Hill, 120 Mason Farm Road, CB 7240, Chapel Hill, North Carolina 27599, USA. [25]Center for Comparative Genomics and Bioinformatics, The Pennsylvania State University, Wartik Laboratory, University Park, Pennsylvania 16802, USA. [26]Department of Biochemistry and Molecular Biology, The Pennsylvania State University, 304 Wartik Laboratory, University Park, Pennsylvania 16802, USA. [27]Program in Bioinformatics, Boston University, 24 Cummington Street, Boston, Massachusetts 02215, USA. [28]RIKEN Omics Science Center, RIKEN Yokohama Institute, 1-7-22 Suehiro-cho, Tsurumi-ku, Yokohama, Kanagawa 230-0045, Japan. [29]Division of Biology, California Institute of Technology, 156-291200 East California Boulevard, Pasadena, California 91125, USA. [30]Developmental and Cell Biology and Center for Complex Biological Systems, University of California Irvine, 2218 Biological Sciences III, Irvine, California 92697-2300, USA. [31]Genome Technology Branch, National Human Genome Research Institute, 5625 Fishers Lane, Bethesda, Maryland 20892, USA. [32]Department of Biochemistry and Molecular Pharmacology, Bioinformatics Core, University of Massachusetts Medical School, 364 Plantation Street, Worcester, Massachusetts 01605, USA. [33]Howard Hughes Medical Institute and Department of Pathology, Massachusetts General Hospital and Harvard Medical School, 185 Cambridge St CPZN 8400, Boston, Massachusetts 02114, USA. [34]National Human Genome Research Institute, National Institutes of Health, 31 Center Drive, Building 31, Room 4B09, Bethesda, Maryland 20892-2152, USA. [35]National Human Genome Research Institute, National Institutes of Health, 5635 Fishers Lane, Bethesda, Maryland 20892-9307, USA. [36]Department of Pediatrics, Division of Medical Genetics, Duke University School of Medicine, Durham, North Carolina 27710, USA. [37]National Human Genome Research Institute, National Institutes of Health, 5625 Fishers Lane, Rockville, Maryland 20892, USA. [38]Affymetrix, Inc., 3380 Central Expressway, Santa Clara, California 95051, USA. [39]Departament de Ciències Experimentals i de la Salut, Universitat Pompeu Fabra, Barcelona, Catalonia 08002, Spain. [40]Department of Genome Sciences, Box 355065, and Department of Medicine, Division of Oncology, Box 358081, University of Washington, Seattle, Washington 98195-5065, USA. [41]Institute for Genomics and Systems Biology, The University of Chicago, 900 East 57th Street, 10100 KCBD, Chicago, Illinois 60637, USA. [42]Beckman Institute, California Institute of Technology, 156-29 1200 E. California Boulevard, Pasadena, California 91125, USA. [43]Department of Biochemistry and Biophysics, University of North Carolina School of Medicine, Campus Box 7260, 120 Mason Farm Road, 3010 Genetic Medicine Building, Chapel Hill, North Carolina 27599, USA. [44]Centro Nacional de Análisis Genómico (CNAG), C/Baldiri Reixac 4, Torre I, Barcelona, Catalonia 08028, Spain. [45]Genomics, Affymetrix, Inc., 3380 Central Expressway, Santa Clara, California 95051, USA. [46]Center for Integrative Genomics, University of Lausanne, Genopode Building, 1015 Lausanne, Switzerland. [47]Genome Technology and Biology, Genome Institute of Singapore, 60 Biopolis Street, 02-01, Genome, Singapore 138672, Singapore. [48]Computational and Systems Biology, Genome Institute of Singapore, 60 Biopolis Street, 02-01, Genome, Singapore 138672, Singapore. [49]Department of Genetic Medicine and Development, University of Geneva Medical School, and University Hospitals of Geneva, 1 rue Michel-Servet, 1211 Geneva 4, Switzerland. [50]Department of Genetics, The University of North Carolina at Chapel Hill, 5078 GMB, Chapel Hill, North Carolina 27599-7264, USA. [51]Department of Biostatistics, Gillings School of Global Public Health, The University of North Carolina at Chapel Hill, 408 Fordham Hall, Chapel Hill, North Carolina 27599-7445, USA. [52]Center for Advanced Computing Research, California Institute of Technology, MC 158-79, 1200 East California Boulavard, Pasadena, California 91125, USA. [53]Department of Statistics, Stanford University, Sequoia Hall. 390 Serra Mall, Stanford, California 94305-4065, USA. [54]DOE Joint Genome Institute, Walnut Creek, California, USA. [55]Genomics Division, Lawrence Berkeley National Laboratory, One Cyclotron Road, MS 84-171, Berkeley, California 94720, USA. [56]Structural Computational Biology, Spanish National Cancer Research Centre (CNIO), Melchor Fernandez Almagro, 3, 28029 Madrid, Spain. [57]School of Life Sciences, Tsinghua University, School of Life Sciences, Tsinghua University, 100084 Beijing, China. [58]Department of Pathology and Laboratory Medicine, Institute for Computational Biomedicine, Weill Cornell Medical College, 1305 York Avenue, Box 140, New York, New York 10065, USA. [59]Computer Science and Engineering, Washington University in St Louis, St Louis, Missouri 63130, USA. [60]Department of Genetics, Albert Einstein College of Medicine, 1301 Morris Park Avenue, Room 353A, Bronx, New York 10461, USA. [61]Center for Biomolecular Science and Engineering, Howard Hughes Medical Institute, University of California, Santa Cruz, 1156 High Street, Santa Cruz, California 95064, USA. [62]Genome Center, University of California-Davis, 451 Health Sciences Drive, Davis, California 95616, USA. [63]Department of Molecular, Cellular, and Developmental Biology, Yale University, 266 Whitney Avenue, New Haven, Connecticut 06511, USA. [64]Biological Chemistry and Molecular Pharmacology, Harvard Medical School, 240 Longwood Avenue, Boston, Massachusetts 02115, USA. [65]Biochemistry and Molecular Biology, University of Southern California, 1501 San Pablo Street, Los Angeles, California 90089, USA. [66]Department of Biomedical Informatics, Ohio State University, 3172C Graves Hall, 333 W Tenth Avenue, Columbus, Ohio 43210, USA. [67]Department of Genetics, Yale University, Yale University School of Medicine, 333 Cedar Street, New Haven, Connecticut 06510, USA. [68]Department of Cellular and Structural Biology, Children's Cancer Research Institute–UTHSCSA, Mail code 7784- 7703 Floyd Curl Dr, San Antonio, Texas 78229, USA. [69]Centre for Organismal Studies (COS) Heidelberg, University of Heidelberg, Im Neuenheimer Feld 230, 69120 Heidelberg, Germany. [70]Basic Sciences Division, Fred Hutchinson Cancer Research Center, 825 Eastlake Avenue East, Seattle, Washington 98109, USA. [71]Department of Medicine, Division of Medical Genetics, Box 357720, University of Washington, Seattle, Washington 98195-7720, USA. [72]Division of Human Biology, Fred Hutchinson Cancer Research Center, 825 Eastlake Avenue East, Seattle, Washington 98109, USA. [73]Department of Psychiatry and Behavioral Sciences, Box 356560, University of Washington, Seattle, Washington 98195-6560, USA. [74]Microarray Informatics Group, European Bioinformatics Institute (EMBL-EBI), Wellcome Trust Genome Campus, Hinxton, Cambridgeshire CB10 1SD, UK. [75]Genomics and Regulatory Systems Group, European Bioinformatics Institute (EMBL-EBI), Wellcome Trust Genome Campus, Hinxton, Cambridgeshire CB10 1SD, UK. [76]Department of Pathology, Department of Genetics, Stanford University, 300 Pasteur Drive, Stanford, California 94305, USA. [77]Department of Computer Science and Engineering, 185 Stevens Way, Seattle, Washington 98195, USA. [78]Department of Electrical Engineering, University of Washington, 185 Stevens Way, Seattle, Washington 98195, USA. [79]Center for Biomedical Informatics, Harvard Medical School, 10 Shattuck Street, Boston, Massachusetts 02115, USA. [80]Departments of Biology and Mathematics and Computer Science, Emory University, Atlanta, Georgia 30322, USA. †Present addresses: Computer Science and Artificial Intelligence Laboratory, Massachusetts Institute of Technology, 32 Vassar Street, Cambridge, Massachusetts 02139, USA (A.K.); UCLA Biological Chemistry Department, Eli and Edythe Broad Center of Regenerative Medicine and Stem Cell Research at UCLA, Jonsson Comprehensive Cancer Center, 615 Charles E Young Dr South, Los Angeles, California 90095, USA (J.E.); Department of Statistics, 514D Wartik Lab, Penn State University, State College, Pennsylvania 16802, USA (Q.L.); Department of Biostatistics and Bioinformatics and the Institute for Genome Sciences and Policy, Duke University School of Medicine, 101 Science Drive, Durham, North Carolina 27708, USA (T.E.R.); Department of Computer Science and Engineering, The Chinese University of Hong Kong, Shatin, New Territories, Hong Kong (K.Y.Y.); Department of Genetics, Washington University in St Louis, St Louis, Missouri 63110, USA (R.F.L.); Department of Cell Biology and Molecular Genetics, University of Maryland, College Park, Maryland 20742, USA (L.A.L.D.); National Cancer Institute, National Institutes of Health, Bethesda, Maryland 20892, USA (J.Z.); University of California, Davis Population Biology Graduate Group, Davis, California 95616, USA (J.R.W.); Illumina Cambridge Ltd., Chesterford Research Park, Little Chesterford, Saffron Walden, Essex CB10 1XL, UK (E.H.M.); BlueGnome Ltd., CPC4, Capital Park, Fulbourn, Cambridge CB21 5XE, UK (F.K.); Institut de Génétique et Développement de Rennes, CNRS-UMR6061, Université de Rennes 1, F-35000 Rennes, Brittany, France (T.D.); Caltech, 1200 East California Boulevard, Pasadena, California 91125, USA (K.F.-T.); A*STAR-Duke-NUS Neuroscience Research Partnership, 8 College Road, Singapore 169857, Singapore (M.J.F.); St Laurent Institute, One Kendall Square, Cambridge, Massachusetts 02139, USA (P.K.); Department of Genetics, Stanford University, Stanford, California 94305, USA (H.T.); Biomedical Sciences (BMS) Graduate Program, University of California, San Francisco, 513 Parnassus Avenue, HSE-1285, San Francisco, California 94143-0505, USA (S.L.P.); Monterey Bay Aquarium Research Institute, Moss Landing, California 95039, USA (M.J.v.B.); Department of Machine Learning, NEC Laboratories America, 4 Independence Way, Princeton, New Jersey 08540, USA (R.M.); Neuronal Circuit Development Group, Unité de Génétique et Biologie du Développement, U934/UMR3215, Institut Curie–Centre de Recherche, Pole de Biologie du Développement et Cancer, 26, rue d'Ulm, 75248 Paris Cedex 05, France (T.A.); Cancer Research UK, Cambridge Research Institute, Li Ka Shing Centre, Robinson Way, Cambridge CB2 0RE, UK (M.L.); Unidade de Bioinformatica, Rua da Quinta Grande, 6, P-2780-156 Oeiras, Portugal (D.S.); Department of Genome Sciences, University of Washington, 3720 15th Avenue NE, Seattle, Washington 98195-5065, USA (M.W.L.); Center for Bioinformatics and Computational Biology, 3115 Ag/Life Surge Building 296, University of Maryland, College Park, Maryland 20742, USA (A.D.S.).